plants

Water and Ion Transport in Plants

New and Older Trends Meet Together

Edited by

Vadim Volkov, Lars H. Wegner and Mary Beilby

Printed Edition of the Special Issue Published in *Plants*

www.mdpi.com/journal/plants

MDPI

Water and Ion Transport in Plants: New and Older Trends Meet Together

Water and Ion Transport in Plants: New and Older Trends Meet Together

Editors

Vadim Volkov
Lars H. Wegner
Mary Beilby

MDPI • Basel • Beijing • Wuhan • Barcelona • Belgrade • Manchester • Tokyo • Cluj • Tianjin

Editors

Vadim Volkov
Department of Plant Sciences,
University of California,
Davis, One Shields Avenue,
Davis, CA 95616, USA

Lars H. Wegner
International Research Center
for Environmental Membrane
Biology, Foshan University,
18 Jiang-wanyi-lu,
Chancheng, Foshan, China

Mary Beilby
School of Physics, Biophysics,
The University of
New South Wales,
Kensington, NSW 2052,
Australia

Editorial Office
MDPI
St. Alban-Anlage 66
4052 Basel, Switzerland

This is a reprint of articles from the Special Issue published online in the open access journal *Plants* (ISSN 2223-7747) (available at: https://www.mdpi.com/journal/plants/special_issues/water_ion_transport).

For citation purposes, cite each article independently as indicated on the article page online and as indicated below:

LastName, A.A.; LastName, B.B.; LastName, C.C. Article Title. *Journal Name* **Year**, *Volume Number*, Page Range.

ISBN 978-3-0365-4517-2 (Hbk)
ISBN 978-3-0365-4518-9 (PDF)

Cover image courtesy of Vadim Volkov.

Contents

About the Editors

Vadim Volkov

Vadim Volkov is currently a Leading Research Scientist in K.A. Timiriazev Institute of Plant Physiology, Russian Academy of Sciences. He graduated from the Moscow State University, USSR and further worked in many areas of plant science and biomedicine with main accent on biophysical aspects of water and ion transport at the cellular level. After getting PhD Degree from K.A. Timiriazev Institute of Plant Physiology, Russian Academy of Sciences he worked at University of Glasgow (Scotland, UK) as a postdoctoral researcher on specific properties of ion transport in a halophyte relative of Arabidopsis thaliana, at University of Paisley (Scotland, UK) on barley ion channels, at Imperial College of London on action potentials in human cardiomyocytes, at Royal Veterinary College (UK) on ion transport in renal tubules, at London Metropolitan University on system biology of ion transport in yeast cells, at University of California, Davis on a new electromechanical microtensiometer to measure water potential in plants and at several other Universities in the UK and the Netherlands. His recent research interests also included effects of light sources with different statistics of photons (laser vs thermal) and single photon sources on ion currents in individual isolated rod cells of visual system of animals. His current research is on ion transport in salt tolerant plants. He is an Author of over 30 papers including 5 Book Chapters which summarized the results of the research, Co-Editor of eBook on ion transport and salinity tolerance in plants and also a member of Editorial Boards of several Journals.

Lars H. Wegner

Lars H. Wegner was born in 1965 in Soest (Westfalia), Germany. He studied biology with plant physiology as a major and physical chemistry as a minor at the University of Göttingen where he started to work on loading of nutrients into the root xylem under the supervision of Klaus Raschke. He continued that work at the Vrije Universiteit in Amsterdam, The Netherlands, and received a doctorate in 1996. He was then working as a postdoc in Germany at the University of Würzburg, and as an independent group leader at the Karlsruhe Institute of Technology. After a brief intermezzo in industrial research, he is a distinguished professor at the International Research Center for Environmental Membrane Biology (School of Food Science and Horticulture) at Foshan University in China since 2019. His fields of interest include electric field effects on membranes, plant electrophysiology, water relations, membrane transport, and systems biology. Lars is an associate editor for Frontiers in Plant Science, section Plant Biophysics and Modelling. He is married and has 2 children.

Mary Beilby

Born 20 January 1948 in Prague, then Czechoslovakia. My parents escaped the Communist regime and migrated to Australia, leaving me with my grandmother. In 1964 I was allowed to join my parents in Sydney. I finished my basic education at Randwick Girls High School Sydney. I got a scholarship to study at University of NSW (UNSW). I finished B. Sc. and joined Biophysics group of Prof. Hans Coster at UNSW. After obtaining my Ph. D., working on electrophysiology of model plant Chara, I had several postdoctoral positions with Prof. N.A. Walker (Sydney University) and Prof. Enid MacRobbie (University of Cambridge, UK). In 1992 I got a Lectureship/Senior Lectureship with School of Physics, UNSW, and worked there for 22 years. Most of my research has been done on various Characeae, but I also looked at electrophysiology of marine plant *Valonia ventricosa*. I am now retired from teaching and became Honorary Senior Lecturer, still in regular contact with the members of the Biophysics group. I am married with one daughter and one grandson. For more details and my publications, see my website: http://newt.phys.unsw.edu.au/~mjb/.

Preface to "Water and Ion Transport in Plants: New and Older Trends Meet Together"

This book was established after closing the Special Issue "Water and Ion Transport in Plants: New and Older Trends Meet Together", edited by Dr. Vadim Volkov, Professor Lars Wegner, and Dr Mary Beilby as Guest Editors and Mr. Everett Zhu as Managing Editor.

The transport of water and ions underlies all organised fluxes in plants, fluxes that secure homeostasis and provide the matrix for biochemical reactions, orchestrated cellular events, and development. At the cellular level, water and ions pass via cell membranes using a set of aquaporins as well as specific ion channels and transporters; transport follows thermodynamic and electrochemical gradients. At the whole-plant level, specialised tissues such as xylem and phloem have evolved to transport ions and water from roots to shoots and metabolites in the reverse direction. At the level of the ecosystem and for agricultural productivity, the supply and transport of water and ions form the basis for crop yield and productivity of ecosystems. All the processes for this exceptionally wide topic could not be covered within a single Special Issue, so the aim was to recall the main concepts established for water and ion transport, to introduce new ideas, including controversial ones, and to link these ideas to generate directions of potential research and progress. Therefore, this book represents a small collection of thoughtfully selected papers related to water and ion transport in plants. The collection represents and outlines the main existing concepts while stimulating the further interest in the intensively developing area of research.

This Special Issue consists of one review and four research papers. In the first paper, https://www.mdpi.com/2223-7747/9/10/1311, Zhang et al. found the surprisingly unexpected link between the activity of vacuolar NXH-type cation–proton antiporters and auxin transport. NXH-type transporters are known as one of determinants of salinity tolerance responsible for vacuolar sodium sequestration, their role in vacuolar potassium homeostasis was subsequently demonstrated. Here, the importance of these transporters for determining the abundance of auxin efflux carrier PIN2 in plasma membrane was demonstrated in *Arabidopsis thaliana* using quadruple knockout mutants, through cell biology and auxin sensor imaging means. The mutant plants exhibit morphological defects and altered gravitropism, which are related to disruptions in auxin transport that were caused by impacts on intracellular trafficking and PIN2 distribution.

The second paper, https://www.mdpi.com/2223-7747/10/1/38, is a Review contributed by the Guest Editor of the Special Issue Vadim Volkov and Co-Authored by Heiner Schwenke, who developed an elegant model of root exudation 30 years ago. The comprehensive Review analyses the phenomenon of plant root and stem exudation, which was quantitatively described about 300 years ago. Still, we are far from having a complete understanding of the processes underlying exudation. The Authors describe several different existing concepts aimed at explaining root exudation, add their own earlier unpublished data, link water transport with ion transport and the expression of aquaporins based on the literature, and develop upon their own earlier ideas about the role of metabolism and mechanosensitive ion channels in generating the root exudation phenomenon.

In the third paper, https://www.mdpi.com/2223-7747/10/4/814, Thorne et al. provide results on the recent introduction of fertilisation with silicon, which is not an essential element for plants, and its effects on drought tolerance of 98 wheat landraces. Apart from the general discussion and introduction about fertilisation by silicon, the Authors demonstrate the lack of effect on the drought tolerance of these landraces due to silicon, contrary to some earlier similar experiments. It is suggested that the reported favourable effects of silicon are not universal and depend on the

genotypes of the agricultural plants.

The fourth paper, https://www.mdpi.com/2223-7747/10/12/2667, by Matalin et al. explores expression of two putative P-type plasma membrane ATPases in unicellular marine algae *Dunaliella maritima*. The ATPases are the primary source of membrane energisation and seem to be extremely important for the exclusion of sodium under salt shock; the algal cells lack large vacuoles, so presumably have sodium-ATPase in the plasma membrane. Bioinformatic analysis and temporal expression of two P-type ATPases in algal cells under salt shock over three hours, paralleled by measurements of sodium concentrations, suggests that the cloned gene *DmHA1* corresponds to H^+-ATPase, while the cloned gene *DmHA2* corresponds to Na^+-ATPase in the algae.

In the fifth paper, https://www.mdpi.com/2223-7747/11/3/409, Nedelyaeva et al. describe cloning and characterization of three genes of the chloride channel family (CLC) from the halophyte *Suaeda altissima* (L.) Pall. The halophyte is able to grow at concentrations of NaCl exceeding 750 mM, which is above the level of salinity of sea water. This plant accumulates large amounts of sodium and chloride under salinity. Interestingly, the cloned CLC genes were similar to the ones from Arabidopsis, and their heterologous expression in yeast and bioinformatic analysis indicated that SaCLCd is likely a Cl^-/H^+ antiporter, while SaCLCf and SaCLCg are chloride channels. The expression of all three genes linearly increased with salinity proportional to the increasing chloride concentrations in leaves.

We thank all researchers that have been contributed to this Special Issue. We hope that this book can be a short teaser, serving as an introduction for further diving into the depths of water and ion transport research in plants.

Vadim Volkov, Lars H. Wegner, and Mary Beilby
Editors

plants

MDPI

Article

Auxin Homeostasis and Distribution of the Auxin Efflux Carrier PIN2 Require Vacuolar NHX-Type Cation/H^+ Antiporter Activity

Shiqi Zhang [1], Hiromi Tajima [2], Eiji Nambara [3], Eduardo Blumwald [2] and Elias Bassil [4,*]

1 Boyce Thompson Institute, Ithaca, NY 14850, USA; shqzhang@ucdavis.edu
2 Department of Plant Sciences, University of California, Davis, CA 95616, USA; htajima@ucdavis.edu (H.T.); eblumwald@ucdavis.edu (E.B.)
3 Department of Cell and Systems Biology, University of Toronto, Toronto, ON M5S 1A1, Canada; eiji.nambara@utoronto.ca
4 Horticultural Sciences Department, Tropical Research and Education Center, University of Florida, Homestead, FL 33031, USA
* Correspondence: ebassil@ufl.edu

Received: 2 September 2020; Accepted: 29 September 2020; Published: 3 October 2020

Abstract: The *Arabidopsis* vacuolar Na^+/H^+ transporters (NHXs) are important regulators of intracellular pH, Na^+ and K^+ homeostasis and necessary for normal plant growth, development, and stress acclimation. *Arabidopsis* contains four vacuolar NHX isoforms known as AtNHX1 to AtNHX4. The quadruple knockout *nhx1nhx2nhx3nhx4*, lacking any vacuolar NHX-type antiporter activity, displayed auxin-related phenotypes including loss of apical dominance, reduced root growth, impaired gravitropism and less sensitivity to exogenous IAA and NAA, but not to 2,4-D. In *nhx1nhx2nhx3nhx4*, the abundance of the auxin efflux carrier PIN2, but not PIN1, was drastically reduced at the plasma membrane and was concomitant with an increase in PIN2 labeled intracellular vesicles. Intracellular trafficking to the vacuole was also delayed in the mutant. Measurements of free IAA content and imaging of the auxin sensor DII-Venus, suggest that auxin accumulates in root tips of *nhx1nhx2nhx3nhx4*. Collectively, our results indicate that vacuolar NHX dependent cation/H^+ antiport activity is needed for proper auxin homeostasis, likely by affecting intracellular trafficking and distribution of the PIN2 efflux carrier.

Keywords: vacuole; potassium; homeostasis; NHX; auxin distribution; PIN; intracellular trafficking

1. Introduction

Plant nutrients are essential to numerous biochemical and physiological processes needed for plant growth and development. Many cellular processes depend on specific steady-state ion concentrations within intracellular compartments. Given the fundamental importance of cellular ion homeostasis, plants contain conserved primary and secondary transport systems and sophisticated mechanisms to regulate their activities to facilitate homeostasis [1]. Primary transporters are H^+-translocating enzymes, such as H^+-ATPases on the plasma membrane (PM) and intracellular organelles and vacuolar pyrophosphatase, which use the hydrolysis of ATP and PPi to establish an electrochemical H^+ gradient across membranes [2]. Secondary transporters use the H^+ gradient generated by the H^+-pumps, to drive the uptake of ions and molecules against their electrochemical gradients [1,3,4]. One important group of secondary transporters, known as the NHX-type cation-H^+ antiporters, mediate the electroneutral exchange of H^+ for either Na^+ or K^+ and, therefore, play key roles in pH regulation, Na^+ sequestration, and intracellular K^+ homeostasis. In plants, K^+ is vital to biosynthesis, osmotic regulation, and charge balance, hence its intracellular levels are tightly regulated [5]. Most plants

with known genomes have three orthologous groups of NHX-type antiporters that localize to distinct intracellular compartments. In *Arabidopsis*, four isoforms known as AtNHX1 through AtNHX4 localize to vacuoles [6,7], AtNHX5 and AtNHX6 localize to Golgi, the *trans*-Golgi network (TGN) and pre-vacuolar compartments [8–12], while the two divergent isoforms AtNHX7/SOS1, AtNHX8 localize on the PM [13,14].

Several studies provided compelling evidence to support the role of NHX-type antiporters in the regulation of pH and transport of K^+ into the vacuole. The *Arabidopsis nhx1nhx2* knockout mutant NHXs displayed acidic pH and 70% less vacuolar K^+ compared to wild type (WT) plants [6,15]. The *nhx1nhx2* mutant also showed aberrant flower development, reduced vegetative growth, overall smaller cells likely caused by reduced vacuolar K^+ uptake and insufficient turgor needed to drive cell expansion. Surprisingly, the *nhx1nhx2* mutant also showed severe growth reduction when treated with high K^+ concentration in the growth media but did not show a similar phenotype in the presence of equimolar Na^+ concentrations [6]. Moreover, moderate amounts of Na^+ in the grow media improved its growth. A recent study assessed the contribution of each of the four *Arabidopsis* vacuolar NHXs (NHX1, NHX2, NHX3 and NHX4) to vacuolar Na^+ and K^+ transport [16]. Using *nhx* triple and quadruple knockout mutants, the affinity of each vacuolar NHX for Na^+ and K^+ and the kinetics of the cation/H^+ were analyzed [16]. While all four vacuolar NHX antiporters were able to mediate Na^+ transport, only NHX1, NHX2 and NHX4 but not NHX3 were able to mediate K^+ transport. Therefore, in the *nhx1/2* or *nhx1/2/3/4* mutant, the loss of major vacuolar K^+ uptake could lead to an accumulation of K^+ in the cytosol, as evidenced previously for *nhx1nhx2* [6,15].

It has been suggested that K^+ transport and cellular K^+ homeostasis play critical roles in auxin homeostasis. *Arabidopsis* mutants lacking HAK/KUP/KT K^+ transporters showed defects in root gravitropism, cell expansion and shoot development and abnormal distribution of auxin reporters [17–23]. Auxin homeostasis is largely regulated by polar auxin transport. In the shoot, auxin flows from the shoot apical meristem, its primary site of biosynthesis, down to the root [24,25] where it moves in two antiparallel streams. Shoot-derived auxin flows down toward the root apex through the central stele, then travels to the outer cells and is redirected to the base of the root [26–28]. The downward auxin flow to the root tip (acropetal auxin transport) is mainly associated with an auxin efflux carrier, PIN1(PIN-FORMED 1), whereas the auxin transport from the root tip to the base (basipetal auxin transport) relies on another auxin efflux carrier, PIN2 [29,30]. The PIN family and the ATP-binding cassette (ABC) superfamily of transporters are the main efflux carriers for the polar auxin transport and play important roles in regulating auxin distribution between cells [31].

Little is known about the role of vacuolar ion homeostasis, in auxin homeostasis. Here, using the quadruple knockout *nhx1nhx2nhx3nhx4* lacking vacuolar K^+/H^+ exchange activity, we assessed auxin-related phenotypes and the distribution of auxin efflux carriers. Our results strongly suggested that the vacuolar NHXs play an important role in modulating auxin homeostasis, likely by affecting PIN2 distribution.

2. Results

2.1. The Morphological Phenotype of nhx1nxh2nhx3nhx4 Knockout Mutants

The loss of vacuolar NHX activity resulted in plant growth reduction with reduced rosette diameter and decreased growth [16]. When grown under normal growth conditions, the *nhx1nhx2nhx3nhx4* knockout displayed shorter shoots, losses of apical dominance and a profusely 'bushy' shoot phenotype (Figure 1a). Shoot branches did not display abnormal phyllotaxy (Figure 1b), suggesting that the knockout did not shift its meristem identity [32]. Close observation of the temporal manifestation of the 'bushy' phenotype revealed that the shoot tissue immediately below the inflorescence cluster dies (Figure 1c; arrow) before seed set. This is then followed by the growth of lower second-order shoots, (presumably because they are no longer suppressed by the primary shoot tip). Secondary order shoots exhibit the same shoot tip death as described for the primary shoot and its inflorescences.

This is then followed by the growth of third-order shoot buds, and so forth, so that the sequence of shoot tip death and lower order bud outgrowth is repeated until a profusely bushy shoot occurs as shown in Figure 1a. We also examined the root growth and responses to the gravity of the *nhx1nhx2nhx3nhx4* mutant. Mutant roots were much shorter than WT roots grown under the same conditions (Figure 1d). Notably, roots of *nhx1nhx2nhx3nhx4* showed altered gravitropism in which a half of the roots displayed incomplete root bending upon gravistimulation under 1 mM K^+ and a complete loss of gravitropism in the presence of 30 mM K^+ (Figure S1). *nhx1nhx2nhx3nhx4* roots grown on 30 mM K^+ medium also showed aberrant curling away from the gravity vector and is likely to be associated with altered cortical microtubule organization as reported previously [7]. Collectively, the bushy shoot phenotype, the losses of shoot apical dominance and abnormal root gravitropism in the *nhx1nhx2nhx3nhx4* mutant suggest that auxin-associated processes and/or homeostasis could be affected.

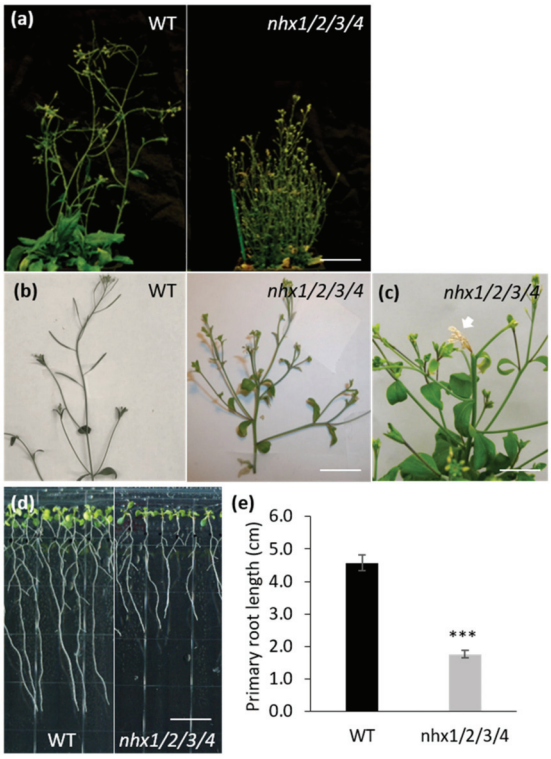

Figure 1. Shoot and root morphological phenotypes of *nhx1nhx2nhx3nhx4* knockout mutant. (**a**), WT (Col-0) and *nhx1/nhx2nhx3nhx4 (nhx1/2/3/4)* were grown in soil under 12-h days for 7 weeks. Scale bar, 4 cm. (**b**), Lateral branches of 4-week-old WT and *nhx1nhx2nhx3nhx4*. Scale bar, 2 cm. (**c**), Shoot apical meristem death of *nhx1nhx2nhx3nhx4* mutants when the plants were 4-week-old. Arrow in (**c**) indicates dead shoot apex and meristem. Scale bar, 0.5 cm. (**d**), WT and *nhx1nhx2nhx3nhx4* grown on standard nutrient plates with 8-h daylight for 7 days. Scale bar, 1 cm. (**e**), Primary root length of WT and the *nhx1nhx2nhx3nhx4* mutant showed in A. Values are mean ± S.D. ***, significant difference ($p < 0.001$; *t* test). n = 50.

2.2. The nhx1nhx2nhx3nhx4 Knockout Mutant Exhibited Altered Responses to Auxin

To evaluate whether the growth phenotypes displayed by the *nhx1nhx2nhx3nhx4* mutant correlated with auxin-associated perturbations, we assessed the root growth responses to

supplemental natural auxin (IAA), and the synthetic auxins NAA (1-Naphtaleneacetic acid) and 2,4-D (2,4-Dichlorophen-oxyacetic acid). The transport of IAA is conducted by both auxin influx and efflux systems, however, unlike IAA, 2,4-D transport is favored by auxin influx carriers such as AUX1, but not the auxin efflux carriers PIN2 [33,34]. NAA transport is favored by auxin efflux carriers but not by the influx carriers [35–37], as shown by the *aux1* mutant's resistance to exogenous 2,4-D but not NAA and the *pin2* mutant's hypersensitivity to exogenous NAA but not 2,4-D. Four-day-old WT and *nhx1nhx2nhx3nhx4* mutant seedlings were transferred to plates containing designated concentrations of IAA, NAA or 2,4-D and grown for 5 days. The root elongation of the primary root was measured and normalized to that of no auxin control (Figure 2). The root elongation of *nhx1nhx2nhx3nhx4* mutant was less sensitive to IAA or NAA compared with that of the WT, whereas the response to 2,4-D is similar to WT seedlings. Altered sensitivity of *nhx1nhx2nhx3nhx4* mutant to IAA and NAA, but not to 2,4-D, suggests that auxin efflux could be affected.

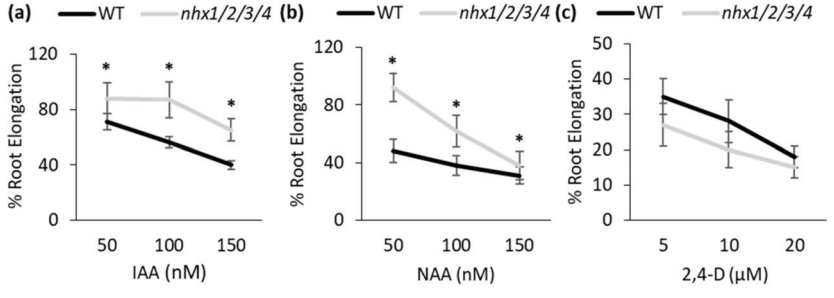

Figure 2. The *nhx1nhx2nhx3nhx4* mutant exhibited less sensitivity to IAA and NAA but not to 2,4-D. (**a**–**c**). Primary root growth of WT and mutant grown on medium supplemented with IAA (**a**), NAA (**b**) and 2,4-D (**c**). Values are the mean ± S.D. (n = 15). Stars indicate significant differences between wild type (WT) and *nhx1nhx2nhx3nhx4 (nhx1/2/3/4)* in the same concentration of auxin. $p < 0.05$ by *t* test.

2.3. Decreased PIN2 Abundance on the PM of nhx1nhx2nhx3nhx4 Mutant

To assess defects in auxin transport in the *nhx1nhx2nhx3nhx4* mutant, we generated translational fusion reporter lines expressing labelled auxin efflux carriers, PIN1 and PIN2, in the *nhx1nhx2nhx3nhx4* background. Confocal microscopy indicated only a slight difference in the PM-localized signal of PIN1 in the stele cells of the mutants compared to WT (Figure 3a,c) under 1 mM K^+ condition. The PM-localized PIN2 signal, however, was severely reduced in *nhx1nhx2nhx3nhx4* root cells (Figure 3b,d). Quantitative real-time PCR indicated no difference in the expression of PIN1 and PIN2 transcripts between WT and *nhx1nhx2nhx3nhx4* (Figure S2), suggesting that the reduced PM-localized PIN2 in the mutant was not due to transcriptional regulation. Furthermore, no differences in the subcellular distribution of PIN1 (basal side of stele cells) between WT and *nhx1nhx2nhx3nhx4* were noted (Figure 3h,i,l). However, numerous autofluorescent bodies were seen in *nhx1nhx2nhx3nhx4* root cells (Figure 3e,f,g). These bodies were relatively static and absent from WT roots. To further assess the nature of the PIN2-GFP signal, we used a Leica TCS SP8 confocal microscope equipped with the LightGate function. LightGate is an adjustable temporal window of emission detection that reduces autofluorescence signals. When a pulsed laser beam excites a fluorophore, a strong burst occurs that decays over time, with autofluorescence typically occurring late in the pulse. LightGate can exclude emission from this period thus reducing autofluorescence signals. This particular feature enabled us to adjust the desired imaging window during fluorophore decay to optimize signal collection and to resolve signals emitted from the autofluorescent bodies. Following image optimization, we were able to resolve apparent autofluorescence from an additional signal associated with PIN2-GFP vesicles in the mutant but not WT PIN2-GFP (Arrows in Figure 3j,k). In *nhx1nhx2nhx3nhx4*, PIN2-GFP was also seen on the apical side of the PM as expected but at relatively lower amounts. Quantification of the

ratio of PIN2-GFP fluorescence intensity associated with vesicles to that on the PM, was significantly higher in *nhx1nhx2nhx3nhx4* mutant root cells (Figure 3l).

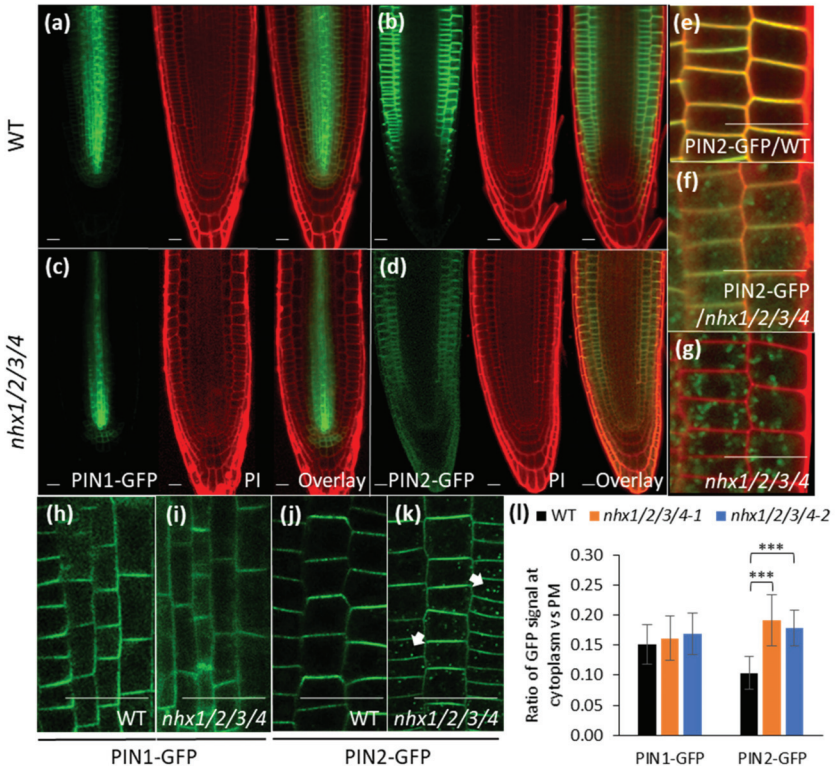

Figure 3. Expression and subcellular localization of PIN1 and PIN2. wild type (WT) and *nhx1nhx2nhx3nhx4* (*nhx1/2/3/4*) root tips are shown in (**a**,**b**) respectively. Localization of PIN1-GFP (**a**) and PIN2-GFP (**b**) in WT; and PIN1-GFP (**c**) and PIN2-GFP (**d**) in *nhx1nhx2nhx3nhx4*. Closeup of PIN2-GFP in WT (**e**) and *nhx1nhx2nhx3nhx4* (**f**). (**g**), autofluorescence signal (green) in *nhx1nhx2nhx3nhx4* roots. Roots were counter stained with propidium iodide (PI) in (**a**–**g**). (**h**,**i**), the subcellular localization of PIN1-GFP in WT (**h**) and *nhx1nhx2nhx3nhx4* (**i**). (**j**,**k**), the subcellular localization of PIN2-GFP in WT (**j**) and *nhx1nhx2nhx3nhx4* (**k**). Arrows in (**k**) indicate the intracellular PIN2-GFP vesicles. (**l**), the ratio of PIN1-GFP and PIN2-GFP signal intensity in the cytosol to that at the PM (values are mean ± SD; $n \geq 10$; ***, $p < 0.001$ by t test). Scale bar, 20 μm.

In addition, we conducted a λ (wavelength) scan and linear unmixing of signals obtained from WT PIN2-GFP, *nhx1nhx2nhx3nhx4* PIN2-GFP as well as *nhx1nhx2nhx3nhx4* to further resolve the nature of the signal from auto-fluorescent bodies (Figure S3a). Linear unmixing also enabled the separation of two distinct signals, one that emanated from autofluorescent bodies and another vesicle-like signal only present in *nhx1nhx2nhx3nhx4* expressing PIN2-GFP (Figure S3b). Results from both imaging approaches suggest the existence of bona fide PIN2 containing vesicles in *nhx1nhx2nhx3nhx4* root cells but not WT. Additionally, the subcellular localization of PIN2 in the *nhx1nhx2nhx3nhx4* under 30 mM K^+ condition were observed because the severe loss of gravitropism occurred under this condition. Surprisingly, no difference in the intracellular PIN2 containing vesicles was found compared to the low K^+ condition (Figure S4). An accumulation of PIN2-containing vesicles in *nhx1nhx2nhx3nhx4* could result in lower levels of PM-localized PIN2, suggesting defects in the distribution of PIN2.

2.4. Intracellular Trafficking to the Vacuole is Affected in the nhx1nhx2nhx3nhx4 Mutant

Given the presence of abundant PIN2-GFP expressing vesicles in *nhx1nhx2nhx3nhx4* and the known constitutive cycling of PIN2 between the PM and endosomal compartments [38,39], we asked whether intracellular trafficking in the mutant might be affected. Because the fluorescence signal of PIN2 is extremely low and not easily discernable without resolving additional autofluorescent signals present in *nhx1nhx2nhx3nhx4* (described above), we used instead the lipophilic dye FM4–64 to observe endomembrane labeling and trafficking in the mutant. In the root tip cells, FM4–64 initially labels the PM and then quickly internalizes into endosomal bodies that traffics and label initially the TGN [40], following other endomembrane compartments including the tonoplast [41]. WT and the mutant roots were stained with 4 μM FM4–64 for 5 min. In both WT and mutant root tips, FM4–64 labeled endosomes became evident after approximately 20 min (Figure 4a,c). As expected, labeling of the vacuolar membrane occurred after approximately 80 min in the WT, but in the mutant, only large FM4–64 endosomal aggregates were noted without any significant labeling of the tonoplast (Figure 4b,d). Instead, vacuolar staining in the mutant occurred after 150 min (Figure 4e). This observation suggested that trafficking from the TGN or pre-vacuolar compartment to the vacuole may be delayed in the *nhx1nhx2nhx3nhx4* mutant.

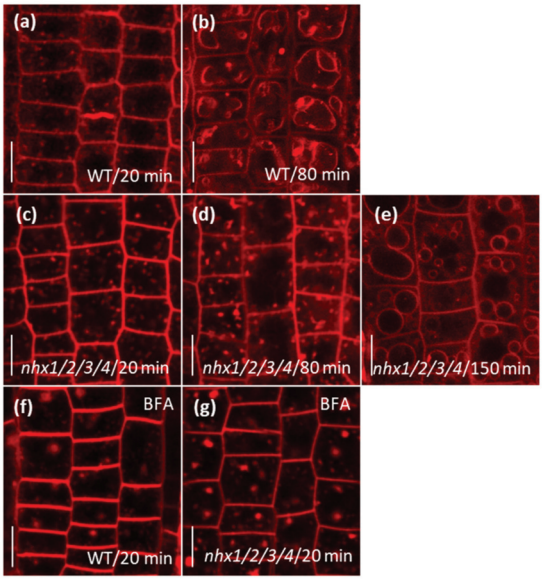

Figure 4. Trafficking to the vacuole is delayed in the *nhx1nhx2nhx3nhx4 mutant.* (**a**,**b**), wild type (WT) root tip cells after 20 min (**a**) or 80 min (**b**) after FM4–64 application. (**c**–**e**), nhx1nhx2nhx3nhx4 (*nhx1/2/3/4)* root tip cells after 20 min (**c**), 80 min (**d**) or 150 min (**e**) after FM4–64 application. (**f**,**g**), formation of BFA bodies in the root tip cells of the WT (**f**) or *nhx1nhx2nhx3nhx4* mutant (**g**). Scale bars, 10 μm.

Given the extensive use of Brefeldin A in assessing endomembrane trafficking processes, we used it to assess whether PIN2 cycling between the PM and endosomal compartments could be affected [39,42] in *nhx1nhx2nhx3nhx4*. Roots were pretreated with 25 μM BFA, then stained with FM4–64 and monitored for the progression of endomembrane labeling. In both WT and *nhx1nhx2nhx3nhx4* root tips pre-treated with BFA, similar-sized BFA bodies were observed after 20 min of FM4–64 application (Figure 4f,g), which suggests that the early internalization of PIN2 and its trafficking to the TGN (which is particularly sensitive to BFA) are not likely to be affected in the *nhx1nhx2nhx3nhx4* mutant.

2.5. Auxin Accumulated in the Root Tip Cells of nhx1nhx2nhx3nhx4 Mutant

The decrease in PM-localized PIN2, but not PM-localized PIN1, suggested that the basipetal movement of auxin, but not its acropetal movement, was perturbed in *nhx1nhx2nhx3nhx4* roots. Thus, auxin transported down to the root tip via PIN1 could be accumulated at the root tip. To test this hypothesis, we transformed *nhx1nhx2nhx3nhx4* mutants with the genetically encoded auxin sensor, DII-Venus [43]. DII-Venus is a tandem fusion of a fast-maturing form of YFP fused to the auxin interaction domain, Domain II of Aux/IAA, which is rapidly degraded in response to increases in auxin levels. Therefore, the DII-Venus signal is negatively correlated to the intracellular auxin content., i.e., a decrease in DII-Venus signal intensity indicates an increase in cellular auxin contents. In wild-type plants, the DII-Venus signal was easily detected and abundant (Figure 5a). In *nhx1nhx2nhx3nhx4*, however, DII-Venus decreased drastically in the root tip, meristem, and part of the elongation zone. In cells of the elongation zone, the DII-Venus signal was more similar to WT roots (arrows in Figure 5a), indicating that auxin was accumulating in mutant root tips. To further confirm these observations, we measured the free-IAA content in roots using LC-ESI-MS/MS and found that *nhx1nhx2nhx3nhx4* root tips had double the IAA content compared to wild type root tips (Figure 5b).

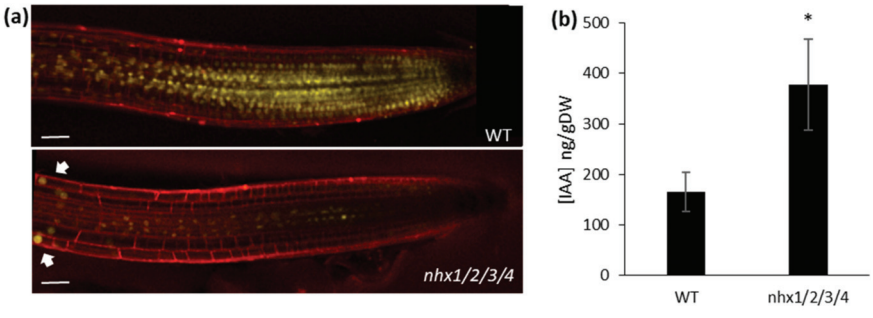

Figure 5. Root cells of *nhx1nhx2nhx3nhx4* accumulate high levels of auxin. (**a**), DII-Venus expression in WT (upper) and *nhx1nhx2nhx3nhx4 (nhx1/2/3/4)*. *nhx2nhx3nhx4 (nhx1/2/3/4)* mutant grown under control conditions. Cells were labeled with propidium iodide (red) as a counter stain to show cell organization. Arrows indicate DII-Venus signals recovery in the elongation zone. Scale bar, 50 μm. (**b**), Free-IAA content measured from the whole root of WT and *nhx1nhx2nhx3nhx4*. Values are the Mean ± SD (n = 3). Star indicates statistical significance ($P < 0.05$ by *t* test).

3. Discussion

The *nhx1nhx2nhx3nhx4* mutant displayed significant growth and developmental phenotypes that could be auxin-related, including the loss of shoot apical dominance, aberrant branching and reduced root growth (Figure 1). We evaluated whether such phenotypes were associated with perturbations in auxin homeostasis, by examining the growth response of the *nhx1nhx2nhx3nhx4* mutant to three auxin isoforms. The *nhx1nhx2nhx3nhx4* mutant showed less sensitivity to IAA and NAA but not to 2,4-D (Figure 2), suggesting that the mutant may be defective in root auxin efflux. Using GFP reporters and confocal microscopy, we examined the distribution of two important auxin efflux carriers, PIN1 and PIN2. Imaging in root tip cells indicated that the PIN1 was similar between the *nhx1nhx2nhx3nhx4* mutant and WT, however, PIN2 abundance at the PM was drastically reduced in *nhx1nhx2nhx3nhx4*. In the mutant, we noted PIN2 labeled vesicles that were observed in WT root cells (Figure 3) suggesting that the cellular distribution of PIN2 could be affected in the mutant. We performed endomembrane labeling experiments using FM-4–64 to monitor intracellular trafficking to the vacuole and whether this was affected in the *nhx1nhx2nhx3nhx4* mutant (Figure 4), and could explain the low abundance of PIN2 at the PM and its presence in intracellular vesicles in *nhx1nhx2nhx3nhx4* roots cells. A lack of PM-localized PIN2 protein could lead to impaired basipetal auxin transport, further resulting

in auxin accumulation as evidenced by a low DII-Venus expression and higher free IAA content in mutant root tips (Figure 5).

Vacuolar NHX-type antiporters function coordinately with other primary and secondary transporters to maintain intracellular pH and K^+ homeostasis [5]. A lack of any vacuolar NHX activity, as shown in the *nhx1nhx2nhx3nhx4* mutant [16], results in acidic vacuoles and little to no vacuolar K^+ uptake [16]. This could cause aberrant accumulation of K^+ in the cytosol because of the lack of K^+ exchange with the vacuole to modulate changes in K^+ uptake and maintain constant cytosolic K^+ concentrations [5,6,15,16]. Not much is known about how K^+ homeostasis could affect intracellular auxin homeostasis but indirect evidence could suggest possible connections. A K^+ carrier TRH1 (Tiny Root Hair 1) was shown to be involved in auxin transport in *Arabidopsis* roots [21]. Also in *Arabidopsis* roots, ZIFL1.1, one of two alternate splice isoforms of vacuolar-membrane localized ZIFL1 (Zinc-Induced Facilitator-Like 1) displayed H^+-coupled K^+ transport activity and was indirectly modulating basipetal auxin efflux likely by regulating the abundance of PIN2 at the PM [44,45]. Other intracellular antiporters of the same family, NHX5 and NHX6 which localize to the TGN, could affect auxin transport by affecting pH of the endoplasmic reticulum [46]. Very recently, Yang et al. demonstrated in rice that a PM H^+/K^+ symporter, OsHAK5, indirectly regulates auxin transport by affecting pH [47]. Collectively, such findings, together with our results, highlight the importance of intracellular pH and/or K^+ homeostasis in maintaining auxin homeostasis.

The molecular mechanism by which vacuolar NHX activity affects the abundance of PIN2 at the PM remains unclear. It is known that the abundance of PIN2 at the PM is maintained by endocytic internalization from the PM and its recycling back to the PM [48–50]. During PIN2 cycling, a population of PIN2 containing vesicles is targeted to the vacuole for degradation [39]. It is possible, therefore, that the accumulation of PIN2 vesicles we observed in the *nhx1nhx2nhx3nhx4* mutant, could be a consequence of defective trafficking to the vacuole, vesicle to vacuole fusion or maturation of late endosomes into vacuoles. It is unlikely that the internalization of PIN2 could be a main cause for the aberrant distribution of PIN2 from PM to vesicles because we did not observe an overall effect of endocytosis in the mutant. Notably, compared to PIN2, the subcellular localization and abundance of PIN1 appear to be less affected in the *nhx1nhx2nhx3nhx4* mutant root tips. One reason could be that PIN1 is under different regulation from PIN2 and may be less affected by intracellular ion homeostasis [30,51]. It is also possible that homeostasis in stele cells, where PIN1 is mainly expressed, is less affected by vacuolar NHX activity because the main NHXs involved in vacuolar K^+ uptake, NHX1, NHX2 and NHX4 [16], are less expressed in these cells [52,53].

4. Materials and Methods

4.1. Arabidopsis Seeds, Agrobacteria Strains, Growth Conditions and Treatments

Seedlings of the following lines were used in this study: *Arabidopsis thaliana* ecotype Columbia-0 as WT (Col-0); the mutants *nhx1–1/nhx2–1/nhx3–1/nhx4–1* (*nhx1nhx2nhx3nhx4*) and *nhx1–2/nhx2 crispr/nhx3–2/nhx4 crispr* in the Col-0 background; the transgenic lines are *35s::*DII-Venus (DII-Venus) used in [43], (Col-0 seeds and constructs obtained from the ABRC stock center; https://abrc.osu.edu/), *pPIN1::*PIN1-GFP (PIN1-GFP), *pPIN2::*PIN2-GFP (PIN2-GFP) used in [39,54] (Col-0 seeds and constructs kindly provided by Dr. Jiri Friml, IST Austria) in Col-0 and *nhx1–1/nhx2–1/nhx3–1/nhx4–1*. Because homozygous quadruple knockouts produce few seeds, heterozygous NHX1/*nhx1–1/nhx2–1/nhx3–1/nhx4–1* were used for transformation. Transformation of mutant plants was performed by floral dip [55], and the transgenic plants were screened with 20ug/l hygromycin. Multiple independent lines were selected, selfed, and T_2 and its progenies were used for imaging. All results were confirmed with two independent lines.

Seeds were treated, germinated on modified Murashige and Skoog media (Control) [56] as described previously [6]. Media were supplemented with either KCl or NaCl as indicated in specific experiments. Indole-3-acetic acid (IAA, Sigma), 1-Naphthaleneacetic acid (NAA, Sigma)

and 2,4-Dichlorophen-oxyacetic acid (2,4-D, Sigma) were applied in designated concentrations as a supplementation to the solid growth media. 4 μM of FM4–64 or 25μM BFA was applied to 5-day-old seedlings in liquid growth media supplemented with. Procedures were the same as Bassil et al. [8]. At least five biological replicates were performed for each experiment.

4.2. Assays for Root Elongation and Root Gravitropism

To assess the effect of auxin on root growth, WT and *nhx1nhx2nhx3nhx4* seedlings were grown on control plates for 5 d and then transferred to a control medium supplemented with different concentrations of IAA, NAA or 2,4-D. Root length was measured 6 or 7 d after transfer. The percentage of root elongation is measured as described in Yamada et al. [57]. To determine the gravitropic response of the roots, seedlings were grown on corresponding media for six days. Then plates were rotated 90° clockwise. After an additional of 5 d, plates were scanned with an Epson Perfection V370 Photo scanner. Image quantification was performed using ImageJ (https://imagej.nih.gov/ij/).

4.3. Fluorescence Microscopy

Confocal laser scanning microscopy was performed on a Carl Zeiss confocal microscope LSM 710 (Zeiss Axio Observer Z.1) unless indicated otherwise. DII-Venus was excited at 458 nm, PIN1-GFP and PIN2-GFP at 488nm and FM4–64 at 514 nm. Imaging of PIN1-GFP and PIN2-GFP was also performed on a Leica confocal microscope (Leica TCS SP8 STED 3X) using the LightGate function to reduce autofluorescence of intracellular bodies visible in the GFP emission wavelengths in the *nhx1nhx2nhx3nhx4* knockout. LightGate is an adjustable time window that can turn off emission collection during pulsed white light excitation and which reduces background fluorescence. Linear unmixing was performed using the Zen software of the LSM710 Zeiss confocal microscope. Image quantification was performed using ImageJ (https://imagej.nih.gov/ij/).

4.4. IAA Content Measurement

Extraction, purification and measurement of IAA were performed as described in Lu et al. [58] with minor modifications. Briefly, freeze-dried materials were homogenized by TissueLyser (Qiagen), then extracted with methanol containing 1% acetic acid. D2-IAA (Olchemim) was added to the samples prior to methanol extraction. Solid-phase extraction was performed with Oasis HLB cartridge columns. Samples were subjected to liquid chromatography equipped with electrospray ionization tandem mass spectrometry (LC-ESI-MS/MS, Agilent 6410 TripleQuad LC/MS system, Agilent). LC conditions and MS settings are described in Lu et al. [58].

4.5. RNA Extraction and qPCR

Transcription of *PIN1* and *PIN2* was examined for WT and *nhx1nhx2nhx3nhx4* genotypes by qPCR. RNA from the roots, 50 seedlings per sample, was extracted using the Qiagen RNase kit. cDNA was reverse-transcribed with the Qiagen Quanti-tect kit. The *Arabidopsis* TIP41-like gene (GenBank accession No. At4g34270.1) served as the reference gene. qPCR was amplified using the specific primers 5′-GCCAGCTCTTATAGCAAAGTC-3′ (forward) and 5′- GGTCCAACGACAAATCTCATAG-3′ (reverse) for *PIN1* and 5′- CTGGTCTTGGAATG-GCTA-3′ (forward) and 5′- AGGAGATCACCTCGAATA-3′ (reverse) for *PIN2*. qPCR amplification was performed as described by [6] using the $2-\Delta\Delta C_T$ method [59]. The experiment was performed using three biological replicates, with two technical repeats for each. Means ± standard deviations (SD) were calculated for all biological replicates. Means of replicates were subjected to statistical analysis by a Student's t-test ($P \leq 0.05$) using Prism 6.

5. Conclusions

This study provides evidence to link pH and/or K^+ homeostasis to auxin homeostasis. Using a quadruple *nhx1nhx2nhx3nhx4* mutant which lacks vacuolar NHX-type antiport activity that is severely

affected in vacuolar pH and K^+ uptake, we examined auxin related phenotypes and growth responses. Our data suggest that auxin efflux is disrupted. Imaging of the abundance and localization of the auxin efflux carriers PIN1 and PIN2 in the mutant, showed that PM-localized PIN2 abundance, but not PIN1, was drastically reduced and was concomitant with an increase in PIN2 labelled intracellular vesicles. The *nhx1nhx2nhx3nhx4* mutant also showed delayed intracellular trafficking to the vacuole and auxin accumulation in the root tip. Collectively, these results indicate that the vacuolar NHXs are required for proper cellular and tissue auxin homeostasis, likely by affecting the intracellular trafficking and abundance of PIN2 on the plasma membrane.

Supplementary Materials: The following are available online at http://www.mdpi.com/2223-7747/9/10/1311/s1, Figure S1: Root response to gravistimulation of *nhx1nhx2nhx3nhx4* mutant, Figure S2: The expression level of *PIN1* and *PIN2* genes in WT and *nhx1nhx2nhx3nhx4* mutant roots, Figure S3: Alternate method (linear unmixing) used to eliminate the plastid-like bodies in PIN2-GFP/*nhx1nhx2nhx3nhx4*, Figure S4: Subcellular localization of PIN2 in *nhx1nhx2nhx3nhx4* under 1mM K^+ and 30mM K^+.

Author Contributions: Conceptualization, S.Z., E.B. (Eduardo Blumwald) and E.B. (Elias Bassil); methodology, S.Z., E.N., H.T. and E.B. (Elias Bassil); software, S.Z.; validation, S.Z.; formal analysis, S.Z., E.B. (Eduardo Blumwald) and E.B. (Elias Bassil); writing—original draft preparation, S.Z.; writing—review and editing, S.Z., E.N., E.B. (Eduardo Blumwald) and E.B. (Elias Bassil). All authors have read and agreed to the published version of the manuscript.

Funding: This work was supported by startup funds from the University of Florida to E.B. (Elias Bassil) and by grants from the National Science Foundation (MCB-0343279; IOS-0820112) to E.B. (Eduardo Blumwald).

Acknowledgments: The authors are grateful to the ABRC, Jiri Friml for providing seeds and plasmids employed in this research. The authors also appreciate the advice of Dawei Yan (UC Davis) and the technical assistance of Ayako Nambara (University of Toronto) for the IAA measurement. Undergraduate students played important roles in this research (Min-Yi Zhen, Cari Yang and Emily Zhang).

Conflicts of Interest: The authors declare no conflict of interest.

References

1. Blumwald, E.; Rea, P.A.; Poole, R.J. *Preparation of Tonoplast Vesicles: Applications to H+-Coupled Secondary Transport in Plant Vacuoles, In Methods in Enzymology*; Elsevier: Amsterdam, The Netherlands, 1987; pp. 115–123.
2. Orlowski, J.; Grinstein, S. Emerging roles of alkali cation/proton exchangers in organellar homeostasis. *Curr. Opin. Cell Biol.* **2007**, *19*, 483–492. [CrossRef]
3. Martinoia, E.; Maeshima, M.; Neuhaus, H.E. Vacuolar transporters and their essential role in plant metabolism. *J. Exp. Bot.* **2007**, *58*, 83–102. [CrossRef]
4. Amtmann, A.; Leigh, R. Ion homeostasis. In *Abiotic Stress Adaptation in Plants*; Springer: Berlin/Heidelberg, Germany, 2009; pp. 245–262.
5. Bassil, E.; Coku, A.; Blumwald, E. Cellular ion homeostasis: Emerging roles of intracellular NHX Na^+/H^+ antiporters in plant growth and development. *J. Exp. Bot.* **2012**, *63*, 5727–5740. [CrossRef]
6. Bassil, E.; Tajima, H.; Liang, Y.C.; Ohto, M.; Ushijima, K.; Nakano, R.; Esumi, T.; Coku, A.; Belmonte, M.; Blumwald, E. The Arabidopsis Na^+/H^+ Antiporters NHX1 and NHX2 Control Vacuolar pH and K^+ Homeostasis to Regulate Growth, Flower Development, and Reproduction. *Plant Cell* **2011**, *23*, 3482–3497. [CrossRef] [PubMed]
7. McCubbin, T.; Bassil, E.; Zhang, S.; Blumwald, E. Vacuolar Na^+/H^+ NHX-Type Antiporters Are Required for Cellular K^+ Homeostasis, Microtubule Organization and Directional Root Growth. *Plants* **2014**, *3*, 409–426. [CrossRef]
8. Bassil, E.; Ohto, M.A.; Esumi, T.; Tajima, H.; Zhu, Z.; Cagnac, O.; Belmonte, M.; Peleg, Z.; Yamaguchi, T.; Blumwald, E. The Arabidopsis Intracellular Na^+/H^+ Antiporters NHX5 and NHX6 Are Endosome Associated and Necessary for Plant Growth and Development. *Plant Cell* **2011**, *23*, 224–239. [CrossRef]
9. Martinière, A.; Bassil, E.; Jublanc, E.; Alcon, C.; Reguera, M.; Sentenac, H.; Blumwald, E.; Paris, N. In Vivo Intracellular pH Measurements in Tobacco and Arabidopsis Reveal an Unexpected pH Gradient in the Endomembrane System. *Plant Cell* **2013**, *25*, 4028–4043. [CrossRef] [PubMed]
10. Reguera, M.; Bassil, E.; Tajima, H.; Wimmer, M.; Chanoca, A.; Otegui, M.S.; Paris, N.; Blumwald, E. pH Regulation by NHX-Type Antiporters Is Required for Receptor-Mediated Protein Trafficking to the Vacuole in Arabidopsis. *Plant Cell* **2015**, *27*, 1200–1217. [CrossRef] [PubMed]

11. Dragwidge, J.M.; Ford, B.A.; Ashnest, J.R.; Das, P.; Gendall, A.R. Two Endosomal NHX-Type Na^+/H^+ Antiporters are Involved in Auxin-Mediated Development in Arabidopsis thaliana. *Plant Cell Physiol.* **2018**, *59*, 1660–1669. [CrossRef]
12. Wu, X.X.; Ebine, K.; Ueda, T.; Qiu, Q.S. AtNHX5 and AtNHX6 Are Required for the Subcellular Localization of the SNARE Complex That Mediates the Trafficking of Seed Storage Proteins in Arabidopsis. *PLoS ONE* **2016**, *11*, 25. [CrossRef] [PubMed]
13. Shi, H.Z.; Quintero, F.J.; Pardo, J.M.; Zhu, J.K. The putative plasma membrane Na^+/H^+ antiporter SOS1 controls long-distance Na^+ transport in plants. *Plant Cell* **2002**, *14*, 465–477. [CrossRef] [PubMed]
14. An, R.; Chen, Q.J.; Chai, M.F.; Lu, P.L.; Su, Z.; Qin, Z.X.; Chen, J.; Wang, X.C. AtNHX8, a member of the monovalent cation: Proton antiporter-1 family in Arabidopsis thaliana, encodes a putative Li^+/H^+ antiporter. *Plant J.* **2007**, *49*, 718–728. [CrossRef] [PubMed]
15. Barragán, V.; Leidi, E.O.; Andrés, Z.; Rubio, L.; De Luca, A.; Fernández, J.A.; Cubero, B.; Pardo, J.M. Ion Exchangers NHX1 and NHX2 Mediate Active Potassium Uptake into Vacuoles to Regulate Cell Turgor and Stomatal Function in Arabidopsis. *Plant Cell* **2012**, *24*, 1127–1142. [CrossRef]
16. Bassil, E.; Zhang, S.; Gong, H.; Tajima, H.; Blumwald, E. Cation specificity of vacuolar NHX-type cation/H^+ antiporters. *Plant Physiol.* **2019**, *179*, 616–629. [CrossRef] [PubMed]
17. Rigas, S.; Debrosses, G.; Haralampidis, K.; Vicente-Agullo, F.; Feldmann, K.A.; Grabov, A.; Dolan, L.; Hatzopoulos, P. TRH1 encodes a potassium transporter required for tip growth in Arabidopsis root hairs. *Plant Cell* **2001**, *13*, 139–151. [CrossRef]
18. Rigas, S.; Ditengou, F.A.; Ljung, K.; Daras, G.; Tietz, O.; Palme, K.; Hatzopoulos, P. Root gravitropism and root hair development constitute coupled developmental responses regulated by auxin homeostasis in the Arabidopsis root apex. *New Phytol.* **2013**, *197*, 1130–1141. [CrossRef]
19. Elumalai, R.P.; Nagpal, P.; Reed, J.W. A mutation in the Arabidopsis KT2/KUP2 potassium transporter gene affects shoot cell expansion. *Plant Cell* **2002**, *14*, 119–131. [CrossRef]
20. Desbrosses, G.; Josefsson, C.; Rigas, S.; Hatzopoulos, P.; Dolan, L. AKT1 and TRH1 are required during root hair elongation in Arabidopsis. *J. Exp. Bot.* **2003**, *54*, 781–788. [CrossRef]
21. Vicente-Agullo, F.; Rigas, S.; Desbrosses, G.; Dolan, L.; Hatzopoulos, P.; Grabov, A. Potassium carrier TRH1 is required for auxin transport in Arabidopsis roots. *Plant J.* **2004**, *40*, 523–535. [CrossRef]
22. Osakabe, Y.; Arinaga, N.; Umezawa, T.; Katsura, S.; Nagamachi, K.; Tanaka, H.; Ohiraki, H.; Yamada, K.; Seo, S.-U.; Abo, M. Osmotic stress responses and plant growth controlled by potassium transporters in Arabidopsis. *Plant Cell* **2013**, *25*, 609–624. [CrossRef]
23. Daras, G.; Rigas, S.; Tsitsekian, D.; Iacovides, T.A.; Hatzopoulos, P. Potassium transporter TRH1 subunits assemble regulating root-hair elongation autonomously from the cell fate determination pathway. *Plant Sci.* **2015**, *231*, 131–137. [CrossRef] [PubMed]
24. Okada, K.; Ueda, J.; Komaki, M.K.; Bell, C.J.; Shimura, Y. Requirement of the auxin polar transport system in early stages of Arabidopsis floral bud formation. *Plant Cell* **1991**, *3*, 677–684. [CrossRef] [PubMed]
25. Rashotte, A.M.; Poupart, J.; Waddell, C.S.; Muday, G.K. Transport of the two natural auxins, indole-3-butyric acid and indole-3-acetic acid, in Arabidopsis. *Plant Physiol.* **2003**, *133*, 761–772. [CrossRef] [PubMed]
26. Mitchell, E.; Davies, P. Evidence for three different systems of movement of indoleacetic acid in intact roots of Phaseolus coccineus. *Physiol. Plant.* **1975**, *33*, 290–294. [CrossRef]
27. Tsurumi, S.; Ohwaki, Y. Transport of 14C-lableled indoleacetic acid in Vicia root segments. *Plant Cell Physiol.* **1978**, *19*, 1195–1206. [CrossRef]
28. Rashotte, A.M.; Brady, S.R.; Reed, R.C.; Ante, S.J.; Muday, G.K. Basipetal auxin transport is required for gravitropism in roots of Arabidopsis. *Plant Physiol.* **2000**, *122*, 481–490. [CrossRef]
29. Křeček, P.; Skůpa, P.; Libus, J.; Naramoto, S.; Tejos, R.; Friml, J.; Zažímalová, E. The PIN-FORMED (PIN) protein family of auxin transporters. *Genome Biol.* **2009**, *10*, 249. [CrossRef]
30. Adamowski, M.; Friml, J. PIN-Dependent Auxin Transport: Action, Regulation, and Evolution. *Plant Cell* **2015**, *27*, 20–32. [CrossRef]
31. Zazímalová, E.; Murphy, A.S.; Yang, H.; Hoyerová, K.; Hosek, P. Auxin transporters—Why so many? *Cold Spring Harb. Perspect. Biol.* **2010**, *2*, a001552. [CrossRef]
32. Bartlett, M.E.; Thompson, B. Meristem identity and phyllotaxis in inflorescence development. *Front. Plant Sci.* **2014**, *5*, 5. [CrossRef]

33. Delbarre, A.; Muller, P.; Imhoff, V.; Guern, J. Comparison of mechanisms controlling uptake and accumulation of 2,4-dichlorophenoxy acetic acid, naphthalene-1-acetic acid, and indole-3-acetic acid in suspension-cultured tobacco cells. *Planta* **1996**, *198*, 532–541. [CrossRef]
34. Marchant, A.; Kargul, J.; May, S.T.; Muller, P.; Delbarre, A.; Perrot-Rechenmann, C.; Bennett, M.J. AUX1 regulates root gravitropism in Arabidopsis by facilitating auxin uptake within root apical tissues. *EMBO J.* **1999**, *18*, 2066–2073. [CrossRef]
35. Chen, R.J.; Hilson, P.; Sedbrook, J.; Rosen, E.; Caspar, T.; Masson, P.H. The Arabidopsis thaliana AGRAVITROPIC 1 gene encodes a component of the polar-auxin-transport efflux carrier. *Proc. Natl. Acad. Sci. USA* **1998**, *95*, 15112–15117. [CrossRef] [PubMed]
36. Muller, A.; Guan, C.H.; Galweiler, L.; Tanzler, P.; Huijser, P.; Marchant, A.; Parry, G.; Bennett, M.; Wisman, E.; Palme, K. AtPIN2 defines a locus of Arabidopsis for root gravitropism control. *EMBO J.* **1998**, *17*, 6903–6911. [CrossRef] [PubMed]
37. Luschnig, C.; Gaxiola, R.A.; Grisafi, P.; Fink, G.R. EIR1, a root-specific protein involved in auxin transport, is required for gravitropism in Arabidopsis thaliana. *Genes Dev.* **1998**, *12*, 2175–2187. [CrossRef] [PubMed]
38. Abas, L.; Benjamins, R.; Malenica, N.; Paciorek, T.; Wirniewska, J.; Moulinier-Anzola, J.C.; Sieberer, T.; Friml, J.; Luschnig, C. Intracellular trafficking and proteolysis of the Arabidopsis auxin-efflux facilitator PIN2 are involved in root gravitropism. *Nat. Cell Biol.* **2006**, *8*, 249–256. [CrossRef] [PubMed]
39. Kleine-Vehn, J.; Leitner, J.; Zwiewka, M.; Sauer, M.; Abas, L.; Luschnig, C.; Friml, J. Differential degradation of PIN2 auxin efflux carrier by retromer-dependent vacuolar targeting. *Proc. Natl. Acad. Sci. USA* **2008**, *105*, 17812–17817. [CrossRef]
40. Dettmer, J.; Hong-Hermesdorf, A.; Stierhof, Y.D.; Schumacher, K. Vacuolar H^+-ATPase activity is required for Endocytic and secretory trafficking in Arabidopsis. *Plant Cell* **2006**, *18*, 715–730. [CrossRef]
41. Bolte, S.; Talbot, C.; Boutte, Y.; Catrice, O.; Read, N.D.; Satiat-Jeunemaitre, B. FM-dyes as experimental probes for dissecting vesicle trafficking in living plant cells. *J. Microsc.* **2004**, *214*, 159–173. [CrossRef]
42. Kleine-Vehn, J.; Langowski, L.; Wisniewska, J.; Dhonukshe, P.; Brewer, P.B.; Friml, J. Cellular and Molecular Requirements for Polar PIN Targeting and Transcytosis in Plants. *Mol. Plant* **2008**, *1*, 1056–1066. [CrossRef]
43. Brunoud, G.; Wells, D.M.; Oliva, M.; Larrieu, A.; Mirabet, V.; Burrow, A.H.; Beeckman, T.; Kepinski, S.; Traas, J.; Bennett, M.J.; et al. A novel sensor to map auxin response and distribution at high spatio-temporal resolution. *Nature* **2012**, *482*, 103. [CrossRef] [PubMed]
44. Remy, E.; Baster, P.; Friml, J.; Duque, P. ZIFL1.1 transporter modulates polar auxin transport by stabilizing membrane abundance of multiple PINs inArabidopsisroot tip. *Plant Signal. Behav.* **2013**, *8*, e25688. [CrossRef] [PubMed]
45. Remy, E.; Cabrito, T.R.; Baster, P.; Batista, R.A.; Teixeira, M.C.; Friml, J.; Sá-Correia, I.; Duque, P. A major facilitator superfamily transporter plays a dual role in polar auxin transport and drought stress tolerance in Arabidopsis. *Plant Cell* **2013**, *25*, 901–926. [CrossRef] [PubMed]
46. Fan, L. Na^+, K^+/H^+ antiporters regulate the pH of endoplasmic reticulum and auxin-mediated development. *Plant Cell Environ.* **2018**, *41*, 850–864. [CrossRef]
47. Yang, T.; Zhao, L.; Hu, H.; Li, W.; Novák, O.; Strnad, M.; Simon, S.; Friml, J.; Shen, J.; Jiang, L.; et al. The Potassium Transporter OsHAK5 Alters Rice Architecture via ATP-Dependent Transmembrane Auxin Fluxes. *Plant Commun.* **2020**, *1*, 100052. [CrossRef]
48. Geldner, N.; Friml, J.; Stierhof, Y.-D.; Jürgens, G.; Palme, K. Auxin transport inhibitors block PIN1 cycling and vesicle trafficking. *Nature* **2001**, *413*, 425–428. [CrossRef]
49. Dhonukshe, P.; Aniento, F.; Hwang, I.; Robinson, D.G.; Mravec, J.; Stierhof, Y.-D.; Friml, J. Clathrin-mediated constitutive endocytosis of PIN auxin efflux carriers in Arabidopsis. *Current Biol.* **2007**, *17*, 520–527. [CrossRef]
50. Kleine-Vehn, J.; Dhonukshe, P.; Sauer, M.; Brewer, P.B.; Wiśniewska, J.; Paciorek, T.; Benková, E.; Friml, J. ARF GEF-dependent transcytosis and polar delivery of PIN auxin carriers in Arabidopsis. *Current Biol.* **2008**, *18*, 526–531. [CrossRef]
51. Li, K.; Kamiya, T.; Fujiwara, T. Differential Roles of PIN1 and PIN2 in Root Meristem Maintenance Under Low-B Conditions in Arabidopsis thaliana. *Plant Cell Physiol.* **2015**, *56*, 1205–1214. [CrossRef]
52. Birnbaum, K.; Shasha, D.E.; Wang, J.Y.; Jung, J.W.; Lambert, G.M.; Galbraith, D.W.; Benfey, P.N. A Gene Expression Map of the *Arabidopsis* Root. *Science* **2003**, *302*, 1956. [CrossRef]

53. Nawy, T.; Lee, J.-Y.; Colinas, J.; Wang, J.Y.; Thongrod, S.C.; Malamy, J.E.; Birnbaum, K.; Benfey, P.N. Transcriptional Profile of the Arabidopsis Root Quiescent Center. *Plant Cell* **2005**, *17*, 1908. [CrossRef] [PubMed]
54. Benkova, E.; Michniewicz, M.; Sauer, M.; Teichmann, T.; Seifertova, D.; Jurgens, G.; Friml, J. Local, efflux-dependent auxin gradients as a common module for plant organ formation. *Cell* **2003**, *115*, 591–602. [CrossRef]
55. Clough, S.J.; Bent, A.F. Floral dip: A simplified method for Agrobacterium-mediated transformation of Arabidopsis thaliana. *Plant J.* **1998**, *16*, 735–743. [CrossRef] [PubMed]
56. Spalding, E.P.; Hirsch, R.E.; Lewis, D.R.; Qi, Z.; Sussman, M.R.; Lewis, B.D. Potassium uptake supporting plant growth in the absence of AKT1 channel activity—Inhibition by ammonium and stimulation by sodium. *J. Gen. Physiol.* **1999**, *113*, 909–918. [CrossRef] [PubMed]
57. Yamada, M.; Greenham, K.; Prigge, M.J.; Jensen, P.J.; Estelle, M. The TRANSPORT INHIBITOR RESPONSE2 Gene Is Required for Auxin Synthesis and Diverse Aspects of Plant Development. *Plant Physiol.* **2009**, *151*, 168. [CrossRef] [PubMed]
58. Lu, G.; Coneva, V.; Casaretto, J.A.; Ying, S.; Mahmood, K.; Liu, F.; Nambara, E.; Bi, Y.M.; Rothstein, S.J. OsPIN5b modulates rice (Oryza sativa) plant architecture and yield by changing auxin homeostasis, transport and distribution. *Plant J.* **2015**, *83*, 913–925. [CrossRef] [PubMed]
59. Schmittgen, T.D.; Livak, K.J. Analyzing real-time PCR data by the comparative CT method. *Nat. Protoc.* **2008**, *3*, 1101. [CrossRef]

plants

MDPI

Review

A Quest for Mechanisms of Plant Root Exudation Brings New Results and Models, 300 Years after Hales

Vadim Volkov [1,2,*,†] and Heiner Schwenke [3,*,†]

[1] Department of Plant Sciences, College of Agricultural and Environmental Sciences, University of California, Davis, CA 95616, USA
[2] K.A. Timiriazev Institute of Plant Physiology RAS, 35 Botanicheskaya St., Moscow 127276, Russia
[3] Max Planck Institute for the History of Science, Boltzmannstraße 22, 14195 Berlin, Germany
* Correspondence: vadim.s.volkov@gmail.com (V.V.); heiner.schwenke@gmail.com (H.S.)
† Both Authors contributed equally to the text.

Abstract: The review summarizes some of our current knowledge on the phenomenon of exudation from the cut surface of detached roots with emphasis on results that were mostly established over the last fifty years. The phenomenon is quantitatively documented in the 18th century (by Hales in 1727). By the 19th century, theories mainly ascribed exudation to the secretion of living root cells. The 20th century favored the osmometer model of root exudation. Nevertheless, growing insights into the mechanisms of water transport and new or rediscovered observations stimulated the quest for a more adequate exudation model. The historical overview shows how understanding of exudation changed with time following experimental opportunities and novel ideas from different areas of knowledge. Later theories included cytoskeleton-dependent micro-pulsations of turgor in root cells to explain the observed water exudation. Recent progress in experimental biomedicine led to detailed study of channels and transporters for ion transport via cellular membranes and to the discovery of aquaporins. These universal molecular entities have been incorporated to the more complex models of water transport via plant roots. A new set of ideas and explanations was based on cellular osmoregulation by mechanosensitive ion channels. Thermodynamic calculations predicted the possibility of water transport against osmotic forces based on co-transport of water with ions via cation-chloride cotransporters. Recent observations of rhizodermis exudation, exudation of roots without an external aqueous medium, segments cut from roots, pulses of exudation, a phase shifting of water uptake and exudation, and of effects of physiologically active compounds (like ion channel blockers, metabolic agents, and cytoskeletal agents) will likely refine our understanding of the phenomenon. So far, it seems that more than one mechanism is responsible for root pressure and root exudation, processes which are important for refilling of embolized xylem vessels. However, recent advances in ion and water transport research at the molecular level suggest potential future directions to understanding of root exudation and new models awaiting experimental testing.

Keywords: root pressure; exudation; xylem embolism; mechanosensitive ion channels; ion transporters; aquaporins; water transport

Citation: Volkov, V.; Schwenke, H. A Quest for Mechanisms of Plant Root Exudation Brings New Results and Models, 300 Years after Hales. *Plants* **2021**, *10*, 38. https://dx.doi.org/10.3390/plants10010038

Received: 16 November 2020
Accepted: 21 December 2020
Published: 25 December 2020

1. Introduction

Roots of many plant species show extrusion of liquid from their cut surface, typically when located in wet soil or submerged in distilled water or a solution. The observation of root exudation goes at least back to Theophrastus (*Historia plantarum* 9,1,6). Albertus Magnus tried to explain it by a *spiritus pulsatilis* (*De vegetabilibus* 2,1,3; see also 6,1,15). About 300 years ago, Hales seems to be the first who did quantitative measurements of the pressure that arises from exudation [1]. He attached mercury manometers to cut roots and branches of typically 3–5-year-old grapevines (Figure 1). Hales found that the observed pressure developing by the extruded sap was around 0.1 MPa (1 bar or approximately 10 m of water column) in spring months for leafless plants. Results on the prevalence of

root exudation vary. Clark, for example, reported in 1874 that he tested "more than sixty species of trees and shrubs . . . , by boring a three-quarter inch hole usually to the depth of two inches into the sap-wood near the earth", and apparently found that only a minority "showed any tendency to bleed" ([2], pp. 26–27). Recently, a study of tropical vines and woody plants found that only 61 of 109 species exhibited predawn root exudation from shoots or lateral branches [3]. On the contrary, 19th century researcher Kraus, who focused on the youngest parts of the roots, observed root exudation in all of the almost hundred herbaceous and seventeen woody species he examined: among them were seven coniferous species [4]. He therefore considered it highly probable that all younger root parts can exude from cross sections. In 1893, Wieler who listed 188 species from 65 families showing exudation after cutting all or a part of the epigeal parts, came to a similar conclusion [5]. However, it obviously depends very much on the method and the physiological status of the root, whether exudation can be observed or not. For example, in conifers, root exudation could be stimulated by long-term cold storage [6], while earlier any exudation was rarely observed in situ for whole conifer root stocks [7].

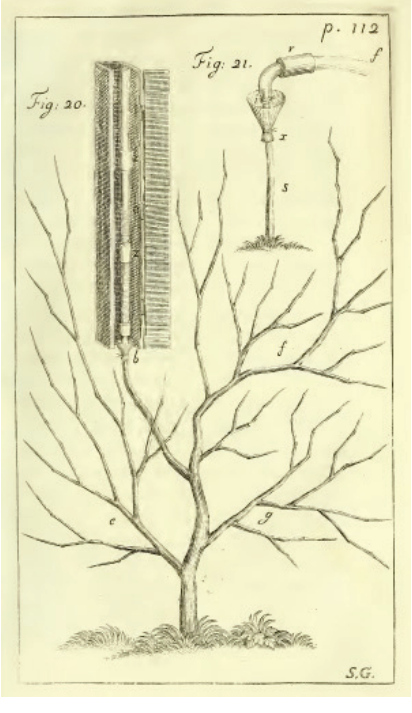

Figure 1. A sketch illustrating experiments done by Hales before 1727 [1] where mercury manometers were tightly connected to the cut branches of leafless grapevines to measure the pressure of the sap extruded by roots (reproduced from [1] with the permission based on https://library.si.edu/digital-library/book/vegetablestatick00hale).

Most experiments on root exudation and root pressure were conducted with herbaceous plants (tomato, maize, cotton, castor beans, kidney beans, sunflower, barley, onion etc.), which are often simpler for experimental procedures and faster to grow than woody species (a short non-comprehensive representative list of references (mostly arranged by years) includes: [8–37].

2. Root Pressure and the Ascent of Sap

Although many investigations only determined root pressures in the range from slightly above zero to 1.5 bar (see [5], p. 112, for various woody and herbaceous species; [18]: 1.2–1.4 bars for maize; [38]: 0.5–1.5 bars for oak; [3]: 0.02 to 1.48 bars for 61 tropical vines and woody species; and [39]: 0.01–0.08 bars as estimates for two submerged aquatic angiosperms, *Lobelia dortmanna* and *Sparganium emersum*), higher pressures have been occasionally reported. Wieler measured more than 1.8 bar in *Betula alba* ([5], p. 123) and Clark 2.5 bar in *Betula lenta* ([2], p. 33). Values from 1.3 to 4.0 bars were registered for barley roots [37]. For detached roots of *Zea mays*, [17] reported root pressure values around four bars. The maximal measured and reported values of root pressure were above six bars for tomato roots [8,9].

Such values suggest that water might be raised to heights below 10–40 m. However, simple comparison with water potentials (Ψ_w) driving transpiration under low humidity shows that root pressure is relatively low: change in air humidity from 100% to 99% results in decrease of Ψ_w by 1.38 MPa ($R \times T/V \times 0.99$, about 13.8 bars) where R is the universal gas constant equal to 8.31 J/(K × mole), T is temperature in K, V is the partial molar volume of water equal to 18 cm^3. Hence, the root pressure might be important under low transpiration for leafless non-transpiring plants or in a highly saturated humidity.

The importance of root pressure and exudation can be considered from an integrative point of view when the water flow transfers ions, metabolites, and physiologically active compounds linking all parts of the plants. Root pressure unites the parts of a multicellular organism when large transport fluxes are carried by directed water fluxes. This revives the idea of circulatory system of plants which was—apparently independently—developed between 1665–1668 by Johann Daniel Major, Christopher Merret, Claude Persault, and Edme Mariotte ([40], p. 1); for recent proponents see [25,41,42] and references therein). From the more common point of view, root pressure is important for refilling the cavitated/embolized xylem vessels in the spring time and under low transpiration (e.g., [43]).

Embolism of xylem vessels (filling with air with consequent loss of conductivity for xylem sap) occurs under water stress, winter freezing, or sometimes after attacks of pathogens [43,44]. The process may result in wilting and further death of plants: if all the conductive elements are embolized then water cannot be transported to shoots. Hence, root pressure is important for refilling the xylem vessels for small trees and vines. For wild grapevines over winter, the xylem vessels are filled with air with usually no sap inside; in spring before the leaf expansion the root pressure in some of the vines reaches up to five bars filling the xylem vessels [43]. Measurements for 15 vines in spring registered root pressure up to twofold above the required pressure based on the height of the vines (up to 30 m); for transpiring vines in summer the root pressure was quite low if any. The experiments also revealed that the water path might be more complex in vines with (partially) embolized xylem and, interestingly, higher root pressure corresponded to taller vines [43]. Refilling of xylem by root pressure in grapevines requires either dry pit structures between vessels with expulsion of air or more complex mechanisms [44,45] when air is dissolved within individual vessels separated by hydrated pit fields. Evidently, this is applicable to other plants. The pit structures/membranes connecting xylem vessels have narrow pores of submicrometer to-nanometer range, e.g., with maximal diameters of 39 nm in *Vitis vinifera* and 225 nm in *Betula pendula*: [46] (reviewed in: [47]).

Wet pit membranes seal individual xylem vessels with pressures typically over 1.5–3 MPa (15–30 bars) in accordance with the simplified Young–Laplace equation:

$$\Delta P = 2\,\gamma / r \quad (1)$$

where ΔP is access pressure formed, γ is surface tension of water (about 72 mN/m with slight dependence on temperature), and r is the radius of the pore. A new tensiometer with a nanoporous membrane obeying the Young–Laplace equation was designed recently [48] and is being used in trials to determine stem water potential in grapevines, apple trees, almond [49]; it cavitates below −100 bars. The same equation can be applied to the air in

wet embolized xylem vessels. The air is pressurized by thin water film adjoining the surface of the vessels, the extra pressure for xylem vessel with diameter 10 μm is about 0.3 bars (30 kPa). Hence, to dissolve the air in the xylem vessel with radius r an extra pressure over $2\gamma/r$ is required. It is produced mostly by root pressure in grapevines [43,45], maize [50], many tropical plants [3], 53 of 53 studied bamboo species [51]. When root pressure is not generated or not sufficient for xylem refilling, the more complicated mechanisms of xylem refilling at the expenses of water and ion transport of xylem parenchyma cells are involved [52–55]; the mechanisms of which are not discussed here in detail, although their nature could be similar to that of water transport in roots (see about osmotic and nonosmotic components of root pressure below). Obviously, the mechanisms may operate for refilling the xylem conduits in tall trees such as sequoia (when possible) where the gravitational part of water potential Ψ_w exceeds -1 MPa (-10 bars), even leading to symptoms of water deficit for high leaves [56].

One more expression of root pressure is guttation or release of water by plants from their leaves, often via specialised structures named hydathodes. Guttation occurs less frequently than root pressure and exudation: for 109 tropical vines and woody plants, 61 of 109 species exhibited predawn exudation while predawn guttation was recorded for only 15 [3]; guttation was reported for 8 of 53 bamboo species with detected root pressure [51]. Moreover, guttation did not always correspond to high root pressure. Species with maximal root pressure from 0.16 to 1.2 bars had guttation; root pressure for the set of measured species varied from 0.02 to 1.5 bars [3]. For guttating bamboo species, the osmotic pressures of the extruded liquid were often over 10 times higher than the recorded by manometer root pressures; the researchers suggested low reflection coefficients (see below) for the coupling of water and ion fluxes [51]. More details about guttation and its implications for the life of plants are reviewed in [57–59] with extensive description and references therein).

3. Origin of Exudate

Rowan, McCully, and Canny [35] investigated the origin of the root exudate on cut surfaces of detached maize roots, root segments and cortical sleeves by means of optical microscopy and cryomicroscopy. After preparation of a specimen, they waited until a dome of exudate had formed on the cut surface, blotted it and observed the appearance of further fluid over the various types of tissue during the seconds following the blotting. They found that the exudate from the cut surface came from all cell types. It appeared from the cortex, epidermis, and hypodermis first, and only later from the xylem vessels, pith parenchyma, and aerenchyma spaces [35]. These results confirmed and added to a number of early investigations that were carried out by means of a hand lens by Dutrochet ([60], p. 13; [61], p. 369), Rominger [62], Brücke [63], Kraus [64], and James and Baker [65]. By far the most comprehensive study of this kind was carried out by Kraus ([64]; see for his method [4], pp. 19–20). After studying numerous herbaceous and woody plants, he concluded that the exudate originated from living cells of various types of tissue ([64], pp. 2–9, 31). James and Baker, who examined the exudation of sycamore roots and stems with a hand lens on cut surfaces and also with live stains, found that the primary source of exudate was living tissue and not the vessels, opposite to most earlier observations with other plants [65].

However, xylem elements are definitely the main pathway for ascending water flow in plants as confirmed by magnetic resonance imaging (MRI) experiments for 6-d-old castor bean seedlings (*Ricinus communis*) [66]. The measured rate of flow in xylem of intact plants under low transpiration was similar to exudation rates measured for detached roots of castor bean seedlings of the same age [67]. MRI experiments also demonstrated large recirculation of water between xylem and phloem and similar flow rates (Stokes flow with rates around 2 m/h) for the two specialised tissues while larger cross-section xylem area ensured higher total fluxes in the xylem [66]. MRI experiments demonstrated higher xylem flow under transpiration with precise spatial resolution of individual large vessels and refilling of cavitated xylem vessels in cucumber [68]. The results of MRI for plant

water transport in xylem and phloem are widely reviewed (see, e.g., [69,70] and references therein). So, the large water exudation flows via detached roots, such as 11,260 mm^3 exudation fluid from a decapitated *Urtica urens* (annual nettle) over 2.5 days, although the volume of the root was only 1450 mm^3 [71], are to be via specialised water-conducting xylem tissues with high hydraulic conductivity.

Another approach to determine the origin of the exudate was to analyze its chemical composition. According to pH, ion composition, contents of amino acids and soluble sugars, the exudate of detached roots of maize seedling comes mainly from the xylem, not from the phloem (Table 1, based on calculations of osmotic pressure, see the next chapter, ions and amino acids make up 90% of osmotic pressure of this exudate with sugars below 5%) [23,24]. Amino acid analysis demonstrated that Asn and Gln were the main free amino acids of exudate making up to 40% of all free amino acids; these were followed by Val and Ser (20% more) [24]. Phloem exudates are more alkaline (pH over 7.2–7.5) with much higher osmotic pressure (over 8 bars) and different chemical composition [72–74] and references therein.

Table 1. Osmotic pressure (II_i), pH values, concentrations of K^+, Ca^{2+}, Cl^- (mM), free amino acids (mM), sugars (μg/0.1 mL) in exudate from detached roots of *Zea mays* L. seedlings.

	II_i, MPa	K^+	Ca^{2+}	Cl^-	Amino Acids	Sucrose	Fructose	pH
Exudation from detached roots	0.13 ± 0.03	17.2 ± 2.9	2.4 ± 0.8	18.7 ± 3.2	7.8 ± 3.5	6 ± 1	29 ± 11	5.2 ± 0.2

Data are given as means ± SD. Exudate was collected and united for thirty-sixty detached roots (apical 5 cm of roots of 5–7 days old seedlings) after 1 h of exudation at 30 °C and frozen if stored before analyses. Based on the results from [23,24].

A xylem origin of exudate was evident in other experiments with maize [17], castor beans [75], tomato [76], tobacco [77], poplar [78], kiwifruit vines [79], grapevines [80,81], and even in the much earlier experiments with maize and *Impatiens balsamina* [82]. Similar results were obtained for conifers [83]. (However, chemical composition of exudates exhibited certain variability depending on the time of the day and even the month of exudate collection for field-grown plants [76,78,80].)

4. Initial Concepts and Further Models for Understanding Mechanisms of Root Pressure and Exudation

Hales explained the rising of the sap in the plants with the "strong attraction of the capillary sap vessels [...] assisted by the brisk undulations and vibrations, caused by the sun's warmth" ([1], p.136). After Nollet discovered osmosis in 1748 [84], it took almost eighty years before Dutrochet attempted to explain root exudation in osmotic terms [60]. Like Hofmeister and Sachs later on, he saw the main cause of this phenomenon in the water expulsion from turgescent root cells ([60], p. 162; [85], p. 175; [86], p. 204). Pressure secretion from living cells was the leading exudation concept of the 19th century (see [5] for the most comprehensive overview of 19th century exudation research). However, only Pfeffer was able to develop physically correct models of root exudation. He built the first functioning osmometer, the so-called Pfeffer's cell [87]. Based on his measurements, van't Hoff formulated the law named after him [88], which is in its simplest version

$$\pi = c \times R \times T \quad (2)$$

where π is the osmotic pressure, c is the concentration of the solutes, R is the universal gas constant (8.31 J/(K × mole)), and T is the temperature in Kelvin. Rough estimates show that 40 mM of solute which does not dissociate (or 20 mM for completely dissociating salt XY producing monovalent ions X^+ and Y^- etc.) make up 1 bar (about 0.1 MPa) of osmotic pressure.

Pfeffer basically considered two variants of exudation by pressure secretion. According to the first, the permeability of plasma membrane to dissolved substances would be different on opposite sides of a cell. Today, we would say that the reflection coefficient of the

plasma membrane varies at different sides of the cell. This would allow the cell to absorb water on one side while releasing it from another. The second model employs an intracellular gradient of solutes. Thus, a pressure secretion of water on the side of the lower osmotic pressure can be achieved. Pfeffer also considered what he called passive or plasmolytic secretion. In this case, the water is sucked from the cell by dissolved substances outside the plasma membrane. This would be the basic idea of the osmometer model of root exudation, which became popular later. Pfeffer considers this mechanism suitable for exudation from nectaries, but not the main cause of root exudation. He found the exudate often lacking significant amounts of dissolved substances and stated that exudation pressure was not correlated with the osmotic concentration of the exudate. Moreover, his co-worker Wieler could not obtain any exudation in inactive plants when he filled the glass tube, which was attached to decapitated stumps, with 0.1–1 percent solution of potassium nitrate. In any case, Pfeffer regarded exudation as a consequence of energy-consuming activity of living cells, referring to experiments by Wieler on the effect of chloroform and oxygen deprivation on exudation ([5]; [87], pp. 224–234; [89], pp. 299–319; [90], pp. 265–267; [91], pp. 234–268).

Since the publications of Atkins [92], Priestley [93] and Sabinin [82] the osmometer model of root exudation has been increasingly favored. The driving force for root exudation is assigned exclusively to the difference in osmotic pressure between the xylem and the external medium, although studies from the 19th century had already shown that this explanation does not fit the data well. Nevertheless, the osmometer model became the leading exudation model in the 20th century (see, e.g., [94,95]). Its main appeal may have been that it offered a simple mathematical formula for the driving force behind root exudation.

Further development of exudation studies in the 20th century productively absorbed Onsager's framework of irreversible processes (reviewed in: [96] and the references therein). Instead of the earlier simple Equation (2), Kedem and Katchalsky applied Onsager's theorems on linear irreversible thermodymanics from membrane processes [97] to fluxes of ions and water via membranes [98–100]. The approach introduced equations for water (for living systems or solvent in general) and ion/solute fluxes with several additional coefficients:

$$J_w = -L_p \times (\Delta P - \sigma \times \Delta C_s \times R \times T) \quad (3)$$

$$J_s = -\omega \times \Delta C_s + (1 - \sigma) \times C_s \times J_w \quad (4)$$

where J_w is water (or solvent) flux across the membrane, L_p is hydraulic conductivity of membrane, ΔP corresponds to difference of hydrostatic pressures across the membrane, the second term of (3) corresponds to difference of osmotic pressures across the membrane multiplied by the reflection coefficient σ J_s is solute flux, ω is solute permeability, and C_s is similar to averaged solute concentration for compartments (more precise definitions of the parameters require more complex explanation and could be found in the cited papers). The equations were swiftly and productively applied to plant water relations (commencing from Dainty [101]) and then to models of root exudation (Figure 2; Table 2). For water fluxes, the reflection coefficient σ varies from 0 to 1 and determines how osmotic forces are translated into the driving forces for water transport. The reflection coefficient σ is a measure of leakiness of biomembranes for solutes (σ equals 1 for a membrane completely non-permeable for solutes).

We briefly describe the models of root exudation (Figure 2; Table 2) which are mainly based on an osmotic explanation of exudation alone, starting from the earlier one membrane models with two compartments (with all the root tissues assumed as one membrane between compartments of external medium and root xylem) to more complicated two membrane models with three compartments (compartments of external medium—root tissues—xylem, each has specific ion concentrations and similar or different reflection coefficients for fluxes between external medium—root tissues, root tissues—xylem).

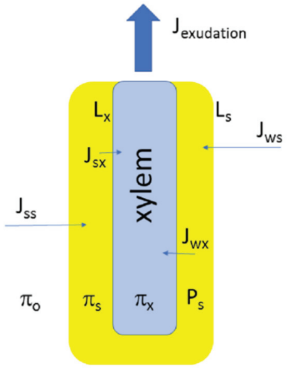

Figure 2. Basic scheme of root often considered for modelling exudation flow $J_{exudation}$. L_s and L_x are hydraulic conductivities of symplast and at the boundary symplast-xylem, correspondingly. The fluxes of solutes (mainly ions) are symbolized by s (J_{ss}, J_{sx}), the flow of water by w (J_{ws}, J_{wx}), the second subscript (s or x) indicates the layer (s for symplast) or boundary (x for symplast-xylem, correspondingly). The outer osmotic pressure is taken as π_o, the osmotic pressure of xylem is π_x. More complex models add osmotic π_s and turgor P_s pressures of symplast; then specific reflection coefficients σ are introduced for the models for different compartments which show the coupling between water and ion fluxes. The relations between water J_w and solute J_s fluxes are based on Equations (3) and (4) of linear irreversible thermodynamics. The sketch is a generalized scheme since each model usually has numerous specific features.

Models of root exudation with a simple osmotic explanation and one important membrane stem from Atkins [92], Priestley [93], and Sabinin [82], followed later by, for example, Eaton [94]. Calculations (where provided) from the investigators demonstrated a linear relation between exudation rate and external osmotic pressure (or even between exudation rate and the difference of exudate and external osmotic pressures) confirmed in experiments. Further approach from linear thermodynamics added the reflection coefficient σ and more complexity. The simple osmometer models of exudation could be partially amended (when failing to explain new experiments, e.g., by van Overbeek [102] etc.) by using variable reflection coefficients and variable hydraulic conductivities for the membranes involved. However, more complex models gained more attention and looked promising (see below). Again, the models mostly operated at the level of a whole root, averaging tissues, and summing up their properties with several membranes having specific reflection coefficients and determined hydraulic conductivities with associated water and solute fluxes. The membranes and compartments are defined with the parameters of fluxes, reflection coefficients and also turgor pressure of cells (for root symplast) (Figure 2; Table 2). These models of exudations include that of (1) Anderson, Aikman and Meiri [103] who proposed a concentration gradient within the vessel lumens; (2) Ginsburg [104] for iso-osmotic flow; (3) Katou, Taura and Furumoto [105] with standing gradient flow; (4) Lyalin [106] with a reverse-osmosis model and (5) the recent model of Pickard [36,107], precisely describing numerous introduced parameters for water and ion transport via roots. Most models and their limitations are well reviewed in [22] (where another classification of the models is introduced): the models can explain potential exudation against reverse osmotic gradients but still many aspects of root exudation are not predicted by the models. For example, the predicted standing gradient of osmotic pressure in xylem vessels [103] was not revealed for maize roots [108]. In contrast to the predictions of the osmometer models, osmotic pressure in the same xylem vessels was relatively stable under changing osmotic pressure of external solution while osmoregulation occurred in the vacuoles of the living root cells [109]. Exudation of roots exhibited sharp pulses within tens of seconds, responded to a wide set of selective inhibitors and metabolic regulators (see below).

Table 2. Main types of quantitative models for describing the phenomenon of root exudation ×.

Type of Model, Main Feature	Short Description	Principle	Proponents, References
Macroscopic	Simple osmotic idea that exudation is caused purely by difference of osmotic pressures between xylem sap and external medium; exudation rate is linearly proportional to this difference	osmotic	Atkins [92], Priestley [93], Sabinin [82], Eaton [94] and others
Macroscopic	Concentration gradient within the vessel lumens drives water flow and exudation	osmotic, standing gradient flow	Anderson, Aikman and Meiri [103]
Macroscopic	Iso-osmotic flow is realized due to different parameters and reflection coefficients for membranes located in a row	osmotic, iso-osmotic flow	Ginsburg [104]
Macroscopic	Concentration gradient exists within the cell walls inside the root stele; water follows osmotic forces which are caused by solute transport, potentially at the expenses of energy for ion fluxes	osmotic, standing gradient flow	Katou, Taura and Furumoto [105]
Macroscopic	High turgor pressure in the root symplast allows reverse osmosis and nonlinear dependence between exudation rate and difference in osmotic pressures between exudate and external medium	reverse osmosis at the level of whole root symplast	Lyalin [106]
Macroscopic	Detailed model with over tens of coefficients, microscopic coefficients are based on structure of plasmalemma and applied to averaged membrane interface between symplast and xylem; assumes active ion fluxes	models osmotic effects with reference to the microscopic level without irreversible thermodynamics	Pickard [36,107]
Subcellular	Reverse osmosis is realized in each plasmodesma of root endodermal cells; turgor oscillations within the cells at 1 Hz frequency result in pumping of water to the root xylem, produce uphill water flux and exudation; energy is pumped into the system via mechanic constrictions and cytoskeleton	reverse osmosis at cellular and subcellular levels	Kundt, Robnik [110,111]
Molecular	The first known model introducing specific ion channels to water transport; alterations in reflection coefficient due to mechanosensitive ion channels explain oscillations in exudation; combination with reverse osmosis may explain visible non-osmotic effects	alterations in reflection coefficient between root compartments with potential implications of reverse osmosis	Schwenke [21], Schwenke, Wagner [22]
Molecular	Model of active water transport based on water cotransport with cation-chloride cotransporters, transferred to plants from animal physiology; suggests the mechanism of water transport to xylem vessels; applicable to root exudation	energetically uphill water transport due to water molecules cotransport with cation-chloride cotransporters	Wegner [112–114]; Fricke [115]

× Due to the large number of models, the Authors are not able to include all of them here; more models and details are given in [22]. Moreover, many models do not provide exact quantitative description, so it is difficult to classify them within the frames we have used.

Here we pay more attention to the recent models that provide links to the cellular details of root structure and to molecular entities for ion and water transport. Over the last decades models of exudation and description of water fluxes in plants gained a lot from molecular studies when ions channels, transporters and specialised proteins, aquaporins for facilitated water flow, were discovered. The model with periodically changing reflection coefficients [21,22] was the first (in our knowledge) where macroscopic properties were linked to the known molecular dynamics of individual mechanosensitive ion channels. Our knowledge of mechanosensitive ion channels of plants is still insufficient (see below) to identify individual ion channels to confirm or amend the model.

The other ion transporting proteins suggested to participate in root water transport are cation chloride cotransporters [112–115]. The cotransporters of cations and glucose proved to additionally transfer hundreds of water molecules per transported substrate in animal systems and can be put under heterologous expression in *Xenopus* oocytes [116–119]. The existence of a similar mechanism in plants was explored thermodynamically and consid-

ered feasible for water transport to xylem vessels [112–115]. Again, we await experimental confirmation of the hypothesis for plants.

The discovery of aquaporins posed questions of their importance to the basics of water transport in plants (see, e.g., [120]); their role in water transport via roots was demonstrated (see, e.g., [121,122]) and developed into a wide, intensively growing area for research. Questions of whether the discovery requires modification of basic equations of linear thermodynamics for water and solute fluxes still remain (see, e.g., [120]). The membrane reflection coefficient generated by many individual aquaporins depends on the nature of solutes at the sites of the aquaporins (these aquaporins are permeable to low molecular weight uncharged molecules); hence, knowledge of the solutes generating the osmotic gradients is required. Aquaporins can be concentrated in specific areas within membranes generating high hydraulic conductivity and so contribute to the formation of mosaic composite membranes at different spatial scales (as suggested by, e.g., [123]). Anyway, the evident effect of aquaporins on root hydraulic conductivity L_p has been demonstrated in most conducted experiments (from 0% up to 90% of L_p is linked to aquaporins as summarized in [122]).

5. Rhizodermis Exudation

The phenomenon of root exudation presumably requires polarity in water flows. The axial, and to a lesser extent radial, polarity is ensured by root morphology and the direction of transport processes by the distribution of transporters, uneven osmotic pressures of liquids and even by measured polarity in hydraulic conductivity for water flows (see, e.g., [18] for conductivity measurements). Since water is usually absorbed by roots, the observation that roots of maize seedlings exuded liquid radially to the outside of the roots over days, simultaneously to xylem exudations ([22]; see below), was unexpected. The middle part of roots was encased and exuded water to a closed water-free compartment over several days at constant temperature (Figure 3). At the same time exudation into micropipettes attached to the cut end of the root was observed [21,22]. These phenomena were reproduced in another study [124] using similar equipment. Rhizodermis and xylem exudation were absent in maize roots boiled for 5 min in tap water [124]. Water condensation as the explanation of the phenomenon was rejected [22,124]. Moreover, 11 woody species (*Abies alba*, *Acer pseudoplatanus*, *Alnus glutinosa*, *Betula nigra*, *Carpinus betulus*, *Fagus sylvatica*, *Fraxinus excelsior*, *Prunus avium*, *Quercus robur*, *Quercus rubra*, and *Vitis vinifera*) were examined. All of the species showed concomitant rhizodermis and xylem exudation, except *Carpinus betulus* where only the cut surface became moist [124].

Similar results were obtained by a different experimental approach: efflux of water from the surface of field-grown roots of maize, oats, barley, and crabgrass was confirmed by means of cryo-scanning electron microscopy. This efflux from the root surface coincided with guttation from leaves. From the convex shape of the droplets it was concluded that water was not drawn passively from the root by lower potential of the soil. Excavated and subsequently frozen roots of the plants were analyzed, at the point where ice crystals on their surface evidenced the extrusion of water to the soil. These crystallized droplets of water were abundant in the early morning; none or very few were observed for roots collected at midday. The chemical X-ray analysis indicated the presence of carbon, potassium, phosphorus, and calcium in the regions of the droplets [125].

There had been much earlier reports of water efflux from the surface of roots, mostly from root hairs. According to De Candolle ([126], p. 248), Brugmans was the first to observe small droplets oozing from the tips of the rootlets of *Viola arvensis* at night. In 1888, Molisch [127] reported that he quite often observed liquid excretions of roots, similar to guttation from leaves. He judged the droplets were not dew because they appeared only at the tip of healthy roots hairs, on healthy root hairs only, and they would also appear when the roots were kept in a room whose temperature was gradually increased so that no condensation of water would occur. In the same year, Stahl ([128], p. 42) reported drop formation on root hairs of *Circaea lutetiana* observed under a microscope. Czapek [129]

found it easy to demonstrate liquid root excretions. If young seedlings of grasses were grown in steam-saturated rooms, as soon as an abundant development of root hairs has occurred, fine, colorless droplets would be seen on many of the latter. These droplets would appear only when the hair cells were highly turgid. Pfeffer ([91], p. 257) wrote that water droplets are generally excreted by root hairs in a saturated atmosphere and considers intracellular excretion under pressure to be the probable cause. When there is bleeding pressure (from the xylem of a root), some of the otherwise absorbing parts of the root would excrete water. Thereby, he seemed to postulate the simultaneity of xylem exudation and rhizodermis exudation. In the 20th century, Rogers [130] documented by microphotography copious droplet formation on the surface of apple roots in the regions with older root hairs. Richardson [131] observed droplets on root hairs of *Acer pseudoplatanus* but ascribed them without further experimental scrutiny to condensation. Cailloux [132–135] measured exudation from oat root hairs and normal rhizodermal cells at high resolution by means of a micro-potometer. Head [136] filmed droplet development on the hairs of apple roots by time-lapse cine-photomicrography.

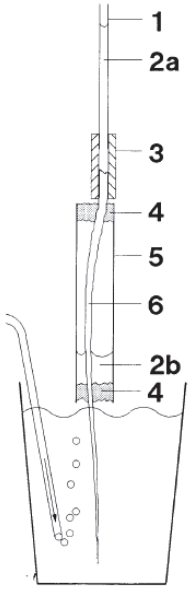

Figure 3. Experimental setup for demonstrating rhizodermis exudation: (1) capillary; (2a) xylem exudation; (2b) rhizodermis exudation; (3) rubber joint; (4) silicon rubber cement; (5) glass cylinder; and (6) maize root. The lower part of the root was immersed in aerated distilled water at constant temperature of 23 °C. The experiments lasted 2.5 days, rhizodermis exudation occurred in all 25 maize roots tested. Reproduced from [22] with the permission of the publisher John Wiley and Sons.

For detached roots of 40–60 days old sunflower plants, which were removed from water and their surfaces dried, exudation continued for days if the roots were contained in dry sealed glass flasks. At the same time, some water also accumulated at the bottom of the flasks: this water was explained by evaporation from external root surface. Howeverthe possibility of rhizodermis exudation was not widely known or discussed at the time [27,29]. For one of the experiments, a root lost, on the average, 11 g of water within two days (from 65 g to 54 g), the weight of root exudate was 5 g while 6 g were collected from the bottom of the vessel containing the root [29].

Rhizodermis exudation could help explaining the unexpected observation of increasing soil water contents towards the root surface, measured by neutron tomography, in

chickpea, white lupin, and maize ([137], for further discussion see [138]). It seems likely that rhizodermis exudation contributes to the phenomenon of hydraulic redistribution. Hydraulic redistribution is the transport of water from moist to dry soil zones via the root system during periods of low transpiration [139–141]. It can take place upward (hydraulic lift) [142,143], downward (inverse hydraulic lift) [144,145] (see earlier: [146,147]) and laterally [148]. Through hydraulic redistribution, plants can create a water buffer outside the roots and improve the availability of nutrients [138,149,150]. Because hydraulic redistribution allows for water parasitism, it can be used for a natural irrigation system in agriculture through the combined cultivation of shallow-rooted crops with deep-rooted plants capable of a pronounced hydraulic lift [151–153].

The efflux of water and organic matter with ions from the roots to rhizosphere is important for interactions of plants with soil microorganisms, soil insects and nematodes and with the other plants. The subject is intensively studied nowadays with fruitful practical and theoretical implications for plant life and stress tolerance (see, e.g., for questions posed earlier and references in: [10], recent reviews and research papers include: [154–158]. Roots release a wide spectrum of metabolites ranging from amino acids and sugars to alcohols, organic acids, nucleic bases and nucleotides, secondary metabolites such as alkaloids, phenylpropanoids, acylsugars, and terpenes (see, e.g., [157–159] with references therein). The concentrations and proportions of the metabolites released provide specific biochemical signatures of growing roots along their length [157], presumably function in root-to-root signalling [159] and serve as a competitive trait of fine roots under field conditions [160]. The profile of root-released metabolites changes under drought and influences rhizosphere-inhabiting microbes [161]. Similarly, the alleviating effect of certain microbial communities was shown under salinity stress for some plants (see, e.g., [156] on specific strain of *B. subtilis* for clover). Mechanisms of transport for the released metabolites involve specific ABC and MATE transporters and simple and facilitated diffusion [157]. However, it is very likely that the metabolites make up only a very small fraction of osmotic pressure in any root exudates (e.g., compare to Table 1). Therefore, understanding of the rhizodermal liquid exudation would help to predict how the concentrations of metabolites are regulated in rhizospheres. *Visa versa*, the study of genetic and molecular basis for release of metabolites to rhizospheres would provide more information to aid understanding of the phenomenon of rhizodermis exudation.

6. Exudation of Root Segments without Root Apex and Stem Exudation

Effects of axial polarity and axial differentiation of roots arose in experiments with excised segments from roots. Exudation from root segments without a root apex and with xylem vessels cut at both ends was demonstrated for onion roots in a saturated atmosphere with several potometers attached along the roots [10,11]. The 25 mm long onion root segments absorbed water from three attached potometers along the axis and then exuded at the basal end (distal to the original apex), while the direction of fluid flow (uptake or efflux) at the apical end depended on the length of removed apical tissue (Figure 4A). Similarly, the discovery that root segments with vessels cut at both ends exude in both directions was later made independently for roots of maize seedlings in an attempt to check the single membrane osmotic concept of exudation [23–26].

Segments with the same length of 5 cm were cut from maize roots (the apical 2 cm were discarded, the next 5 cm of root were used in the experiments); these segments demonstrated exudation from basal end and also from the apical end [23–26]. The exudation rate from the basal end (distal to the original apex; direction for the exudation of detached roots) was usually 2–3 times higher than for exudation from the apical end (opposite direction to exudation of detached roots; 1.6 ± 1.2 μL/(h × cm^2) compared to 0.7 ± 0.5 μL/(h × cm^2), means ± SD; [25]). The chemical composition of exudates for segments from maize seedlings was similar to the exudate of detached roots, indicating xylem exudation, but exudate from the apical end (proximal to the original root apex) with slower exudation was more concentrated ($II_i = 0.28 \pm 0.03$ MPa compared to 0.13 ± 0.03 MPa).

The energy activation (expressed in Q_{10}) for the faster exudation from the basal end was higher than from the apical end (see sections below for more explanations); exudation from both ends responded to metabolic inhibitors and stimulators and was stopped by the same external osmotic pressure from PEG 6000 (see sections below for more explanations) [23–25]. Exudation of maize root segments with the same length of 5 cm but cut at different distances from the root apex decreased as the segments were cut further from the apex. For exudation from the apical end (proximal to original apex) the highest exudation was for segments cut 3 cm from the original apex (Figure 4B). Sealing the apical end of maize root segments (2–7 cm from the root apex) with glue increased exudation from the basal end from 2.9 ± 0.3 μL/(h × cm^2) to 4.7 ± 0.6 μL/(h × cm^2) (means ± SE); sealing the basal end of maize root segments (2–7 cm from the root apex) increased exudation from the apical end from 0.5 ± 0.1 μL/(h × cm^2) to 1.0 ± 0.1 μL/(h × cm^2) (means ± SE) [26]. Presumably, the stage of development of xylem vessels along the roots was the reason for the differences in exudation from the ends of root segments. The phenomenon confirms the multiplex nature of root exudation and complexity of root structure. Interestingly, xylem-like (based on exudate chemical composition) exudation was recorded from the apical part of roots of maize seedlings exposed to air with 100% humidity when the apical 3–5 cm of the roots were cut off [162,163]; the researchers suggested that xylem pressure was generated in humid air and resulted in exudation after removing the hydraulically insulating root tip.

Still it is important to set the frameworks in generalizing our knowledge from several herbaceous plants to all plant species, especially for trees where measured xylem pressure could be caused by either by root pressure or by stem pressure. For example, xylem sap pressure in sugar maple *Acer saccharum* Marsh. is a basis for commercial production of maple syrup. The sap contains plenty of sugars (over 3%) and even flows under low temperatures from upright detached pieces of stem (trunks) and, moreover, from the reverted upside down stem pieces when they have their lower (morphologically apical) part in water [164]. The flow from maple stems exhibited large variability even from sections of one stem, dependent on temperature and required living tissues [165]. Likely, the mechanisms for the stem pressure and flow in some trees may differ from the mechanisms for root pressure in maize; in experiments with 17-years-old orchard walnuts both root and stem pressure were detected and separated based on temperature dependence and time of the year when they were dominant [166]. Xylem pressures up to 1.6 bars were recorded in autumn and spring, correlated with soil temperature, the pressures constituted about 55% of the calculated values based on xylem sap osmolarity and were attributed to root pressure. Lower xylem pressures up to 0.35 bars occurred in winter and were about 7% of the calculated values of sap osmolarity; these pressures were of stem origin [166]. So, several mechanisms could be in operation together for xylem exudation in different plants and their tissues.

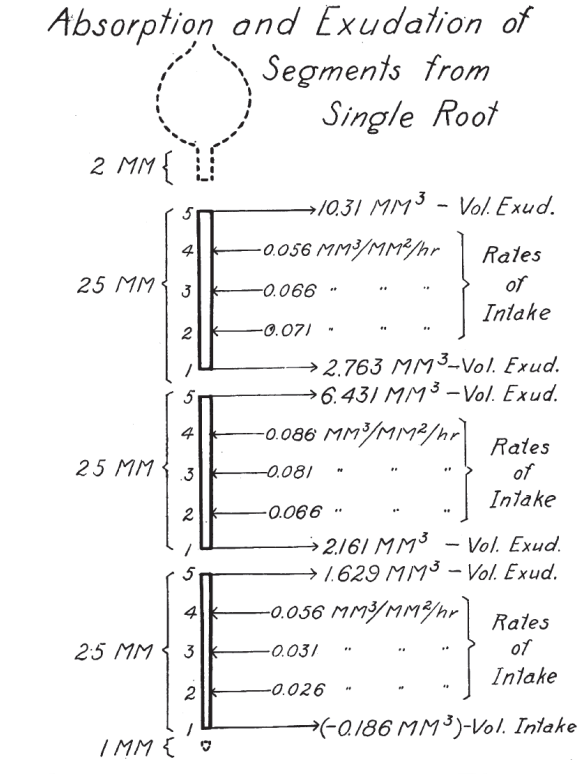

(**A**)

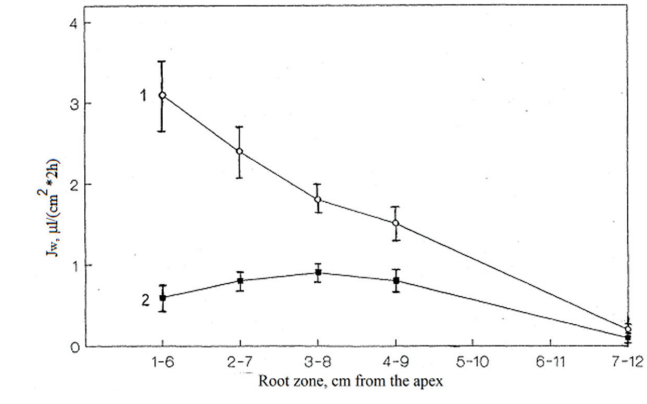

(**B**)

Figure 4. Exudation of root segments isolated from onion roots (**A**); reproduced from: [10] with the permission of American Society of Plant Biologists with further enhancement by AI software and roots of maize seedlings (**B**), reproduced from [26] equivalent to Figure 1 from [24]. A Diagram of total volume outflow and average rates of intake of water in isolated contiguous segments of the same root. Positions of the potometers are designated by the arrows numbered 1, 2, 3, 4, and 5. Observations were made during a 20-h period. B Exudation rate (J_w) from basal (1) and the apical (2) ends of 5 cm root segments cut out from various root zones. Data are given as means ± SE. Exudation time was 2 h; the similar regularity was observed after the first 20 min of exudation and later on.

7. Pulses and Oscillations in Exudation Rate, Coordinated Activity of Cells, and Estimates for Potential Changes of Cell Volume and Turgor Required

An extremely intriguing aspect of the phenomenon of root exudation is the sudden sharp pulses and oscillations in the rate that occurred at the scale of minutes for some (not all) detached roots of maize seedlings ([19] with references therein for earlier publications for different plant species; [22]) and for roots detached from 40 to 60-day-old sunflower plants [31,32]. The more pronounced pulses were in the observations with maize roots at 23 °C (Figure 5A reproduced from: [22]). The total volume of the studied roots was estimated at about 100 mm × 1 mm^2 × π/4 or 79 mm^3 (=μL); the pulses of 0.16 μL which occurred within 30 s are then 0.2% of the total root volume (including the root central cylinder with xylem vessels) [22]. Larger pulses, up to 1.5 μL at 30 °C making up to 4% of total root volume (these roots were 5 cm long,) were registered with much lower temporal resolution of 20 min in the wider capillaries for root segments of similar maize seedlings [26]. Converting the volume flow in the larger pulses over 20 min to 30 s will lead, however, to only 0.1% of total root volume/30 s (also Q_{10} of exudation at 30 °C compared to 20 °C was 3.2–3.5 [23] proportionally reducing the estimated pulses at 23 °C). Experiments with sunflower roots demonstrated exudation rates about 5–10 μL/minute and oscillations about 1–2 μL/minute for dry roots in air (exuding at the expenses of own intrinsic water) and for roots in tap water [31,32]. Based on the mentioned losses of weight by the roots (the roots were over 10 g), so the pulses were below 0.1%/30 s.

(**A**)

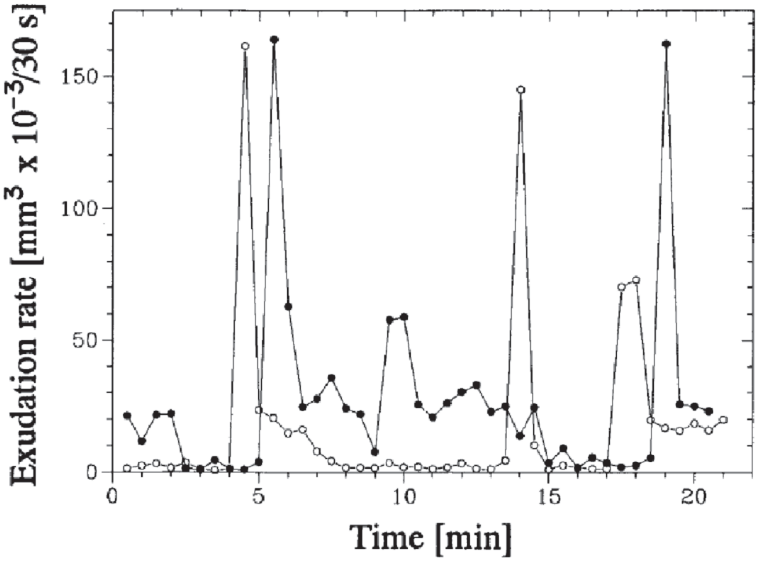

Figure 5. *Cont.*

(**B**)

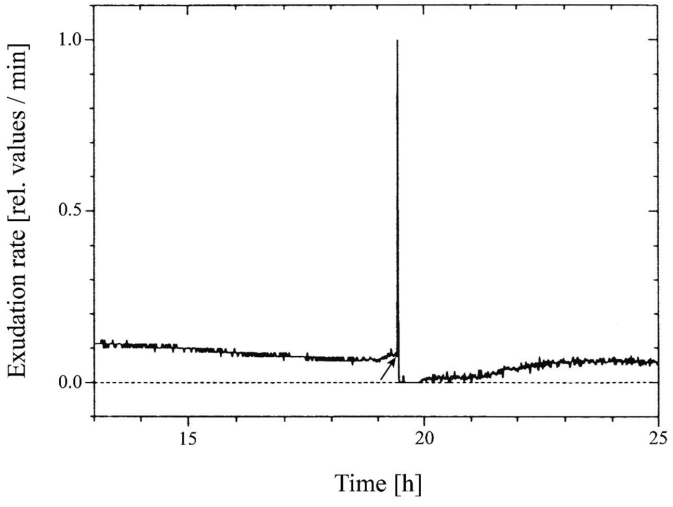

Figure 5. Exudation pulses recorded for detached roots of maize seedlings. (**A**) Rate of xylem exudation of two single maize roots in distilled water at constant temperature of 23 °C measured simultaneously by the micropipette method; standard error is 2.5×10^{-3} mm^3. Reproduced from [22] with the permission of the publisher John Wiley and Sons. Similar results (though with lower temporal resolution) were obtained for detached maize roots of 5–7 days old seedlings at 30 °C [26]. (**B**) Collective exudation rate from the cut surface of 24 four-day old maize roots in aerated distilled water as bathing medium was measured by the micro drop recorder (see for this method [22]). The bathing medium was at a constant 22 °C up to the time indicated by the arrow. At this point, the temperature changed to 4 °C (cold bathing medium by pot change). The ensuing exudation peak started immediately after contact of the roots with the cold bathing medium. Subsequently, the bathing medium was slowly warmed to room temperature (22 °C) without further external manipulation. Reproduced from ([124], p. 31), modified.

Oscillations of water uptake and exudation have been recorded for detached roots of 20–40-day old sunflower plants. The oscillations were in counterphase, were stimulated by 5×10^{-5} M acetylcholine and inhibited by 5 μM cytochalasin B, 10 mM 2,3-butanedione monoxime (potential inhibitor of nonmuscle myosin) and 1 μM CCCP (uncoupler of oxidative phosphorylation) [32]. Though the effect of inhibitors and stimulators could be nonspecific and related to the metabolic and structural components of cellular machinery, the counterphase of oscillations in water uptake and exudation may point to two distinct processes. Similarly, for excised onion roots and root segments directions of changes for fluctuating water uptake and water exudation were often opposite over 2 h intervals; moreover, the ratio between volume absorbed to volume exuded ranged from 0.65 to 1.04 over the intervals for one set of experiments ([10] with references therein to the earlier studies on periodic oscillations in root exudation). Aperiodic or periodic pulses in exudation for over 3 h were sometimes recorded for exudation from detached roots and from both basal and apical ends of maize root segments at the available scale of measurements (20 min) [26]. It is surprising that the sensitivity of measurements was not the factor which determined whether researchers paid attention or not to pulses of exudation. Sabinin [82] concentrated his efforts on the osmotic phenomena surrounding exudation from maize roots and its formalization; he developed high resolution of measurements

below 0.001 μL (1 nl) [82]. However, he did not report and even rejected oscillations in exudation rate (apart from long-term temperature-dependent ones) [82].

Interestingly, for large (over 2–3 weeks old) maize roots when exudation was observed from the whole upper cut root surface, not only from the xylem vessels [35], but there were also periodic oscillations in exudation for some roots. The oscillations had a peak to peak period of 1–1.5 h and reached 1 g/(hour×root) for the large roots (Figure 4 of [35]).

The fastest so far documented exudation pulses of single roots are 0.16 μL/30 s or 0.2% of root volume/30 s (Figure 5 from [22]). These pulses need several factors to be fulfilled with one or several potential mechanisms realized. Firstly, a high hydraulic conductivity L_p should ensure the possibility of fast water fluxes. The known measured root and cell hydraulic conductivities L_p are sufficient to satisfy the observed high water fluxes: L_p of the order of 10^{-7} m s^{-1} MPa^{-1} was measured in hydrostatic experiments (0.94 ± 0.6610^{-7} from 0.1210^{-7} to 2.810^{-7} in endosmotic experiments where the direction of water flow was from the medium into the xylem) and about 10 times lower in osmotic experiments with maize roots [18]. It means that difference of 1 bar in hydrostatic pressure across a root (cell turgor could be involved) would lead to the flux of 10^{-7} m^3 m^{-2} s^- hence per root stele area (based on Figure 1 of [35]: 100 mm × π × 0.4 mm = 125 mm^2) it is 1.25×10^{-2} μL/second or 0.375 μL/30 s. The value twice exceeds the measured exudation pulses of 0.16 μL within 30 s [22]. It seems, however, that L_p could be a limiting factor and also it is unlikely that the exudation pulses could occur at the expense of the osmotic forces only. Secondly, large sudden ion fluxes should appear within the short time of the exudation pulses if we assume that water and ion fluxes are tightly linked. One explanation could be the activation of large mechanosensitive channels (MSC), allowing for the passage of water and ions, or of activating smaller MSCs which in turn activate larger ion channels of another types of ion channels. This would explain the inhibitory effect of gadolinium on exudation because it is known as an inhibitor of MSCs (recent reviews on plant mechanosensitive ion channels include: [167,168]), and also of cytochalasin, which has been shown to decrease the activity of MSCs, probably by reducing their mechanosensitivity [167]. Another option is a potential sharp short-term activation of cation-chloride antiporters [112–114], but since they are not well studied in plants (see for an overview [169]), we do not know whether the option is possible at all and what the mechanisms could be if any. Both mechanisms could be combined. Thirdly, more mechanisms at the subcellular level are proposed that involve changes of turgor pressure but not ion fluxes:

(1) cytoskeleton-based turgor oscillations of root cells constituting the so called metabolic component of root pressure [19];
(2) reverse osmosis realized in the plasmodesmata of endodermis when cell turgor oscillations around 1 Hz frequency lead to reduction of solute osmotic pressure [110,111].

Turgor pressure changes of cortical cells may be required for the oscillation peaks of measured exudation. Elastic modulus ε has been measured for many (39) cortical cells of maize roots from 12 to 211 μm from the root surface [18]. Turgor pressure varied from 1 to 6.6 bars, average hydraulic conductivities L_p were $2.4 \pm 2.0 \times 10^{-7}$ (from 0.5 to 8.7×10^{-7}) m × MPa^{-1} × s^{-1}, while elastic modulus ε varied from 1.3 to 18.1 MPa depending on the cell turgor [18]. We assume the average ε as 10 MPa, the total volume of cortex as 67 μL (total volume of cortex−olume of stele is about 79 mm^3 − 12 mm^3 = 67 mm^3) and suggest that turgor P decreases for all the cortical cells (their diameters were from 26 to 43 μm and lengths from 205 to 305 μm: [18]). Then the estimates give the required ΔP for the cortical cells:

$$\Delta P = 10 \text{ MPa} \times 0.16 \text{ μL}/67 \text{ μL} = 0.024 \text{ MPa or about } 0.25 \text{ bars.}$$

The estimates look reasonable if rather low; it is around the pressure of activation (around 0.1 bars) for some mechanosensitive ion channels of plants (see, e.g., Figure 1 and Supplementary Figures S1 and S7 from: [170]). Several separated symplastic cell domains could be considered within the root cortex (as was demonstrated for lateral root organo-

genesis in *Arabidopsis*: [171]), then the numerical estimates give higher turgor pressure changes/different hydraulic conductivities for the observed exudation pulses. There is a question, posed in [22], of how the activity of the cells within a domain is coordinated; presumably plasmodesmatal connections may link turgor pressures of individual cortical cells within symplastic domains and coordinate their activity.

One more intriguing observation about synchronization of exudation is that a strong exudation pulse was observed for groups of 24 maize roots measured collectively when they were transferred from warm (22 °C) to cold (4 °C) water; the pulse started at the very moment of immersing (resolution of these measurements reached 1 s). Exudation increased 8 to 56 times, went then down to zero, and gradually increased again when the water warmed up slowly ([124], p.31)). The phenomenon was taken as evidence for a biphasic exudation mechanism (Step 1: filling of the symplast, Step 2, release into the xylem) [124]. The exudation pulses were weakened but not totally suppressed by incubating the roots for 2 h in 10 mM KCN plus 10 mM SHAM (Salicylhydroxamic acid, blocking KCN-insensitive electron transport). However, addition of 200 mM sorbitol (4.8 bars or somewhat less) to the bathing medium (water) inhibited exudation completely. Weaker exudation peaks could be triggered by transfer of maize roots from 22 °C to 10–18 °C water [124]. The observation is similar to the earlier results with roots of maize seedlings, which expressed a sharp peak of exudation and contraction of root cross-section on being transferred from 15 ° to 30 °C or from 20 ° to 35 °C. The pulses of exudation (and decrease of measured root cross-section) were inhibited by 2,4-dinitrophenol and by *p*-chloromercuriobenzoate (influencing SH-groups of enzymes) ([13–16] and references therein). The researchers ([13–16] and references therein for similar sharp pulses of exudation revealed for sunflower roots transferred from 12 ° to 27 °C) suggested that cell contractile elements are responsible for the effect. However, the pulses of exudation could be explained by synchronous change of turgor pressure in large domains of root cells. Higher temporal resolution (within seconds) of exudation pulses and oscillations and a better understanding of root symplastic domains and their synchronized activity are the next steps for deeper investigation of oscillations in exudation and the mechanisms of root exudation in general. It is worth mentioning that measurements of root pressure by applied equilibrium hydrostatic pressure [8,9,17,18,37,38,172] did not report any oscillations (though the predicted oscillations are low, and this method could change the root water pathways which were suggested in [34] by influencing mechanosensitive elements). Additionally, as far as we are aware, the measurements of turgor pressure in individual root cortical cells also did not demonstrate any oscillation of turgor pressure at the time scale of minutes or less (e.g., [18] for maize).

8. Effects of Chemical Agents on Exudation and Root Pressure

Numerous publications have explored effects of a wide spectrum of chemical compounds on the exudation and water transport parameters, especially for 4–7 weeks old tomato roots [102], detached roots of 5–7 days old maize seedlings and 20–60 days old sunflowers roots ([19] and references therein for earlier publications, [22–33]). Table 3 illustrates some examples of how different substances influence exudation of detached roots and root segments of maize seedlings (from [23–26]). Further parts of the Sections 8.1–8.3 briefly describe groups of compounds according to their known mode of action with an accent on the ion channel blockers (the other types of compounds are discussed more in: [19] and publications from the laboratory).

Table 3. Effect of 2, 4-dinitrophenol, various inhibitors of contractile proteins and biomediators on exudation rate (J_w) from detached roots and root segments of *Zea mays* at 30 °C over the first 20 min of the process.

Treatment	J_w, μL × cm^{-2} × h^{-1}		
	Detached Roots	Segments	
		Basal End	Apical End
No treatment (water)	1.9 ± 1.0 (100)	1.6 ± 1.2 (100)	0.7 ± 0.5 (100)
2, 4-Dinitrophenol, 2.5×10^{-4} M	0.5 ± 0.4 (26)	0.4 ± 0.4 (25)	0.2 ± 0.3 (29)
Cytochalasin B, $2 \times l0^{-5}$ M	1.3 ± 1.0 (68)	1.2 ± 1.2 (75)	0.5 ± 0.3 (71)
d-Tubocurarine, 6.7×10^{-5} M	1.1 ± 0.5 (58)	0.9 ± 0.8 (56)	0.5 ± 0.3 (71)
Acetylcholine, 10^{-4} M	2.2 ± 0.9 (116)	1.7 ± 0.7 (106)	1.1 ± 0.8 (157)
Noradrenaline, 10^{-5} M	2.3 ± 1.1 (121)	2.1 ± 1.2 (131)	1.2 ± 1.0 (171)

Data are given as means ± SD. 95% confidence intervals are at least 3 times less than SD. Percent of the corresponding control values is given in the parenthesis. The differences from control treatments are significant at $p = 0.95$ level; stimulation of exudation from the apical end by biomediators significantly differs from other root segments at $p = 0.95$ level. Stimulating effect of acetylcholine and noradrenaline increased with time (2nd hour of exudation) for exudation from detached roots and apical end of segments (from: [23–26]).

8.1. Inhibitors of Metabolism and Substances Influencing the Integrity of Cell Membranes and Cytoskeleton

Inhibitors of metabolism or uncouplers of oxidative phosphorylation in roots (KCN, 10^{-4}–10^{-3} M; 2,4-dinitrophenol, 1–5 × 10^{-4} M; carbonyl cyanide-3-chlorophenylhydrazone (CCCP), 10^{-6} M) have a clear inhibiting effects on exudation of sunflower and maize roots ([19,102] and references therein for earlier publications, [23–25,27,28,30–32]).

At the same time, inhibitors or destabilizing agents for intracellular contractile systems and cytoskeleton (*d*-tubocurarine, 6.7×10^{-5}–1.5×10^{-4} M; cytochalasin B, 1–5 × 10^{-6} M; colchicine, 10^{-3} M; 2,3-butanedione monoxime, 1–10 mM; latrunculin B, 10^{-6} M) also inhibited exudation of maize and sunflower roots ([19] and references therein for earlier publications, [23–25,27,28,30–32]).

Substances that influenced the stability of cell membranes had effects on exudation, depending on their effects on membranes stability: compounds decreasing stability of cell membranes (pipolphen, 0.1–1 mM; EDTA, 7 mM) inhibited exudation for maize and sunflower roots while $CaCl_2$ (1 mM) increasing stability of cell membranes stimulated exudation ([19] and references therein for earlier publications, [27,28,31,32]).

The effects clearly demonstrate that the living cells and their intracellular contractile and membrane systems are essential for root exudation and root pressure. Evidently, water and ion fluxes require the functioning of cellular water and ion membrane transport systems which are supported by ongoing cellular metabolism and by membrane interactions with the cytoplasmic cytoskeleton and intracellular compartments. From another point of view, the effects of relatively nonspecific compounds do not indicate the mechanisms of exudation. The application of the inhibitors at high concentrations for a long time could also disrupt root structure; for example, 2,4-dinitrophenol at 2.5×10^{-4} M resulted in the loss of turgor of maize seedling roots after 1–2 h of application [26].

8.2. Plant Hormones, Biologically Active Compounds, and Modifiers of Signal Transduction Chains

A stimulatory effect on exudation was discovered for plant hormones and structurally similar compounds: indole-3-acetyc acid, 10^{-7}–10^{-6} M; kinetin, 10^{-4} M at 30 °C ([19]

and the references therein for earlier publications, [28]) though kinetin at 10^{-9}–10^{-6} M was reported to have inhibitory effect at 23 °C for similar roots of maize seedlings [173]. A stimulatory effect was shown for adenine, 10^{-4} M ([19] and the references therein for earlier publications); ABA, 10^{-9}–10^{-6} M within first 5 h of application with further inhibition [173]; fusicoccin, 10^{-9}–10^{-6} M within first 4–5 h of application with further inhibition [173]. The mechanisms of the phenomenon are not well understood, although some of the researchers ([19] and the references therein for earlier publications, [28] and further publications from the laboratory) suggest that the hormones enhance metabolism of the root cells which in turn results in exudation by activating nonosmotic component of root pressure (see below).

An interesting observation was that some animal neuromediators (acetylcholine, 10^{-5}–10^{-4} M; adrenaline, 10^{-6}–10^{-5} M; noradrenaline, 10^{-5} M; serotonin, 10^{-4} M) stimulated exudation ([19] and the references therein for earlier publications [24,25,28,30–32]). It led to questions about homology of regulatory systems in plants and animals at the cellular level. More specific and selective compounds, guanosine thiodiphosphate (2×10^{-5} M), a specific inhibitor of G-protein activation, and guanosine thiotriphosphate (2×10^{-5} M), a specific activator of G-proteins, also inhibited and stimulated, respectively, exudation of maize roots [33].

8.3. Ion Channel Blockers

Occasionally in the past, the influence of compounds, which later turned out to be ion channel blockers, were examined (see [15,174], and the references in the latter). The first intentional tests of ion channel blockers on exudation were reported [21,22]. Exudation from the cut surface of 24 or 30 maize roots was measured collectively with a micro drop recorder when agents were added to the bathing medium. A general problem with this approach is that it does not allow any statement about whether the agent actually reaches the membranes from which the measured exudate emerges. The most specific, consistent effect was found with gadolinium (Gd^{3+}), which is a blocker of various MSCs [175], but also of (other) non-selective cation channels (see, e.g., [176]). At a concentration of 50 μM in distilled water as the bathing medium, exudation was increased initially, and then decreased down to 20% of the exudation of the control after 20 h [22]. The time lag between application and inhibition might be due to slow penetration of Gd^{3+} into the root (see [177]). The effect is hardly likely to be due to general cytotoxic effects (see [178]), but very recently an impact of rare earth elements like gadolinium and lanthanum at submillimolar concentrations on endoplasmic reticulum-plasma membrane contact sites has been shown [179]. In screening experiments with other potential blockers, La^{3+}, which blocks a number of mechanosensitive ion channels, but not necessarily the same as Gd^{3+} [175], did not show any marked inhibitory effect on exudation at a concentration of 1 mM in the bathing medium [21,22]. This could be used as an argument against the involvement of an MSC, but also against explaining inhibition of exudation observed with gadolinium to less specific effects on membranes reported by [179]. In further screening experiments, the K^+ channel blocker Ba^{2+}, which permeates through Ca^{2+} channels, likewise increased exudation at first, and reduced exudation almost to zero within seven hours at a concentration of 3 mM in the bathing medium [21]. Application of a 3 mM solution of the K^+ channel blocker quinine which permeates the lipid bilayer well resulted in a small and short increase of exudation followed within 2 h increase and a reduction of exudation to about a quarter of the initial level within 2 h and a further reduction to zero within the next 5 h. At a concentration of 100 μM quinine showed some reversible inhibitory effects [21]. Amiloride, inter alia a blocker of Na^+ and of mechanosensitive cation channels (see [180]) showed some decrease of exudation at 100 μM concentration in the bathing medium, and complete exudation inhibition after 8 h at a concentration of 1 mM [21]; TEA^+, a general blocker of K^+ channels, penetrating the cell membrane very poorly, showed at 3–10 mM concentrations in the bathing medium an increase in exudation, but no following decrease [21]. Screenings with agents that interfere with chloride currents (NPPB, DPC, anthracene-9-carboxylic acid,

sodium gluconate, and glutamate) showed inconclusive effects [21]. The results offer some support to the idea that xylem exudation strongly depends on potassium fluxes which are influenced by a mechanosensory system (see, e.g., [181]).

The initial xylem exudation by cationic channel blockers added to distilled water as a bathing medium poses a riddle. One might speculate that xylem exudation increases when rhizodermis exudation is blocked. But exudation also increased (up to double within 15–30 min) when submillimolar concentrations of NaCl and KCl were added to distilled water. Reversibility of the increase was tested for CsCl, $LaCl_3$, KCl, and NaCl and confirmed for all these substances (and $BaCl_2$, $GdCl_3$, and TEA^+), most markedly in the case of CsCl. When another salt was already present in the bathing medium the exudation increase weakened or failed to appear [22].

8.4. Summary on the Effects of Chemicals on Exudation

Though a large array of data has accumulated, it is difficult to decipher the mechanisms behind the inhibition or stimulation of exudation since most of the agents inhibiting and stimulating exudation (apart from probably fast effects of salts at low concentrations) have a complex influence on plant roots and their cells (including effects on metabolism, on membrane stability, intracellular signalling, even on gene expression and profiles of mRNAs, siRNAs, and transcriptional factors). However, generally speaking, the results provide solid support for a conclusion about the complexity of root pressure and exudation as it was described and conceived by Hales [1] and later on envisaged by further researchers at the developing levels of our understanding for biological systems (see, e.g., [19]). More specific inhibitors of ion channels support their role in driving ion fluxes linked to water fluxes. Cytoskeleton modifiers are suggested to directly influence cell turgor of root cells, although cytoskeleton elements are also tightly linked to regulation of ion channels.

9. Energy Activation Barrier and Osmotic Compensation Pressure for Root Exudation

The energy activation barrier for physico-chemical processes is also measured in physiology as Q_{10} (ratio of rates for a process when temperature changes by 10 °C) and often used to indicate the nature of reactions behind a process. Simple diffusion and osmosis have Q_{10} values close to 1 for temperatures 20 °C–30 °C (since ratio of 303 K/293 K in $\Delta\pi = C \times R \times T$ is close to one; the same for the simple diffusion equations). For more complex processes where temperature dependence is stronger and (simplifying the nature of processes) the form for the tail of Maxwell–Boltzmann distribution (developed for gases) is more shaped by temperature, Q_{10} reaches values of 2–3 and more.

For exudation of detached roots of sunflower and maize seedlings, the Q_{10} was around 2.5–4 for exudation rate measured at 30 °C divided by exudation rate at 20 °C (reviewed in ([19] with later references), [23–25,28,31,33]). However, the Q_{10} of root exudation for excised roots of maize dropped from over 3 to 1–1.3 under application of the inhibitors such as 2,4-dinitrophenol, cytochalasin B, colchicine [19], and to 1.7 from 3 after inhibition by guanosine thiodiphosphate with the background of decreased inhibited exudation rate [33]. On the other hand, stimulators of exudation such as $CaCl_2$, indole-3-acetyc acid, acetylcholine, adrenalin, noradrenalin, and guanosine thiotriphosphate increased Q_{10} for excised roots of maize by 3–30% to 2.9–3.6 [19,28,33]. For twice faster exudation from the basal end of segments from the maize roots the Q_{10} was 3.7 ± 1.0 (same was for detached roots), but slower exudation from the apical end of segments had a statistically lower $Q_{10} = 2.7 \pm 1.2$ [24]. The Q_{10} of exudation for surface-dried sunflower roots removed from water was surprisingly higher at 4.6 ± 0.7 compared to 3.6 ± 0.7 for roots in water [31].

Assuming that the mechanism of water transport/root exudation remains the same at the temperatures 20 °C and 30 °C, it is possible to use the simple Arrhenius equation [182] for the ratio of reaction rates k_2/k_1 and calculate the energy activation E_a for root exudation:

$$E_a = R \ln(k_2/k_1)/(1/T_1 - 1/T_2), \quad (5)$$

where T is absolute temperature in K, R is the universal gas constant (8.31 J/(K×mole). For 30 °C and 20 °C and the high Q_{10} of exudation around 2.7 (e.g., Q_{10} = e) E_a corresponds to 73.8 kJ/mole; for a Q_{10} of 5 the values are 1.6 times higher. In positioning this energy among biochemical and water transport parameters it is reasonable to compare the value of the activation barrier for water exudation with the other processes. For a biochemical reaction, 73.8 kJ/mole is about 2.5 moles ATP/mole of transported water (assuming standard free energy of ATP hydrolysis about −30 kJ/mole: see, e.g., [183] although it could be 1.5 less, down to −50 kJ/mole depending on the physiological conditions and concentrations). This estimate for direct active transport is not realistic, so the energy activation for the reaction comes from the other processes. Another comparison also looks unlikely, 73.8 kJ/mole being translated with sign reversion to water potential Ψ_w makes a huge −4350 MPa (−43,500 bars)—the value is over four times below the water potential of vapor with a humidity 0.1%, which probably does not exist on Earth. This high energy barrier of the reaction suggests that complex mechanisms participate in exudation and control the flows and water transport in roots although presumably the processes could be easily achieved by osmotic forces. Still it is not clear why and how the stimulators of exudation increase the energy barrier for exudation (increasing Q_{10} and, hence, energy activation for exudation).

Zholkevich [19] based on earlier results [14] developed the concept of two constituents of root pressure: an osmotic component with a simple physical nature and a Q_{10} around 1, and a so called metabolic component with a Q_{10} around 5 (Figure 6). The metabolic component is highly sensitive to inhibitors and bioregulators, the share of each component determines the rate of oscillations of exudation and the total Q_{10} of exudation [19]. The concept is highly valuable physiologically but still requires exact molecular entities and mechanisms to explain the existence of this metabolic component. A suggestion that cytoskeleton-linked microoscillations in turgor pressure of root cells create the water flow [19] has to be supported by sensitive techniques of cell and root pressure probes or by the methods of advanced imaging. One of the other limitations is that the concept of metabolic and osmotic components of root pressure ([19] and the references therein with further cited here) was developed in experiments with roots of maize seedlings and with sunflower roots only, so may not be applicable to the wider range of plant species including trees and vines.

The potential input and share of non-osmotic forces in root pressure and exudation is often estimated and measured by the osmotic compensatory method where an external solution with high osmotic pressure π_o is applied to stop exudation (Figure 2), this osmotic pressure π_o is taken as compensatory pressure. Then the osmotic pressure of the root exudate π_x is compared to the osmotic pressure of the external solution π_o and the part (if any) of external osmotic pressure exceeding the osmotic pressure of the exudate (π_o–π_x) is taken as the nonosmotic or metabolic component of root pressure (see, e.g., [19,102]). The experiments require sensitive methods to measure exudation and osmotic pressure and also need osmotically active compounds which do not permeate to the root tissues. So, mannitol used in early experiments is nowadays usually replaced by PEG with high molecular weight (e.g., 6000).

Contrary to purely osmotic concepts without nonosmotic forces (simple osmotic models from Table 2), experiments with tomato roots revealed that compensatory pressure is about 1.4 bars in distilled water with about 70% of a nonosmotic component while about 2.7 bars in nutrient solution with about 50% of nonosmotic component [102]. As the compensatory pressure was determined by mannitol solutions, root exudate was collected before the determination of the root compensatory pressure and it is possible that exudate became more concentrated when the exudation was stopped. However, the reversible twofold inhibition of root exudation and compensatory pressure by KCN, 10^{-4} M with lack of nonosmotic component was then in favor of a nonosmotic component [102]. Experiments with detached roots of sunflower demonstrated 40–70% of nonosmotic component for compensatory root pressure (compensatory pressure was equal to 1.6–2.2 bars by PEG) [19]. Another set of experiments with similar sunflower roots showed 40% of nonosmotic

component, 1 bar of compensatory pressure with Q_{10} = 3.6 ± 0.7 for exudation (30 °C to 20 °C), while for the roots exuding without external water the nonosmotic component was 80% and Q_{10} = 4.6 ± 0.7 [31]. Similar experiments with roots and root segments of maize seedlings are in line with the results for sunflower roots. Briefly, the higher Q_{10} corresponded to a higher nonosmotic component of root pressure (measured by compensation method with external PEG 6000); stimulators of exudation increased both Q_{10} and the metabolic component of root pressure: lower exudation corresponded to lower Q_{10} and to the decreased metabolic component of root pressure [19,24,28,33]. Experiments with maize roots [173] demonstrated that exudation stopped at even 4.8–5 bars (not around three bars as in the abovementioned experiments by Zholkevich and colleagues) of external osmotic pressure by PEG 6000 and mannitol, respectively (close to the turgor pressure of the root cells). However, the researcher did not specifically compare the compensatory pressure to the exudate osmotic pressure [173].

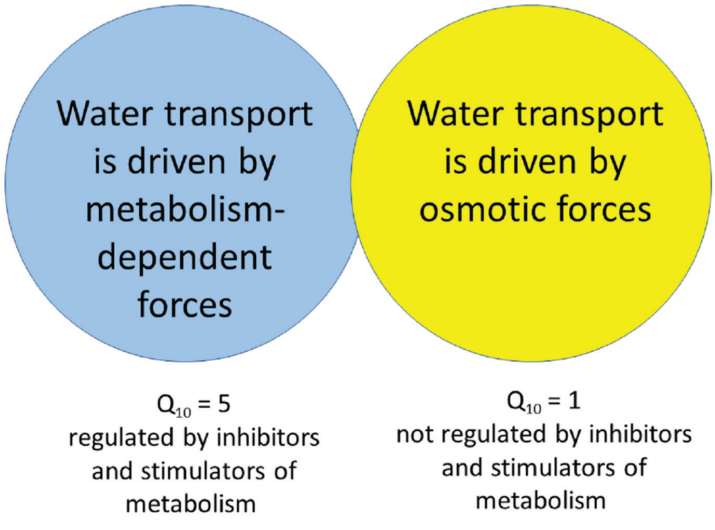

Figure 6. The generalized model of metabolic and osmotic components which constitute the root pressure, and are responsible for the observed exudation (based on: [19]). The separation between the components was based on an assumption that metabolism-dependent forces and processes are not of osmotic origin. The distinction between the components is supported by a complex of coinciding features (activation energy measured as Q_{10} increased parallel to exudation rate and compensation pressure to stop exudation when stimulators were applied; inhibitors decreased the three parameters). Oscillations in turgor pressure of root cells driven by the cytoskeleton (as suggested by in [19] to explain non-osmotic component) were neither supported nor rejected by sensitive single cell methods. The overlap between the circles demonstrates that both mechanisms operate together under most circumstances producing undistinguishable exudation flows.

Interestingly, with this approach at the molecular level a similar nonosmotic component was discovered and characterized under heterologous expression in oocytes for cotransport of water with substrates (sugars or cations) for specific animal transporters [116–119]. Co-transport added an extra component to the osmotic water flow, of nearly 50% (Figures 2 and 7 reproduced from [184]). Similar transporters can function in plants; the transporters could be responsible for the energetically uphill (that is nonosmotic) water transport in roots [112–114]. Calculations for the possible energetically uphill water transport to the xylem were based on measured membrane potential of xylem parenchyma cells and hydraulic conductivity L_p of their plasma membranes. The conclusion was that for typical L_p around 10^{-7} m s^{-1} MPa^{-1} extra root pressure developed by the mechanism may exceed

1.2 bars reaching over 10 bars at 10 times lower (still well within the range of measurements, see above) L_p [112].

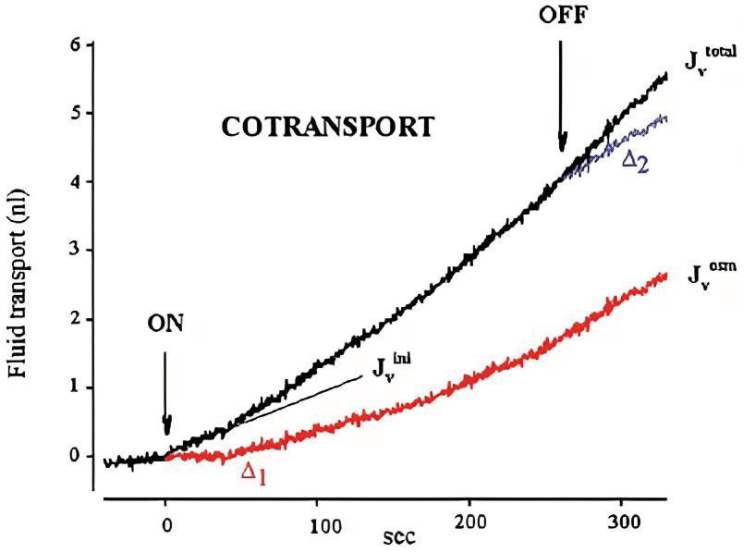

Figure 7. The two components of water transport by sodium–glucose cotransporter SGLT1. At point "ON" sugar was added to the external media, at point "OFF" the Na^+–glucose co-transporter was turned off with a step jump of the membrane voltage to 0 mV. J_v^{total} is the time course of the oocyte volume. There was an initial linear component J_v^{ini} (continuous line, with slope $1.75 \times 10^{-3} \pm 3.85 \times 10^{-19}$ cm s^{-1}). Subtracting this component from the total J_v total yields the osmotic water flow J_v^{osm}. In the steady state, the slope was $4.41 \times 10^{-3} \pm 2.29 \times 10^{-5}$ cm s^{-1}. The osmotic water flow occurred after a 40 s delay (the slope in the steady state was $2.66 \times 10^{-3} \pm 2.29 \times 10^{-5}$ cm s^{-1}). Δ1 and Δ2 are the changes in slope of the fluid transport vs. time curve (i.e., the differences in the rates of fluid transport), which would be predicted if Na^+–glucose cotransport was turned on and off). Reproduced from [184] with the permission of the publisher John Wiley and Sons with further enhancement of pdf by AI software.

Indeed, simple calculations demonstrate that hydrolysis of one mole of ATP molecules (see above) releases 30–50 kJ, while for transport of 1 mole of water against pressure of 1 bar we need only (0.018 kg × 9.81 H/kg × 10 m) 1.77 Joules. So, hydrolysis of one molecule of ATP is energetically sufficient for transport of over 15,000 water molecules against 1 bar of osmotic pressure. For an exudation pulse of 0.16 μL/30 s it would correspond to change of around 6×10^{-10} moles of ATP per a root (equivalent to about 8 μM per a root of 80 mm^3 while regulatory K_m for maize root H^+-ATPase is over 10 times higher [185]). So, we believe that finally the research will lead to molecular identities and mechanisms of how metabolism of living cells is expressed in the measured root exudation.

Still, the experiments with osmotic compensatory pressure need more detailed analysis. Firstly, a check of osmotic pressure π_x for exudates under increasing external osmotic pressure π_o is required. Lower exudation rate may coincide with higher exudate osmotic pressure π_x; hence, it would increase the part of osmotic component (higher π_x at lower exudation was indeed demonstrated by [102] but the interpretation was the opposite to that given here). Under low exudation rate the collection of exudates and measurements of their osmotic pressure π_x may require nanoliter sampling and nanoliter osmometry with further technical advances. Secondly, direct summation of Q_{10} for separate components of the process based on their percentage of the whole root compensatory pressure may not be valid and would require complex models. Thirdly, molecular and genetic manipulations

with ion transporters and mechanosensitive ion channels could help to reveal whether they do participate in the formation of root pressure and its metabolic component. Last, but not least, the experiments with wider range of plants are required to understand the role of the nonosmotic water transport for different groups of plants.

10. Proposed Sketch of the New Mechanism Which Explains Both Xylem and Rhizodermal Types of Exudation; Overall Conclusions and Further Perspectives

Our overview describes how the phenomena of root exudation and root pressure were studied over centuries and how the knowledge in the direction accumulated and interconnected with ideas from the adjacent areas, how it further developed in models being paralleled by experimental advances. Pfeffer [87,91] had already suggested that there might be several mechanisms of root exudation. We also tend to conclude that there are several mechanisms involved in exudation that likely operate under specific conditions for different plant species. Possible mechanisms start with simple osmosis, which is an inevitable consequence of the basic laws of physical chemistry and the likely origin of, for example, stem and xylem pressure for sugar maple [164,165] and for walnut [166]. Other mechanisms employed by more complex models foresee a direct contribution of living cells to exudation involving several other processes: from reverse osmosis at the level of the symplast (e.g., [106]) or at the subcellular level [110,111] to co-transport of water with ions via cation-chloride or other cotransporters [112–114] similar to suggested formation of cerebrospinal fluid in mammals [186]. Here, we paid particular attention to a mechanism with proposed turgor oscillations of root cells due to functioning of cellular cytoskeletal elements ([19] with references therein and further works from the laboratory) and outlined the mechanism whereby activation of mechanosensitive ion channels is suggested as a basis for periodic changes in reflection coefficients of hydraulically isolated domains in roots or compartments, rhizodermis exudation, and pulses of exudation [22]. When we observe the total summed water and ion fluxes, the role and participation of each mechanism often remains obscure and needs further investigation.

Examination of the origin of the plant root liquid exudates showed that they arose at first from all kinds of living cells and only later from open xylem vessels. This observation suggests that at least one type of exudation is caused by the osmoregulation in living cells. Such an explanation would very neatly fit the observation of concomitant rhizodermis and xylem exudation. The observations of Cailloux [132,133] indicate that there might be an individual, independent exudation, and absorption behaviour of single root cells. If the osmoregulation of single cells is synchronized, strong exudation pulses can occur. Still the model of Schwenke and Wagner [22] seems promising in explaining these phenomena. It postulates the involvement of mechanosensitive channels in cellular osmoregulation in order to explain the observed effects of gadolinium and cytoskeleton inhibitors on exudation and also the explosiveness of some exudation pulses. When a threshold turgor is reached, mechanosensitive ion channels open; ions are released from the cell either through the MSC themselves or through other channels triggered by the opening of these MSC. Water may follow osmotically [22] or could be also co-transported with ions through membrane channels [112–114] (Figure 8A). Because no standing gradients in maize root vessels were found [108,109], re-uptake of ions from the vessels should be assumed by the model. Uphill water transport could occur through cation channels where the water-ion coupling ratio is larger for ion efflux than for ion reuptake (see for such a concept in ([112], p. 386, Figure 2). Uphill transport could also be achieved by a higher channel density at the vessel sites than at the root surface (see [22]). The model would also fit nicely observations of a phase shifting of root water uptake and root xylem exudation (see [19] and the references therein for earlier publications; [32]).

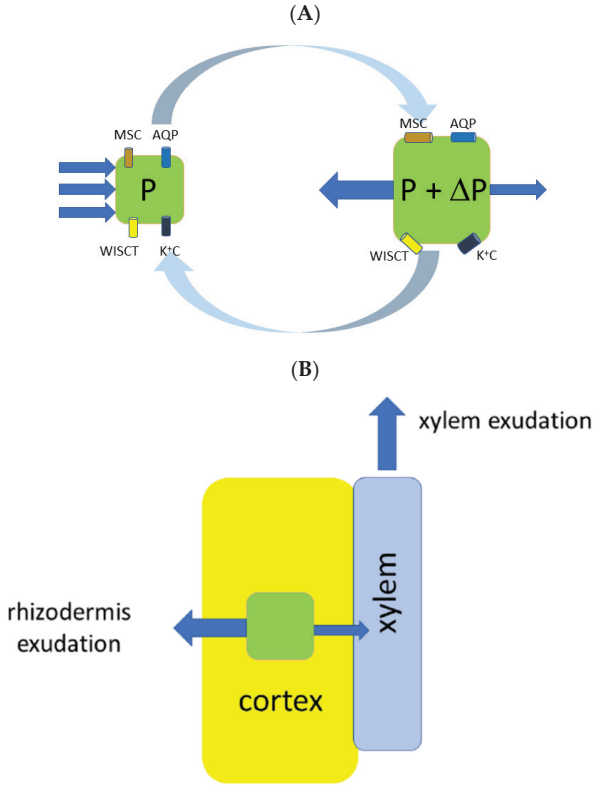

Figure 8. Scheme demonstrating how a domain of hydraulically linked cells in the root cortex potentially generates both xylem and rhizodermis exudation. (**A**). Suggested model for hydraulically linked cells forming a domain with alternating turgor pressure P and water fluxes (blue arrows). The cells within the domain increase their turgor P to the certain threshold of turgor pressure P + ΔP (active water transport could be involved via water-ion/substrate coupling transporters (WISCT) including known cation chloride cotransporters and cation substrate cotransporters), then mechanosensitive ion channels (MCS) activate the opening of other ion channels (e.g., potassium channels K^+C with depolarization of membrane potential and outward K^+ fluxes) or activation of aquaporins (AQP) generating pulses of water flows. The process repeats, the sizes are disproportionally enlarged with more details in the text. (**B**). The resulting water flows from the domain of hydraulically linked cells (green box) produce both strong pulses of xylem exudation and rhizodermis exudation. More details are in the text. It should be noted that not all the roots exhibited exudation pulses, so the scheme is limited to certain roots only.

Here, we introduce a simple sketch for the model at the level of roots (Figure 8B). The model tries also to explain both xylem and rhizodermis exudation with presumed specific features for each type of exudation. The suggestion is that the metabolically-active component of water transport (due to active ion fluxes, turgor oscillations, or activity of the specific transporters) participates in both xylem and rhizodermis types of exudation. Upon reaching a certain threshold of turgor, the mechanosensitive ion channels of cells are activated, which results in the release of ions followed by water (Figure 8A). Most likely opening the channels leads to changes in potassium permeability since the ion is among the main osmolytes and far from thermodynamic equilibrium controlled by membrane potential of the cells. So, for example, depolarization of cells would release plenty of K^+ (based on Nernst equation) followed by outward water fluxes. We further ignore, for the

sake of extreme simplicity, the complex radial root structure and assume homogeneous hydraulic conductivity in both directions but do take into account small volume of xylem compartment with high hydraulic resistance along the xylem vessels and between them; we also assume an unlimited volume of outer compartment with negligible hydraulic resistance (similar to idea of different compartments from the reverse osmotic exudation model: [106]). Hence, any released water would flow both directions, to the xylem and to the outside of the root (Figure 8B). In this way both xylem exudation and rhizodermis exudation would occur with expected pulses in exudation. Presumably, based on the physical assumptions, more water with lower concentration of ions would be released via rhizodermis exudation while less water with higher concentration of ions and higher pulses in exudation would be released via xylem exudation, though the assumption is rather arbitrary and needs calculations with further experimental verification for proof.

In reality, the complex radial root structure, differences in hydraulic conductivities and other numerous factors should be taken into account to compose a detailed picture how concerted activity of cell domains produces observed exudation peculiarities. The existence of domains with higher turgor pressure would not necessarily require the activity of water-ion cotransporters, the water-ion cotransporters could add extra turgor pressure and their role has to be estimated and evaluated separately. The framework of this short review does not allow us to develop here the proposed model in detail. We are at the very beginning of the road since we do not know about the regulation and the properties of the transporters and of the mechanosensitive channels related to water transport: we do not even know which ones are involved in the proposed scheme.

Further study of root exudation would benefit from the new opportunities from genetics and molecular biology with mutants in specific genes, CRISPR editing, and single point mutations in the genes of mechanosensitive ion channels and water-ion/substrate cotransporters which were proposed as molecular candidates for conversion of ATP-driven ion fluxes or turgor changes to directed water fluxes. Still, however, we are at the very beginning of identifying the molecular entities for the processes. At the same time, biophysical experiments combining exudation studies with root pressure probe, cell pressure probe, picoliter osmometry, and with measurements of membrane potential of cells in exuding roots should provide more information about mechanisms of root exudation, a phenomenon which seems an unresolved puzzle yet.

Author Contributions: V.V. and H.S. wrote, corrected, and finalized the manuscript. All authors have read and agreed to the published version of the manuscript.

Funding: The work of V.V. on the Manuscript was partially supported by AVF Grant 2017-2042.

Institutional Review Board Statement: Not applicable.

Informed Consent Statement: Not applicable.

Data Availability Statement: Available data are presented in the manuscript.

Acknowledgments: V.V. thanks Kenneth Shackel for critical comments and discussions during seminars which stimulated the deeper investigation of root exudation. The Authors thank Timothy J. Flowers for advising on the Manuscript before the submission and four anonymous reviewers for their valuable comments and suggestions on our manuscript.

Conflicts of Interest: The authors declare no conflict of interest.

References

1. Hales, S. *Vegetable Staticks: Or, an Account of Some Statical Experiments on the Sap in Vegetables: Being an Essay towards a Natural History of Vegetation. Also a Specimen of an Attempt to Analyse the Air, by a Great Variety of Chymo-Statical Experiments, Which Were Read at Several Meetings before the Royal Society*; W. and J. Innys: London, UK, 1727.
2. Clark, W.S. The circulation of sap in plants. *Mass. State Board Agric. Ann. Rep.* **1874**, *21*, 159–204.
3. Fisher, J.B.; Angeles, G.; Ewers, F.W.; Lòpez-Portillo, J. Survey of root pressure in tropical vines and woody species. *Int. J. Plant. Sci.* **1997**, *158*, 44–50. [CrossRef]

4. Kraus, C. Die Saftleistung der Wurzeln, besonders ihrer jüngsten Theile. I. Ueber Verbreitung und Nachweis des Blutungsdrucks der Wurzeln. *Forschungen auf dem Gebiete der Agriculturphysik* **1882**, *5*, 432–462.
5. Wieler, A. Das Bluten der Pflanzen. *Beitr. Biol. Pflanzen* **1893**, *6*, 1–211.
6. Lopushinsky, W. Occurrence of root pressure exudation in Pacific Northwest conifer seedlings. *For. Sci.* **1980**, *26*, 275–279.
7. O'Leary, J.W.; Kramer, P.J. Root pressure in conifers. *Science* **1964**, *145*, 284–285. [CrossRef]
8. White, P.R. "Root pressure"—An unappreciated force in sap movement. *Am. J. Bot.* **1938**, *25*, 223–227. [CrossRef]
9. White, P. Root-Pressure as a Factor in the Rise of Sap. *Nature* **1938**, *141*, 581–583. [CrossRef]
10. Rosene, H. Water balance in the onion roots: Relation of water intake to volume exudate of isolated roots and root segments. *Plant Physiol.* **1941**, *16*, 447–460. [CrossRef]
11. Rosene, H. Control of water transport in local root regions of attached and isolated roots by means of the osmotic pressure of the external solution. *Am. J. Bot.* **1941**, *28*, 402–410. [CrossRef]
12. O'Leary, J. Root pressure exudation from apical root segments. *Nature* **1966**, *212*, 96–97. [CrossRef]
13. Mozhaeva, L.V.; Pil'shchikova, N.V. Effect of temperature on exudation rate and several aspects of energy exchange of sunflower roots. *Izvestiya Timiryazevskoy Sel'skokhozyaistvennoi Akademii* **1969**, *4*, 14–30.
14. Mozhaeva, L.V.; Pil'shchikova, N.V. Nature of water pumping process by plant roots. *Izvestiya Timiryazevskoy Sel'skokhozyaistvennoi Akademii* **1972**, *3*, 3–15.
15. Mozhaeva, L.V.; Pil'shchikova, N.V.; Zaitseva, N.V. The study of the contractile properties of root cells in relation to rhythmicity of plant exudation. *Izvestiya Timiryazevskoy Sel'skokhozyaistvennoi Akademii* **1975**, *1*, 3–12.
16. Mozhaeva, L.V.; Pil'shchikova, N.V.; Kuzina, V.I. Study on the nature of the motive force of plant exudation with the use of chemical effects. *Izvestiya Timiryazevskoy Sel'skokhozyaistvennoi Akademii* **1979**, *1*, 3–9.
17. Miller, D.M. Studies of root function in *Zea mays*: III. Xylem sap composition at maximum root pressure provides evidence of active transport into the xylem and a measurement of the reflection coefficient of the root. *Plant Physiol.* **1985**, *77*, 162–167. [CrossRef] [PubMed]
18. Steudle, E.; Oren, R.; Schulze, E.D. (1987) Water transport in maize roots: Measurement of hydraulic conductivity, solute permeability, and of reflection coefficients of excised roots using the root pressure probe. *Plant Physiol.* **1987**, *84*, 1220–1232. [CrossRef]
19. Zholkevich, V.N. Root pressure. In *Plant Roots, the Hidden Half*; Waisel, Y., Eshel, A., Kafkafi, U., Eds.; Marcel-Dekker: New York, NY, USA, 1991; pp. 589–603.
20. Zholkevich, V.N.; Chugunova, T.V.; Korolev, A.V. New data on the nature of root pressure. *Stud. Biophys.* **1990**, *136*, 209–216.
21. Schwenke, H. *Der Mechanismus der Wurzelexsudation*; Hochschulverlag: Zurich, Switzerland, 1990; ISBN 3-8107-2233-2.
22. Schwenke, H.; Wagner, E. A new concept of root exudation. *Plant, Cell Environ.* **1992**, *15*, 289–299. [CrossRef]
23. Volkov, V.S.; Zholkevich, V.N. Exudation parameters depending on spatial orientation of root segments of *Zea mays* L. *Dokl. Akad. Nauk* **1993**, *332*, 526–528.
24. Volkov, V.; Zholkevich, V. Oppositely-directed water flows in roots with respect to the plant integral hydrodynamic system. In *Root Demographics and Their Efficiencies in Sustainable Agriculture, Grasslands and Forest Ecosystems. Developments in Plant and Soil Sciences*; Box, J.E., Ed.; Springer: Dordrecht, The Netherlands, 1998; Volume 82, pp. 623–630. [CrossRef]
25. Volkov, V.S. Investigation of oppositely directed water flows in roots as an approach to the identification of the plant's integral hydrodynamic system. *Acta Hortic.* **1998**, *458*, 247–252. [CrossRef]
26. Volkov, V.S. Peculiarities of Water Transport in Segments of *Zea mays* L. Roots. Ph.D. Thesis, K.A. Timiriazev Institute of Plant Physiology, Russian Academy of Sciences, Moscow, Russia, 1999. (In Russian).
27. Zholkevich, V.N.; Korolev, A.V. Air-dried roots as a model for studying the nature of root pressure. *Dokl. Biol. Sci.* **1995**, *344*, 481–483.
28. Zholkevich, V.N.; Chugunova, T.V. Effect of neurotransmitters on the pumping activity of plant roots. *Dokl. Biochem.* **1997**, *356*, 109–112.
29. Zholkevich, V.N.; Zubkova, N.K.; Korolev, A.V. Effect of colchicine and noradrenaline on the exudate secretion by *Helianthus annuus* L. roots in the absence of water uptake from an environment. *Dokl. Akad. Nauk.* **1998**, *359*, 551–553.
30. Zholkevich, V.N.; Puzakov, M.M.; Monakhova, O.F. The involvement of actin in the formation of root pressure. *Dokl. Biochem. Biophys.* **2001**, *380*, 332–335. [CrossRef]
31. Zholkevich, V.N.; Sushchenko, S.V.; Emel'yanova, I.B.; Monakhova, O.F. Peculiarities of root exudation in the absence of water uptake. *Dokl. Biol. Sci.* **2005**, *400*, 42–44. [CrossRef]
32. Zholkevich, V.N.; Emel'yanova, I.B.; Sushchenko, S.V. Self-oscillations of water transport in the plant root. *Dokl. Biol. Sci.* **2005**, *403*, 269–271. [CrossRef]
33. Zholkevich, V.N.; Popova, M.S.; Zhukovskaya, N.V. Stimulatory effects of adrenalin and noradrenalin on root water-pumping activity and the involvement of G-proteins. *Russ. J. Plant Physiol.* **2007**, *54*, 790–796. [CrossRef]
34. Steudle, E. Water uptake by plant roots: An integration of views. *Plant Soil* **2000**, *226*, 45–56. [CrossRef]
35. Rowan, A.; McCully, M.E.; Canny, M.J. The origin of the exudate from cut maize roots. *Plant Physiol. Biochem.* **2000**, *38*, 957–967. [CrossRef]
36. Pickard, W.F. The riddle of root pressure: II. Root exudation at extreme osmolalities. *Funct. Plant Biol.* **2003**, *30*, 135–141. [CrossRef] [PubMed]

37. Knipfer, T.; Fricke, W. Root pressure and a solute reflection coefficient close to unity exclude a purely apoplastic pathway of radial water transport in barley (*Hordeum vulgare*). *New Phytol.* **2010**, *187*, 159–170. [CrossRef] [PubMed]
38. Steudle, E.; Meshcheryakov, A.B. Hydraulic and osmotic properties of oak roots. *J. Exp. Bot.* **1996**, *47*, 387–401. [CrossRef]
39. Pedersen, O. Long-Distance water transport in aquatic plants. *Plant Physiol.* **1993**, *103*, 1369–1375. [CrossRef] [PubMed]
40. Kirschner, S. Die Theorie vom Saftkreislauf der Pflanzen. Ein Wenig Bekanntes Kapitel in der Geschichte der Pflanzenphysiologie. Habilitation Thesis, Ludwig Maximilian University of Munich, Munich, Germany, 2002.
41. Biddulph, S.; Biddulph, O. The circulatory system of plants. *Sci. Am.* **1959**, *200*, 44–49.
42. Zyalalov, A.A. Water flows in higher plants: Physiology, evolution, and system analysis. *Russ. J. Plant Physiol.* **2004**, *51*, 547–556. [CrossRef]
43. Scholander, P.F.; Love, W.E.; Kanwisher, J.W. The rise of sap in tall grapevines. *Plant Physiol.* **1955**, *30*, 93–104. [CrossRef]
44. Tyree, M.T.; Sperry, J.S. Vulnerability of xylem to cavitation and embolism. *Ann. Rev. Plant Physiol. Plant Mol. Biol.* **1989**, *40*, 19–38. [CrossRef]
45. Sperry, J.S.; Holbrook, N.M.; Zimmerman, M.H.; Tyree, M.T. Spring filling of xylem vessels in wild grapevine. *Plant Physiol.* **1987**, *83*, 414–417. [CrossRef]
46. Jansen, S.; Choat, B.; Pletsers, A. Morphological variation of intervessel pit membranes and implications to xylem function in angiosperms. *Am. J. Bot.* **2009**, *96*, 409–419. [CrossRef]
47. Choat, B.; Cobb, A.R.; Jansen, S. Tansley Review: Structure and function of bordered pits: New discoveries and impacts on whole plant hydraulic function. *New Phytol.* **2008**, *177*, 608–625. [CrossRef] [PubMed]
48. Pagay, V.; Santiago, M.; Sessoms, D.A.; Huber, E.J.; Vincent, O.; Pharkya, A.; Corso, T.N.; Lakso, A.N.; Stroock, A.D. A microtensiometer capable of measuring water potentials below -10 MPa. *Lab Chip* **2014**, *14*, 2806–2817. [CrossRef] [PubMed]
49. Lakso, A.N.; Zhu, S.; Santiago, M.; Shackel, K.; Volkov, V.; Stroock, A.D. A microtensiometer sensor to continuously monitor stem water status in woody plants—Design and field testing. *Acta Hortic. (ISHS)* **2021**, in press.
50. Tyree, M.T.; Fiscus, S.D.; Wullschleger, M.A.; Dixon, M.A. Detection of xylem cavitation in corn under field conditions. *Plant Physiol.* **1986**, *82*, 597–599. [CrossRef] [PubMed]
51. Wang, F.; Tian, X.; Ding, Y.; Wan, X.; Tyree, M.T. A survey of root pressure in 53 Asian species of bamboo. *Ann. For. Sci.* **2011**, *68*, 783–791. [CrossRef]
52. Tyree, M.T.; Salleo, S.; Nardini, A.; Lo Gullo, M.A.; Mosca, R. Refilling of embolized vessels in young stems of Laurel. Do we need a new paradigm? *Plant Physiol.* **1999**, *120*, 11–22. [CrossRef]
53. Zwieniecki, M.A.; Holbrook, N.M. Bordered pit structure and vessel wall surface properties: Implications for embolism repair. *Plant Physiol.* **2000**, *123*, 1015–1020. [CrossRef]
54. De Boer, A.H.; Volkov, V. Logistics of water and salt transport through the plant: Structure and functioning of the xylem. *Plant Cell Environ.* **2003**, *26*, 87–101. [CrossRef]
55. Zwieniecki, M.A.; Holbrook, N.M. Confronting Maxwell's demon: Biophysics of xylem embolism repair. *Trends in Plant Science* **2009**, *14*, 530–534. [CrossRef]
56. Williams, C.B.; Næsborg, R.R.; Dawson, T.E. Coping with gravity: The foliar water relations of giant sequoia. *Tree Physiol.* **2017**, *37*, 1312–1326. [CrossRef]
57. Singh, S. Guttation: Path, principles and functions. *Aust. J. Bot.* **2013**, *61*, 497–515. [CrossRef]
58. Singh, S. Root Pressure: Getting to the Root of Pressure. In *Progress in Botany*; Lüttge, U., Cánovas, F., Matyssek, R., Eds.; Springer: Cham, Germany, 2016; Volume 77, pp. 105–150. [CrossRef]
59. Singh, S. *Guttation: Fundamentals and Applications*; Cambridge University Press: Cambridge, UK, 2020. [CrossRef]
60. Dutrochet, H. *L'agent Immédiat du Mouvement Vital Dévoilé dans sa Nature et dans son Mode D'action, Chez les Végétaux et Chez les Animaux*; Dentu: Paris, France, 1826.
61. Dutrochet, H. *Mémoires Pour Servir à L'histoire Anatomique et Physiologique des Vegetaux et des Animaux*; Baillière: Paris, France, 1837.
62. Rominger, C.L. Versuche über die Saftführung der Gefässe. *Bot. Ztg.* **1843**, *1*, 177–185.
63. Brücke, E. Ueber das Bluten des Rebstockes. *Annalen der Physik und Chemie* **1844**, *63*, 177–214. [CrossRef]
64. Kraus, C. *Untersuchungen über den Säftedruck der Pflanzen*; Flora Oder Allgemeine Botanische Zeitung; Regensburgische Botanische Gesellschaft: Regensburg, Germany, 1881–1883.
65. James, W.O.; Baker, H. Sap pressure and the movements of sap. *New Phytol.* **1933**, *32*, 317–343. [CrossRef]
66. Köckenberger, W.; Pope, J.M.; Xia, Y.; Jeffrey, K.R.; Komor, E.; Callaghan, P.T. A non-invasive measurement of phloem and xylem water flow in castor bean seedlings by nuclear magnetic resonance microimaging. *Planta* **1997**, *201*, 53–63. [CrossRef]
67. Schobert, C.; Komor, E. Transport of nitrate and ammonium into the phloem and the xylem of *Ricinus communis* seedlings. *J. Plant Physiol.* **1992**, *140*, 306–309. [CrossRef]
68. Scheenen, T.W.; Vergeldt, F.J.; Heemskerk, A.M.; Van As, H. Intact plant magnetic resonance imaging to study dynamics in long-distance sap flow and flow-conducting surface area. *Plant Physiol.* **2007**, *144*, 1157–1165. [CrossRef]
69. Köckenberger, W. Functional imaging of plants by magnetic resonance experiments. *Trends Plant Sci.* **2001**, *6*, 286–292. [CrossRef]
70. Van As, H. Intact plant MRI for the study of cell water relations, membrane permeability, cell-to-cell and long distance transport. *J. Exp. Bot.* **2007**, *58*, 743–756. [CrossRef]
71. Hofmeister, W. Tabellen zu W. Hofmeisters Aufsatz über Spannung, Ausflussmenge und Ausflussgeschwindigkeit von Säften lebender Pflanzen. *Flora Oder Allgemeine Botanische Zeitung* **1862**, *45*, I–XXXIX.

72. Hocking, P.J. The composition of phloem exudate and xylem sap from tree tobacco (*Nicotiana glauca* Grah.). *Ann. Bot.* **1980**, *45*, 633–643. [CrossRef]
73. Richardson, P.T.; Baker, D.A.; Ho, L.C. The chemical composition of Cucurbit vascular exudates. *J. Exp. Bot.* **1982**, *33*, 1239–1247. [CrossRef]
74. Shelp, B.J. The composition of phloem exudate and xylem sap from broccoli (*Brassica oleracea* var. italica) supplied with NH_4^+, NO_3^- or NH_4NO_3. *J Exp. Bot.* **1987**, *38*, 1619–1636. [CrossRef]
75. Schurr, U.; Schulze, E.D. The concentration of xylem sap constituents in root exudate, and in sap from intact, transpiring castor bean plants (*Ricinus communis* L.). *Plant Cell Environ.* **1995**, *18*, 409–420. [CrossRef]
76. Urrestarazu, M.; Sanchez, A.; Lorente, F.A.; Guzman, M. A daily rhythmic model for pH and volume from xylem sap of tomato plants. *Communications in Soil Science and Plant Analysis* **1995**, *27*, 1859–1874. [CrossRef]
77. Wallace, A.; Abou-Zamzam, A.M.; Motoyama, E. Cation and anion balance in the xylem exudate of tobacco roots. *Plant Soil* **1971**, *35*, 433–438. [CrossRef]
78. Siebrecht, S.; Tischner, R. Changes in the xylem exudate composition of poplar (*Populus tremula* × *P. alba*)—dependent on the nitrogen and potassium supply. *J. Exp. Bot.* **1999**, *50*, 1797–1806. [CrossRef]
79. Clark, C.J.; Holland, P.T.; Smith, G.S. Chemical composition of bleeding xylem sap from kiwifruit vines. *Ann. Bot.* **1986**, *58*, 353–362. [CrossRef]
80. Andersen, P.C.; Brodbeck, B.V. Diurnal and temporal changes in the chemical profile of xylem exudate from *Vitis rotundifolia*. *Physiol. Plant.* **1989**, *75*, 63–70. [CrossRef]
81. Glad, C.; Regnard, J.L.; Querou, Y.; Brun, O.; Morot-Gaudry, J.F. Flux and chemical composition of xylem exudates from chardonnay grapevines: Temporal evolution and effect of recut. *Am. J. Enol. Vitic.* **1992**, *43*, 275–282.
82. Sabinin, D.A. On the root system as an osmotic apparatus. *Perm Univ. Bull.* **1925**, *4*, 1–128.
83. Ketchie, D.O.; Lopushinsky, W. *Composition of Root Pressure Exudate from Conifers*; Research Note PNW-395; USDA, Forest Service: Washington, DC, USA, 1981; pp. 1–6.
84. Nollet, J.-A. Recherches sur les causes du bouillonnement des liquides. In *Mémoires de Mathématique et de Physique, tirés des registres de l'Académie Royale des Sciences de l'année*; Imprimerie Nationale: Tournai, Belgium, 1748; pp. 57–104.
85. Hofmeister, W. Ueber Spannung, Ausflussmenge und Ausflussgeschwindigkeit von Säften lebender Pflanzen. *Flora Oder Allgemeine Botanische Zeitung* **1862**, *45*, 97–108, 113–120, 138–144, 145–152, 170–175.
86. Sachs, J. *Handbuch der Experimental-Physiologie der Pflanzen*; Engelmann: Leipzig, Germany, 1865.
87. Pfeffer, W. *Osmotische Untersuchungen. Studien zur Zellmechanik*; Engelmann: Leipzig, Germany, 1877.
88. Van't Hoff, J.M. *Die Gesetze des chemischen Gleichgewichts*; Engelmann: Leipzig, Germany, 1900.
89. Pfeffer, W. *Zur Kenntniss der Plasmahaut und der Vacuolen nebst Bemerkungen über den Aggregatzustand des Protoplasmas und über osmotische Vorgänge*; Hirzel: Leipzig, Germany, 1890.
90. Pfeffer, W. *Studien zur Energetik der Pflanze*; Hirzel: Leipzig, Germany, 1892.
91. Pfeffer, W. *Pflanzenphysiologie. Ein Handbuch der Lehre vom Stoffwechsel und Kraftwechsel in der Pflanze*, 2nd ed.; Engelmann: Leipzig, Germany, 1897; Volume 1.
92. Atkins, W.R.G. *Some Recent Researches in Plant Physiology*; Whittaker: London, UK, 1916.
93. Priestley, J.H. Further observations upon the mechanism of root pressure. *New Phytol.* **1922**, *21*, 41–47. [CrossRef]
94. Eaton, F. The osmotic and vitalistic interpretations of exudation. *Am. J. Bot.* **1943**, *30*, 663–674. [CrossRef]
95. Kramer, P.J. Physical and physiological aspects of water absorption. In *Encyclopedia of Plant Physiology, 3 (Water Relations of Plants)*; Ruhland, W., Ed.; Springer: Berlin/Göttingen/Heidelberg, Germany, 1956; pp. 124–159.
96. Marbach, S.; Bocquet, L. Osmosis, from molecular insights to large-scale applications. *Chem. Soc. Rev.* **2019**, *48*, 3102–3144. [CrossRef] [PubMed]
97. Staverman, A.J. Non-equilibrium thermodynamics of membrane processes. *Trans. Faraday Soc.* **1952**, *48*, 176–185. [CrossRef]
98. Kedem, O.; Katchalsky, A. Thermodynamic analysis of the permeability of biological membranes to non-electrolytes. *Biochim. Biophys. Acta* **1958**, *27*, 229–246. [CrossRef]
99. Kedem, O.; Katchalsky, A. A physical interpretation of the phenomenological coefficients of membrane permeability. *J. Gen. Physiol.* **1961**, *45*, 143–179. [CrossRef]
100. Kedem, O.; Katchalsky, A. Permeability of composite membranes. Part 1—Electric current, volume flow and flow of solute through membranes. *Trans. Faraday Soc.* **1963**, *59*, 1918–1930. [CrossRef]
101. Dainty, J. Water relations of plant cells. *Adv. Bot. Res.* **1963**, *1*, 279–326.
102. Van Overbeek, J. Water uptake by excised root systems of the tomato due to non-osmotic forces. *Am. J. Bot.* **1942**, *29*, 677–683. [CrossRef]
103. Anderson, W.P.; Aikman, D.P.; Meiri, A. Excised root exudation—A standing-gradient osmotic flow. *Proc. R. Soc. Lond. B Biol. Sci.* **1970**, *174*, 445–458.
104. Ginsburg, H. Model for iso-osmotic water flow in plant roots. *J. Theor. Biol.* **1971**, *32*, 147–158. [CrossRef]
105. Katou, K.; Taura, T.; Furumoto, M. A model for water transport in the stele of plant roots. *Protoplasma* **1987**, *140*, 123–132. [CrossRef]
106. Lyalin, O.O. Theory of transcellular osmosis: Reverse osmosis model of root exudation. *Fiziol. Rast. (Sov. Plant Physiol. Engl. Transl.)* **1989**, *38*, 421–434.

107. Pickard, W.F. The riddle of root pressure: I. Putting Maxwell's demon to rest. *Funct. Plant Biol.* **2003**, *30*, 121–134.
108. Enns, L.C.; McCully, M.E.; Canny, M.J. Solute concentrations in xylem sap along vessels of maize primary roots at high root pressure. *J. Exp. Bot.* **1998**, *49*, 1539–1544. [CrossRef]
109. Enns, L.C.; Canny, M.J.; McCully, M.E. An investigation of the role of solutes in the xylem sap and in the xylem parenchyma as the source of root pressure. *Protoplasma* **2000**, *211*, 183–197. [CrossRef]
110. Kundt, W.; Robnik, M. Water pumps in plant roots. *Russ. J. Plant Physiol.* **1998**, *45*, 262–269.
111. Kundt, W. The hearts of the plants. *Curr. Sci.* **1998**, *75*, 98–102.
112. Wegner, L.H. Root pressure and beyond: Energetically uphill water transport into xylem vessels? *J. Exp. Bot.* **2014**, *65*, 381–393. [CrossRef] [PubMed]
113. Wegner, L.H. A thermodynamic analysis of the feasibility of water secretion into xylem vessels against a water potential gradient. *Funct. Plant Biol.* **2015**, *42*, 828–835. [CrossRef] [PubMed]
114. Wegner, L.H. Cotransport of water and solutes in plant membranes: The molecular basis, and physiological functions. *AIMS Biophys.* **2017**, *4*, 192–209. [CrossRef]
115. Fricke, W. The significance of water co-transport for sustaining transpirational water flow in plants: A quantitative approach. *J. Exp. Bot.* **2015**, *66*, 731–739. [CrossRef] [PubMed]
116. Zeuthen, T. Molecular water pumps. *Rev.Physiol. Biochem. Pharmacol.* **2000**, *141*, 97–151. [PubMed]
117. Zeuthen, T. Water-transporting proteins. *J. Membr. Biol.* **2010**, *234*, 57–73. [CrossRef]
118. Zeuthen, T.; McAulay, N. Cotransport of water by Na^+–K^+–$2Cl^-$ cotransporters expressed in Xenopus oocytes: NKCC1 versus NKCC2. *J. Physiol.* **2012**, *590*, 1139–1154. [CrossRef]
119. Zeuthen, T.; Gorraitz, E.; Her, K.; Wright, E.M.; Loo, D.D.F. Water permeation through transporters. *Proc. Nat. Acad. Sci. USA* **2016**, *113*, E6887–E6894. [CrossRef]
120. Steudle, E.; Henzler, T. Water channels in plants: Do basic concepts of water transport change? *J. Exp. Bot.* **1995**, *46*, 1067–1076. [CrossRef]
121. Javot, H.; Maurel, C. The role of aquaporins in root water uptake. *Ann. Bot.* **2002**, *90*, 301–313. [CrossRef]
122. Gambetta, G.A.; Knipfer, T.; Fricke, W.; McElrone, A.J. Aquaporins and root water uptake. In *Plant Aquaporins. Signalling and Communication in Plants*; Chaumont, F., Tyerman, S., Eds.; Springer: Cham, Germany, 2017; pp. 133–153. [CrossRef]
123. Steudle, E.; Peterson, C.A. How does water get through roots? *J. Exp. Bot.* **1998**, *49*, 775–788. [CrossRef]
124. Blasel, D. Untersuchungen zur Wurzelexsudation an Mais, Rebe und verschiedenen Laubbaumarten. Diploma Thesis, Albert Ludwig University of Freiburg, Freiburg im Breisgau, Germany, 1991.
125. McCully, M.E. Water efflux from the surface of field-grown grass roots: Observations by cryo-scanning electron microscopy. *Physiol. Plant.* **1995**, *95*, 217–224. [CrossRef]
126. De Candolle, A.-P. *Physiologie Végétale*; Béchet Jeune: Paris, France, 1832; Volume 1.
127. Molisch, H. Über Wurzelausscheidungen und deren Einwirkung auf organische Substanzen. *Sitzungsberichte der Wiener Akademie der Wissenschaften Mathematisch-Naturwissenschaftliche Classe* **1888**, *96*, 84–109.
128. Stahl, E. *Pflanzen und Schnecken: Eine Biologische Studie über die Schutzmittel der Pflanze Gegen Schneckenfrass*; Gustav Fischer: Jena, Germany, 1888.
129. Czapek, F. Zur Lehre von den Wurzelausscheidungen. *Jahrbücher für Wissenschaftliche Botanik* **1896**, *29*, 321–390.
130. Rogers, W.S. Root Studies VIII. Apple root growth in relation to rootstock, soil, seasonal and climatic factors. *J. Pomol. Horticult. Sci.* **1940**, *17*, 99–130. [CrossRef]
131. Richardson, S.D. Root growth of *Acer pseudoplatanus* L. in relation to grass cover and nitrogen deficiency. *Mededelingen van de Landbouwhogeschool te Wageningen/Nederland* **1953**, *54*, 75–97.
132. Cailloux, M. Observations sur l'exsudation par les poils radiculaires. *Ann. ACFAS (Assoc. Can.-Fr. Av. Sci.)* **1950**, *16*, 158–162.
133. Cailloux, M. Metabolism and the absorption of water by root hairs. *Can. J. Bot.* **1972**, *50*, 557–573. [CrossRef]
134. Ahmad, M.; Cailloux, M. The effects of malonate on absorption of water by root hairs of *Avena sativa*. *Can. J. Bot.* **1971**, *49*, 521–528. [CrossRef]
135. Ahmad, M.; Cailloux, M. Effects of some respiratory inhibitors on water flux in root hairs of *Avena sativa*. *Can. J. Bot.* **1972**, *50*, 575–579. [CrossRef]
136. Head, G.C. A study of 'Exudation' from the root hairs of apple roots by time-lapse cine-photomicrography. *Ann. Bot.* **1964**, *28*, 495–498. [CrossRef]
137. Moradi, A.B.; Carminati, A.; Vetterlein, D.; Vontobel, P.; Lehmann, E.; Weller, U.; Hopmans, J.W.; Hans-Jörg Vogel, H.-J.; Oswald, S.E. Three-dimensional visualization and quantification of water content in the rhizosphere. *New Phytol.* **2011**, *192*, 653–663. [CrossRef] [PubMed]
138. Carminati, A.; Zarebanadkouki, M.; Kroener, E.; Ahmed, M.A.; Holz, M. Biophysical rhizosphere processes affecting root water uptake. *Ann. Bot.* **2016**, *118*, 561–571. [CrossRef] [PubMed]
139. Prieto, I.; Armas, C.; Pugnaire, F.I. Water release through plant roots: New insights into its consequences at the plant and ecosystem level. *New Phytol.* **2012**, *193*, 830–841. [CrossRef] [PubMed]
140. Neumann, R.B.; Cardon, Z.G. The magnitude of hydraulic redistribution by plant roots: A review and synthesis of empirical and modeling studies. *New Phytol.* **2012**, *194*, 337–352. [CrossRef] [PubMed]

141. Meunier, M.; Rothfuss, Y.; Raynaud, T.B.; Biron, P.; Richard, P.; Durand, J.-L.; Couvreur, V.; Vanderborght, J.; Javaux, M. Measuring and modeling hydraulic lift of *Lolium multiflorum* using stable water isotopes. *Vadose Zone J.* **2017**, *17*, 1–15. [CrossRef]
142. Richards, J.H.; Caldwell, M.M. Hydraulic lift: Substantial nocturnal water transport between soil layers by *Artemisia tridentate* roots. *Oecologia* **1987**, *73*, 486–489. [CrossRef]
143. Caldwell, M.; Dawson, T.; Richards, J. Hydraulic lift: Consequences of water efflux from the roots of plants. *Oecologia* **1998**, *113*, 151–161. [CrossRef]
144. Schulze, E.-D.; Caldwell, M.M.; Canadell, J.; Mooney, H.A.; Jackson, R.B.; Parson, D.; Scholes, R.; Sala, O.E.; Trimborn, P. Downward flux of water through roots (i.e., Inverse hydraulic lift) in dry Kalahari sands. *Oecologia* **1998**, *115*, 460–462. [CrossRef]
145. Burgess, S.S.O.; Adams, M.A.; Turner, N.C.; Ong, C.K. 1998. The redistribution of soil water by tree root systems. *Oecologia* **1998**, *115*, 306–311. [CrossRef]
146. Breazeale, J.F.; Crider, F.J. Plant association and survival, and the build-up of moisture in semi-arid soils. *Tech. Bull. Univ. Ariz.* **1934**, *53*, 95–123.
147. Gessner, F. Die Wasseraufnahme durch Blätter und Samen. In *Encyclopedia of Plant Physiology, 3 (Water Relations of Plants)*; Ruhland, W., Ed.; Springer: Berlin/Göttingen/Heidelberg, Germany, 1956; pp. 215–246.
148. Smart, D.R.; Carlisle, E.; Goebel, M.; Núñez, B.A. Transverse hydraulic redistribution by a grapevine. *Plant Cell Environ.* **2005**, *28*, 157–166. [CrossRef]
149. Emerman, S.H. Towards a theory of hydraulic lift in trees and shrubs. In *Sixteenth American Geophysical Union Hydrology Days*; Morel-Seytoux, H.J., Ed.; Hydrology Days Publication: Atherton, CA, USA, 1996; pp. 147–157.
150. Cardon, Z.G.; Stark, J.M.; Herron, P.M.; Rasmussen, J.A. Sagebrush carrying out hydraulic lift enhances surface soil nitrogen cycling and nitrogen uptake into inflorescences. *Proc. Natl. Acad. Sci. USA* **2013**, *110*, 18988–18993. [CrossRef] [PubMed]
151. White, J.C.; Liste, H.H. Plant hydraulic lift of soil water—Implications for crop production and land restoration. *Plant Soil* **2008**, *313*, 1–17.
152. Izumi, Y.; Okaichi, S.; Awala, S.K.; Kawato, Y.; Watanabe, Y.; Yamane, K.; Iijima, M. Water supply from pearl millet by hydraulic lift can mitigate drought stress and improve productivity of rice by the close mixed planting. *Plant Prod. Sci.* **2018**, *21*, 8–15. [CrossRef]
153. Zhu, L.; Wang, T.T.; Zhao, X.L.; Qi, Y.S.; Xu, X. Study on the hydraulic lift of *Medicago sativa* and *Astragalus laxmannii* and its effect on their neighborhood plants. *Chin. J. Plant Ecol.* **2020**, *44*, 752–762. [CrossRef]
154. Bais, H.P.; Weir, T.L.; Perry, L.G.; Gilroy, S.; Vivanco, J.M. The role of root exudates in rhizosphere interactions with plants and other organisms. *Ann. Rev. Plant Biol.* **2006**, *57*, 233–266. [CrossRef]
155. Badri, D.V.; Vivanco, J.M. Regulation and function of root exudates. *Plant Cell Environ.* **2009**, *32*, 666–681. [CrossRef]
156. Han, Q.Q.; Lü, X.P.; Bai, J.P.; Qiao, Y.; Paré, P.W.; Wang, S.M.; Zhang, J.L.; Wu, Y.N.; Pang, X.P.; Xu, W.B.; et al. Beneficial soil bacterium *Bacillus subtilis* (GB03) augments salt tolerance of white clover. *Front. Plant Sci.* **2014**, *5*, 525:1–525:8. [CrossRef]
157. Canarini, A.; Kaiser, C.; Merchant, A.; Richter, A.; Wanek, W. Root exudation of primary metabolites: Mechanisms and their roles in plant responses to environmental stimuli. *Front. Plant Sci.* **2019**, *10*, 157:1–157:19, Correction in *Front Plant Sci.* **2019**, *10*, 420. [CrossRef]
158. Dietz, S.; Herz, K.; Gorzolka, K.; Jandt, U.; Bruelheide, H.; Scheel, D. Root exudate composition of grass and forb species in natural grasslands. *Sci. Rep.* **2020**, *10*, 10691:1–10691:15. [CrossRef] [PubMed]
159. Korenblum, E.; Dong, Y.; Szymanski, J.; Panda, S.; Jozwiak, A.; Massalha, H.; Meir, S.; Rogachev, I.; Aharoni, A. Rhizosphere microbiome mediates systemic root metabolite exudation by root-to-root signaling. *Proc. Natl. Acad. Sci. USA* **2020**, *117*, 3874–3883. [CrossRef] [PubMed]
160. Sun, L.; Ataka, M.; Han, M.; Han, Y.; Gan, D.; Xu, T.; Guo, Y.; Zhu, B. Root exudation as a major competitive fine-root functional trait of 18 coexisting species in a subtropical forest. *New Phytol.* **2021**, *229*, 259–271. [CrossRef] [PubMed]
161. Williams, A.; de Vries, F.T. Plant root exudation under drought: Implications for ecosystem functioning. *New Phytol.* **2020**, *225*, 1899–1905. [CrossRef]
162. Solov'ev, V.A.; Verenchikov, S.P. Characterization of xylem exudate obtained without shoot detachment. *Fiziol. Rast. (Sov. Plant Physiol. Engl. Transl.)* **1987**, *34*, 554–559.
163. Ionenko, I.F.; Zyalalov, A.A. Effect of potassium and abscisic and indole-3-acetic acids on maize root xylem exudation and potassium efflux. *Biol. Plant.* **1999**, *42*, 137–141. [CrossRef]
164. Stevens, C.L.; Eggert, R.L. Observations on the causes of flow of sap in red maple. *Plant Physiol.* **1945**, *20*, 636–648. [CrossRef]
165. Marvin, J.W.; Greene, M.T. Temperature induced sap flow in excised stems of Acer. *Plant Physiol.* **1951**, *26*, 565–580. [CrossRef]
166. Ewers, F.W.; Améglio, T.; Cochard, H.; Martignac, M.; Vandame, M.; Bodet, C.; Cruiziat, P. Seasonal variation of xylem pressure in walnut trees: Root and stem pressure. *Tree Physiol* **2001**, *21*, 1123–1132. [CrossRef]
167. Hamilton, E.S.; Schlegel, A.M.; Haswell, E.S. United in diversity: Mechanosensitive ion channels in plants. *Ann. Rev. Plant. Biol.* **2015**, *66*, 113–137. [CrossRef]
168. Basu, D.; Haswell, E.S. Plant mechanosensitive ion channels: An ocean of possibilities. *Curr. Opin. Plant Biol.* **2017**, *40*, 43–48. [CrossRef] [PubMed]
169. Henderson, S.; Wege, S.; Gilliham, M. Plant cation-chloride cotransporters (CCC): Evolutionary origins and functional insights. *Int. J. Mol. Sc.* **2018**, *19*, 492. [CrossRef]

170. Tran, D.; Galletti, R.; Neumann, E.D.; Dubois, A.; Sharif-Naeini, R.; Geitmann, A.; Frachisse, J.-M.; Hamant, O.; Ingram, G.C. A mechanosensitive Ca^{2+} channel activity is dependent on the developmental regulator DEK1. *Nat. Commun.* **2017**, *8*, 1009. [CrossRef] [PubMed]
171. Benitez-Alfonso, Y.; Faulkner, C.; Pendle, A.; Miyashima, S.; Helariutta, Y.; Maule, A. Symplastic intercellular connectivity regulates lateral root patterning. *Dev. Cell.* **2013**, *26*, 136–147. [CrossRef] [PubMed]
172. White, P.R.; Schuler, E.; Kern, J.R.; Fuller, F.H. "Root pressure" in gymnosperms. *Science* **1958**, *128*, 308–309. [CrossRef]
173. Rhizopoulou, S.; Wagner, E. Probing short-term root exudation in *Zea mays*. *Environ. Exp. Bot.* **1998**, *40*, 229–235. [CrossRef]
174. Bose, J.C. *The Motor Mechanism of Plants*; Longmans, Green: London, UK, 1928.
175. Martinac, B.; Cox, C.D. Mechanosensory transduction: Focus on ion channels. In *Reference Module in Life Sciences*; Elsevier: Amsterdam, The Netherlands, 2017; 46p, ISBN 978-012-809-633-8. [CrossRef]
176. Han, X.; Zhang, C.; Wang, C.; Huang, Y.; Liu, Z. Gadolinium inhibits cadmium transport by blocking non-selective cation channels in rice seedlings. *Ecotoxicol Environ Saf.* **2019**, *179*, 160–166. [CrossRef]
177. Quiquampoix, H.; Ratcliffe, R.G.; Ratkovic, S.; Vucinic, Z. Proton and phosphorus-31 NMR investigation of gadolinium uptake in maize roots. *J. Inorganic Biochem.* **1990**, *38*, 265–276. [CrossRef]
178. Millet, B.; Pickard, B.G. Gadolinium ion is an inhibitor suitable for testing the putative role of stretch-activated ion channels in geotropism and thigmotropism. *Biophys. J.* **1998**, *53*, 155a.
179. Lee, E.; Santana, B.V.N.; Samuels, E.; Benitez-Fuente, F.; Corsi, E.; Botella, M.A.; Perez-Sancho, J.; Vanneste, S.; Friml, J.; Macho, A.; et al. Rare earth elements induce cytoskeleton-dependent and PI4P-associated rearrangement of SYT1/SYT5 endoplasmic reticulum–plasma membrane contact site complexes in *Arabidopsis*. *J. Exp. Bot.* **2020**, *71*, 3986–3998. [CrossRef]
180. Lane, J.W.; McBride, D.W., Jr.; Hamill, O.P. Amiloride block of the mechanosensitive cation channel in Xenopus oocytes. *J. Physiol.* **1991**, *441*, 347–366. [CrossRef] [PubMed]
181. Moran, N.; Fox, D.; Satter, R.L. Interaction of depolarization-activated K^+ channel of *Samanea saman* with inorganic ion: A patch-clamp study. *Plant Physiol.* **1990**, *94*, 424–431. [CrossRef] [PubMed]
182. Smith, I.W.M. The temperature-dependence of elementary reaction rates: Beyond Arrhenius. *Chem. Soc. Rev.* **2008**, *37*, 812–826. [CrossRef] [PubMed]
183. Volkov, V. Quantitative description of ion transport via plasma membrane of yeast and small cells. *Front. Plant Sci.* **2015**, *6*, 425. [CrossRef]
184. Loo, D.D.; Wright, E.M.; Zeuthen, T. Water pumps. *J. Physiol.* **2002**, *542 Pt 1*, 53–60. [CrossRef]
185. Ramos, R.S.; Caldeira, M.T.; Arruda, P.; De Meis, L. The two Km's for ATP of corn-root H^+-ATPase and the use of Glucose-6-Phosphate and Hexokinase as an ATP-Regenerating System. *Plant Physiol.* **1994**, *105*, 853–859. [CrossRef]
186. Steffensen, A.B.; Oernbo, E.K.; Stoica, A.; Gerkau, N.J.; Barbuskaite, D.; Tritsaris, K.; Rose, C.R.; MacAulay, N. Cotransporter-mediated water transport underlying cerebrospinal fluid formation. *Nat. Commun.* **2018**, *9*, 2167:1–2167:13. [CrossRef]

plants

MDPI

Article

The Effect of Silicon on Osmotic and Drought Stress Tolerance in Wheat Landraces

Sarah J. Thorne [1], Susan E. Hartley [2] and Frans J. M. Maathuis [1,*]

[1] Department of Biology, University of York, York YO10 5DD, UK; st945@york.ac.uk
[2] Department of Animal and Plant Sciences, University of Sheffield, Sheffield S10 2TN, UK; s.hartley@sheffield.ac.uk
* Correspondence: frans.maathuis@york.ac.uk

Abstract: Drought stress reduces annual global wheat yields by 20%. Silicon (Si) fertilisation has been proposed to improve plant drought stress tolerance. However, it is currently unknown if and how Si affects different wheat landraces, especially with respect to their innate Si accumulation properties. In this study, significant and consistent differences in Si accumulation between landraces were identified, allowing for the classification of high Si accumulators and low Si accumulators. Landraces from the two accumulation groups were then used to investigate the effect of Si during osmotic and drought stress. Si was found to improve growth marginally in high Si accumulators during osmotic stress. However, no significant effect of Si on growth during drought stress was found. It was further found that osmotic stress decreased Si accumulation for all landraces whereas drought increased it. Overall, these results suggest that the beneficial effect of Si commonly reported in similar studies is not universal and that the application of Si fertiliser as a solution to agricultural drought stress requires detailed understanding of genotype-specific responses to Si.

Keywords: silicon fertiliser; wheat; osmotic stress; drought stress; landraces; genotypic variation

Citation: Thorne, S.J.; Hartley, S.E.; Maathuis, F.J.M. The Effect of Silicon on Osmotic and Drought Stress Tolerance in Wheat Landraces. *Plants* **2021**, *10*, 814. https://doi.org/10.3390/plants10040814

Academic Editor: Vadim Volkov

Received: 25 March 2021
Accepted: 19 April 2021
Published: 20 April 2021

1. Introduction

Wheat is the primary source of calories for 30% of the world population [1], with over 765 million tonnes of wheat produced globally in 2019 [2]. However, drought causes average global yield losses of ≈20% for wheat [3]. Anthropogenic climate change is predicted to induce changes in global precipitation patterns, with droughts likely to become more frequent in some areas, further exacerbating yield losses [4,5]. The impacts of abiotic stresses such as drought may be exacerbated by the focus of crop domestication on optimising yields at the expense of reduced stress tolerance and genetic diversity [6]. Current mitigation strategies include crop irrigation, but this often results in soil salinisation [7], and breeding for increased drought tolerance, particularly by using the genetic diversity of landraces to breed cultivars with improved drought tolerance [8]. However, breeding approaches are slow, labour intensive and complicated by genotype-environment interactions [9].

Silicon (Si) is the second most abundant element in the earth's crust [10]. Although not considered an essential element in plants, Si accumulation has been linked to improved growth, especially in plants under stress [11]. However, plants only absorb Si as silicic acid, which is often limited in the soil [12]. In grasses, silicic acid is transported through the roots by the action of two transporters: Lsi1 and Lsi2 [13]. While most silicic acid is transported to the shoots, some is deposited in the roots, predominantly in the tangential and radial walls of endo- and exodermal tissues [14,15]. The majority of absorbed Si passes through the transpiration stream to the shoots [16]. In rice, the Si transporters Lsi2, Lsi3 and Lsi6 are involved in unloading silicic acid out from the xylem into the shoot [17]. High levels of silicic acid in the shoot cause its autopolymerisation into silica [18]. Deposited silica can be found in the form of phytoliths, silicified spines and surface structures, which occur in a

range of shoot tissues [19,20]. Silica also accumulates in or beneath the cuticle layer of the cell wall in epidermal cell layers and tissues that surround the vasculature [18,21–23].

Si fertilisation may improve drought tolerance, although the exact underpinning mechanisms are unknown [24]. Drought stress induces oxidative damage [25], and Si fertilisation has been shown to reduce oxidative damage, notably by increasing antioxidative enzyme activity [26–28]. Additionally, Si fertilisation can improve water use efficiency during drought stress [28–30], for example, via an increase in stomatal conductance, which in turn improves the photosynthetic rate [31–33]. In contrast, other studies showed improved water use efficiency linked to lower transpiration, which may occur via reduction in cuticular water conductance [34,35].

Most studies on wheat report that Si increases growth and yield under drought stress [28,36–38], although there are others reporting no significant effect either in wheat [39] or in other species [40,41]. The inconsistent nature of the observed Si effects may reflect variation in plant species and genotype, as has been found for understanding the Si effect on herbivory tolerance [20,42,43]. For example, genotypic variability in Si accumulation is likely to affect the Si response, and while many studies assessed the effect of Si on cultivars that differ in drought tolerance [44–46], there is a clear lack of studies examining the effect of Si on drought tolerance in a larger range of genotypes, particularly those that vary in Si accumulation.

Although there is increasing interest in the use of local landraces in crop breeding programs to improve stress tolerance [8,47], to date, only a few studies have used landraces to investigate the effect of Si on osmotic and drought stress in wheat [48,49]. In this study, whether there are consistent differences in Si accumulation between wheat landraces was assessed. Whether there is a different effect of Si on osmotic and drought stress in landraces with relatively high Si content compared to those with lower Si content was then examined. It was hypothesised that the impact of Si on stress tolerance in landraces depends on their capacity to accumulate Si.

2. Materials and Methods

2.1. Plant Material, Experimental Design and Growth Conditions

2.1.1. Wheat Diversity Panel

A diversity panel of 98 *Triticum aestivum* landraces, which is part of the 350 landraces YoGI biodiversity panel (Harper, unpublished data), was used. The panel was formed using material from the following collections: The International Maize and Wheat Improvement Center (CIMMYT), Mexico; Crop Research Institute, Prague; and John Innes Germplasm Resource Unit, the Biotechnology and Biological Sciences Research Council Designing Future Wheat programme. A full list of landraces is available in Table S1 in the Supplementary Materials.

2.1.2. Growth of Wheat in Compost

Seeds for each *T. aestivum* landrace were planted in 500 mL pots filled with F2 + S compost (Levington) and placed in controlled glasshouse (15–20 °C, 16:8 hr light:dark). Prior to seed planting, pots filled with compost were treated with Calypso insecticide (Bayer) according to the manufacturer's instructions. One week after germination, the seedlings were thinned to 2 plants per pot. The plants were grown in the glasshouse for 7 weeks and watered as required with tap water. The plants were cultivated with or without Si fertilisation. For plants grown with Si, the plants received 100 mL 1.5 mM sodium metasilicate (Sigma-Aldrich, St. Louis, MO, USA) twice weekly, starting one week after germination and continuing for 42 days when the shoots were sampled. All experiments consisted of four temporally separate replicates, with at least two weeks between experiments, apart from the screen using the diversity panel, which consisted of three replicates. Each replicate consisted of one plant per landrace per treatment. At harvest, the shoot fresh weight was recorded, the plants were oven-dried at 70 °C for 72 h to obtain shoot dry weights, and shoot Si concentration was measured as described below.

2.1.3. Growth of Wheat in Hydroponics

The seeds of landraces were germinated in the glasshouse in sand for 10–11 days, and then, the seedlings were transferred to 9 L hydroponics boxes, filled with 1/2 strength Hoagland's solution supplemented with Si as indicated. The pH was adjusted to 5.6–6.0 using 1 M HCl or 0.1 M KOH. For Si fertilisation, sodium metasilicate (Sigma-Aldrich, St. Louis, MO, USA) was added to achieve final Si concentrations of 0.2, 0.9 or 1.8 mM. Across all levels of Si availability, sodium chloride was used to balance sodium levels. The nutrient solution was changed every 3–4 days. The hydroponics boxes were aerated throughout the experiment. The plants were grown under controlled glasshouse conditions (15–20 °C, 16:8 hr light:dark) and sampled 6 weeks after germination. At the end of the experiment, the roots were washed in deionised water and the shoot and root fresh weights were recorded. The plants were oven-dried at 70°C for 72 h to obtain dry weights. The shoot and root Si concentrations were measured as described below.

2.1.4. Imposition of Stress Conditions

To impose osmotic stress, the hydroponically grown plants were exposed to 8% (*w/v*) polyethylene glycol-(PEG)6000 (Sigma-Aldrich, St. Louis, MO, USA), which was calculated to have an osmotic pressure of −0.12 MPa [50]. The plants were treated for 4 weeks, and the experiment was composed of four replicates, with a minimum of two weeks between replicates.

Drought stress was applied to the soil-grown plants by withholding watering until 40% field capacity (FC) was achieved. All plants were then watered as required to maintain the soil moisture at either control (100% FC) or drought (40% FC) levels. The soil moisture content was checked using a soil moisture probe (ML3 ThetaProbe Soil Moisture Sensor, delta-T). The plants were harvested 6 weeks after sowing. Four replicates were performed, with a minimum of two weeks between replicates and two plants per landrace per treatment per replicate.

2.2. Silicon Measurements

Shoot and root Si concentrations were measured by portable X-ray fluorescence spectroscopy (P-XRF) using the method described in Reidinger et al. [51]. The dried leaf material was ball-milled (Retsch MM400 Mixer mill, Haan, Germany), and the ground material was pressed at 10 tons into pellets using a manual hydraulic press with a 13 mm die (Specac, Orpington, UK). Si analysis (% Si dry weight) was performed using a commercial P-XRF instrument (Nitron XL3t900 GOLDD analyser: Thermo Scientific Winchester, UK) held in a test stand (SmartStand, Thermo Scientific, Winchester, UK). The P-XRF machine was calibrated using Si-spiked synthetic methyl cellulose (Sigma-Aldrich, product no. 274429) and validated using Certified Reference Materials of NCS DC73349 'Bush branches and leaves' obtained from the China National Analysis Center for Iron and Steel. To avoid signal loss by air absorption, the analyses were performed under a helium atmosphere [50]. A reading of each side of the pellet was taken approximately one hour apart to account for u-drift in the instrument (i.e., variation in readings between consecutive runs using identical parameters [52]). The two readings were averaged to estimate the Si concentration (%).

2.3. Statistical Analysis

All statistical analyses were performed using R software [53] (version 3.6.1). Three-way analysis of variance (ANOVA) was used to test the effect of Si fertilisation, stress treatment, and landrace or accumulation type on Si concentration, dry weight and stress tolerance. Stress tolerance in non-fertilised and Si fertilised conditions was calculated as the ratio of growth of stressed plants compared to control plants (Stress/Control and Stress + Si/Control + Si, respectively). In all ANOVAs, temporal replicate was included as a factor to account for variation caused by plants that were grown at different times. Data normality was checked using Shapiro tests, and homogeneity of variance was tested using Levene's tests. Dry weights and stress tolerance were log transformed, and Si concentration was

logit transformed to satisfy the test assumptions. Post hoc Tukey's HSD tests were used when significant interaction terms were present.

3. Results

3.1. Variation in Si Concentration in a Wheat Diversity Panel and Selection of High and Low Accumulators

The 98 landraces were grown in compost and ranked according to their shoot Si levels for both the non-fertilised and Si fertilised conditions. The 10 highest and 10 lowest scoring landraces were then cultivated in hydroponics to control the Si supply more accurately and to assess whether ranking was consistent across growing systems and the amount of Si supplied to the growth medium. These combined analyses allowed for identification of five landraces that consistently showed relatively high and five landraces that consistently showed relatively low shoot Si accumulation for compost grown plants (Figure 1a) and hydroponically grown plants (Figure 1b). Furthermore, the plants from hydroponics showed that the shoot accumulation pattern was reproduced in root tissue (Figure 1b). Based on these data, a 'high' or 'low' Si accumulation type was assigned to each of the 10 landraces.

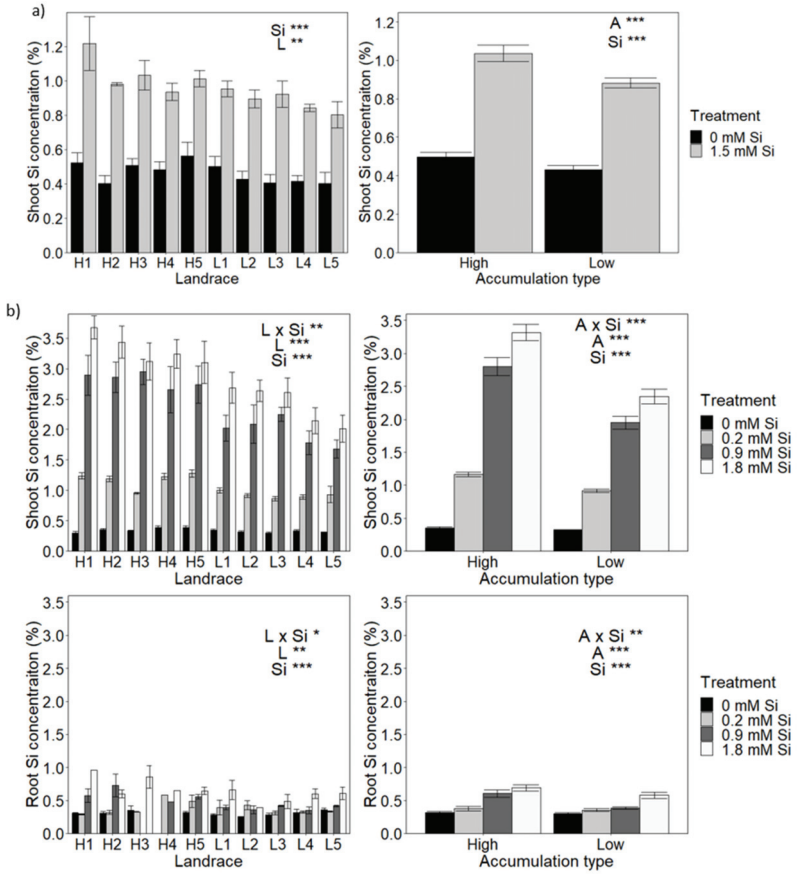

Figure 1. Variation in Si accumulation among selected wheat landraces. Ten wheat landraces were grown in (**a**) compost or (**b**) hydroponically with varying levels of Si fertilisation. Si level was measured for each landrace (left-hand panels). Average Si values, after classification into high and low Si accumulators, are shown in the right-hand panels. Statistically significant impacts and interactions, determined by 3-way ANOVA, are indicated in each panel, where *** $p < 0.001$, ** $p < 0.01$ and * $p < 0.05$. Mean values ± SE are shown. N = 3. L: Landrace, A: accumulation type, Si: level of Si fertilisation.

When cultivated in compost, shoot Si concentration in the selected 10 landraces was significantly affected by both landrace and Si fertilisation, but no interaction was found between these variables (Figure 1a; Table S2 in the Supplementary Materials). When grown with Si, the average Si concentration for the five high Si landraces was 1.04% compared to 0.88% for the five low Si landraces, a small but significant difference between accumulation types (Figure 1a; Table S2).

For hydroponically grown plants, Si fertilisation, landrace and the interaction between these factors, all had significant effects on shoot as well as root Si concentrations (Figure 1b; Table S2). The same pattern of significant effects on shoot and root Si contents were found for accumulation type (Figure 1b; Table S2). Thus, high accumulators not only accumulate more Si but also are more responsive to Si addition. For example, high accumulators showed bigger increases in Si uptake in response to 0.9 mM Si than low accumulators (Figure 1b). Shoot Si concentrations were higher in hydroponic-grown plants than in compost-grown ones, and the difference between high and low accumulators was greater, with an average of 3.24% Si for high accumulators grown in 1.8 mM Si compared to 2.35% Si for low accumulators.

3.2. The Effect of Accumulation Type and Si Supply on Plant Growth during Osmotic Stress

Osmotic stress, Si fertilisation and accumulation type significantly affected shoot dry weight (Table S3). Si improved shoot biomass when plants were exposed to PEG for the high accumulation type only, and the effect of Si fertilisation was relatively small (Figure 2a).

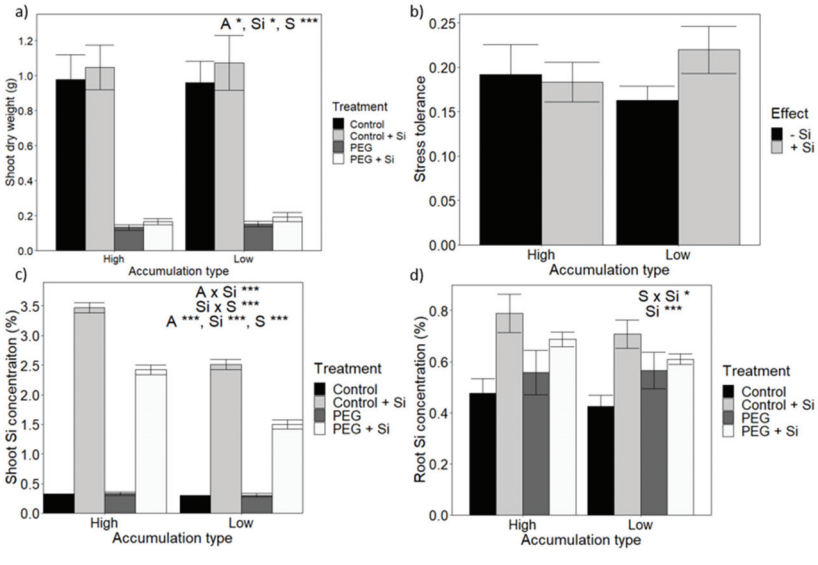

Figure 2. The impact of Si fertilisation on wheat osmotic stress tolerance according to Si accumulation type. (**a**) Shoot dry weight (DW). (**b**) Growth data were normalised to express 'Stress tolerance', defined as the ratio between shoot growth under osmotic stress compared to the control. (**c**) Shoot Si concentration. (**d**) Root Si concentration. Statistically significant impacts and interactions, determined by 3-way ANOVA, are indicated in each panel, where *** $p < 0.001$, ** $p < 0.01$ and * $p < 0.05$. Mean values ± SE are shown. N = 4. L: Landrace, A: accumulation type, Si: level of Si fertilisation, S: osmotic stress treatment.

To facilitate comparisons between high and low Si accumulators, growth data were normalised and expressed as 'Stress tolerance', defined as the ratio of growth during stress compared to growth in the control. The stress tolerance was calculated separately for

–Si and +Si plants. Neither Si fertilisation nor Si accumulation type significantly affected osmotic stress tolerance (Figure 2b).

As can be seen in Figure 2c,d, during osmotic stress, the high and low Si accumulation traits were preserved, with significantly higher shoot and root Si levels for the high Si accumulators. Interestingly, for plants that were Si fertilised, an imposition of osmotic stress itself led to a large reduction in shoot, but not root, Si concentration relative to the results for the non-stressed plants.

Overall, no impact of Si on stress tolerance was observed in either the high or low Si accumulators. This lack of response may be due to the fact that Si impact is insignificant in all of the lines or because the positive Si effect of one line is cancelled by the negative response of another. However, Figure S1 shows that, across all the landraces, there was no significant effect of Si on stress tolerance in any of the landraces, ruling out the latter explanation.

3.3. The Effect of Accumulation Type and Si Supply on Growth during Drought Stress

Osmotic stress applied using chemical agents such as PEG is frequently applied to plants to mimic physiological drought. Such hydroponics-based assays have the advantage of exposing plants to a better controlled and less complex growth substrate and allows access to roots. However, genuine drought stress, i.e., water deficit, better simulates real field conditions. Furthermore, responses to osmotic and drought stress can be very different [54,55]. This study was therefore repeated using compost-grown wheat where water deficits could be applied.

Drought stress (i.e., 40% FC) significantly the lowered shoot dry weight by around 50% (Figure 3a). This reduction in biomass was the same for both high and low Si accumulators, and the addition of Si did not significantly alter the observed pattern (Table S4).

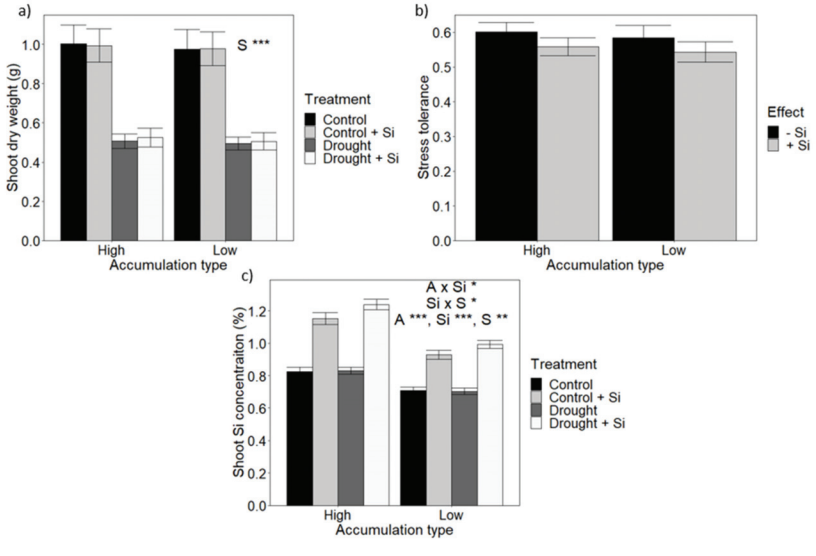

Figure 3. The impact of Si fertilisation on wheat drought stress tolerance. (**a**) Shoot dry weight (DW). (**b**) Growth data were normalised to express 'Stress tolerance', defined as the ratio between shoot growth under drought stress compared to the control. (**c**) Shoot Si concentration. Statistically significant impacts and interactions, determined by 3-way ANOVA, are indicated in each panel, where *** $p < 0.001$, ** $p < 0.01$ and * $p < 0.05$. Mean values ± SE are shown. N = 20. L: Landrace, A: accumulation type, Si: level of Si fertilisation, S: drought stress treatment.

In addition to the effect of Si on absolute growth, the Si effect on stress tolerance was investigated. Stress tolerance (Figure 3b) was the same in high and low Si accumulators; Si fertilisation did not have a significant effect on tolerance to drought stress.

Figure 3c shows that, for compost-grown plants in all four Si × drought treatments, the high accumulators had higher levels of shoot Si than the low accumulators. Furthermore and in contrast to the findings here for osmotic stress, when water availability was lowered, it caused an increase in shoot Si levels of Si fertilised plants (Figure 3c). This increase was larger for the high Si accumulators compared to the low Si accumulators.

As with osmotic stress, the effect of Si on stress tolerance on each landrace was investigated to verify that the lack of Si response was not the result of positive effects in some landraces being cancelled by negative effects in other landraces. There was no significant effect of Si on stress tolerance for any individual landrace (Figure S2).

4. Discussion

Si fertilisation could be a cost-effective method to mitigate water stress in crops. However, reports on its efficacy vary widely and uncertainty regarding the underpinning mechanisms remain. An important question in this regard is whether and how variation in plant Si accumulation relates to Si impact on plant growth during water stress. Previous studies have investigated the differences in Si accumulation between genotypes [20,56,57] and the effect of Si accumulation on growth, including yield. For example, Merah et al. [48] found no significant correlation between Si content and grain yield among 10 durum wheat genotypes. However, to our knowledge, no studies have correlated the differences in Si accumulation with differences in stress tolerance. To address this question, whether there is a different effect of Si on osmotic and drought stress in landraces with high Si content compared to those with low Si content was examined.

In spite of the significant differences in both shoot and root Si contents between the low and high accumulator groups (Figure 1) and with the exception of a small growth improvement for PEG-treated high accumulators (Figure 2), no difference in growth or stress tolerance was observed between accumulator types irrespective of treatment (Figures 2 and 3). A similar conclusion is arrived at when investigating Si impact on individual landraces. Thus, these findings do not corroborate wheat studies that found that Si improves growth under osmotic [58] and drought stress [28,36–38]. Nevertheless, other studies on osmotic and drought-stressed wheat did not report a significant increase in shoot dry weight biomass [39,59]. Furthermore, a lack of response to Si has also been reported for many other crop species. For example, Ruppenthal et al. [60] reported that Si did not improve growth during drought in soybean, although Si did reduce membrane damage and increased peroxidase activity. In the case of barley, osmotic stress led to a rise in tissue Si but it did not alter biomass [40,41], and a similar result was reported in tall fescue [34].

These disparities may be (partly) due to methodological aspects; for instance, many studies used Na or K silicate as the Si treatment but failed to correct for cation concentrations in the control treatment. Hence, it is likely that the observed Si response is in fact due to extra Na or K fertilisation. Interpretational divergence is another potential source of confusion; many studies report a positive impact of Si on tolerance to osmotic or drought stress, when in reality, the effects of Si are already obvious in control treatments and hence are not stress specific.

Genotype-specific Si responses could be another important factor; Hu et al. [61] found that the positive effect of Si on growth in poinsettia under control conditions was cultivar dependent. In sugarcane, the effect of Si under water-deficit conditions varied among cultivars, with a significant positive effect on dry weight observed in only one out of four tested cultivars [62]. Similar, genotype-specific effects of Si under drought stress have also been found when investigating 12 sunflower cultivars [63]. In wheat, Sapre and Vakharia [64] found variation both in the physiological response to osmotic stress and in Si accumulation among 10 wheat cultivars.

Clearly, there is great, genotype-dependent variability in the Si effects, and this could go some way in explaining the lack of responses to Si within an accumulation type if positive and negative changes in stress tolerance for individual landraces tend to cancel each other. This possibility was tested by examining the responses of individual landraces to Si: the impact of Si fertilisation on stress tolerance did vary between landraces from around 25 to +40% during osmotic stress (Figure S1) and from around −30 to +10% during drought (Figure S2), but none of these changes was significant.

Since Si fertilization did not change the stress tolerance, the hypothesis that Si correlates with tissue Si contents could not be properly tested. However, interesting interactions between stress and tissue Si content were found; during osmotic stress, the levels of Si in shoots were greatly reduced, whereas after exposure to drought, the opposite was observed, i.e., Si content increased. These effects were observed consistently across most landraces. Decreased Si accumulation in response to osmotic stress imposed using PEG has been previously reported [41,60,61,65]. Additionally, studies in both wheat [28,66] and other species have reported decreased Si accumulation during drought stress [29,67,68]. Nevertheless, increased Si during drought, as found in this study, has also been reported in the literature [30,69]. It is not clear what, if any, the physiological relevance is of these processes and whether they are part of a mechanistic link between Si accumulation and stress response. The similarity in physiological responses to osmotic and drought stress would, perhaps naively, suggest parallel changes in the accumulation of Si in response to both conditions, though they may be species dependent.

5. Conclusions

In this study, it was shown that wheat landraces varied significantly and consistently in their Si accumulation, such that two groups, high Si accumulators and low Si accumulators, could be identified. Osmotic stress decreased the Si content in both accumulation types whereas drought increased it. However, no significant effect of Si on growth during drought stress was found, and Si was found to improve growth only slightly in high Si accumulators during osmotic stress. The failure reported here to observe clear positive effects of Si suggest that, for wheat, any mitigation of the impacts of water stress by Si is limited. Further research is required to establish whether modern cultivars exhibit a more positive response toward Si fertilization compared to the landraces used in this study.

Supplementary Materials: The following are available online at https://www.mdpi.com/2223-7747/10/4/814/s1, Figure S1: The impact of Si fertilisation on individual wheat landraces under osmotic stress, Figure S2: The impact of Si fertilisation on individual wheat landraces under drought stress, Table S1: Shoot Si concentrations for the 98 landrace diversity panel, Table S2: ANOVA for the effect of Si fertilisation, for landrace or Si accumulation type, and for their interactions on the tissue Si contents of plants grown in compost or hydroponics, Table S3: ANOVA for osmotic stress, Si fertilisation and Si accumulation type and for their interactions on shoot dry weight, Si concentration and stress tolerance in hydroponic-grown plants, Table S4: ANOVA for osmotic stress, Si fertilisation and Si accumulation type and for their interactions on shoot dry weight, Si concentration and stress tolerance in compost-grown plants.

Author Contributions: Conceptualization, S.J.T., S.E.H. and F.J.M.M.; methodology, S.J.T., S.E.H. and F.J.M.M.; formal analysis, S.J.T.; investigation, S.J.T.; data curation, S.J.T.; writing—original draft preparation, S.J.T.; writing—review and editing, S.E.H. and F.J.M.M.; funding acquisition, S.E.H. and F.J.M.M. All authors have read and agreed to the published version of the manuscript.

Funding: This work was supported by the Biotechnology and Biological Sciences Research Council (Award ref 1949569).

Data Availability Statement: Not applicable.

Acknowledgments: The authors thank the Biotechnology and Biological Sciences Research Council for funding of the project. We are grateful to Andrea Harper for providing the seeds for this project.

Conflicts of Interest: The authors declare no conflict of interest. The funders had no role in the design of the study; in the collection, analyses or interpretation of data; in the writing of the manuscript; or in the decision to publish the results.

References

1. Chaves, M.S.; Martinelli, J.A.; Wesp-Guterres, C.; Graichen, F.A.S.; Brammer, S.P.; Scagliusi, S.M.; da Silva, P.R.; Wiethölter, P.; Torres, G.A.M.; Lau, E.Y.; et al. The importance for food security of maintaining rust resistance in wheat. *Food Secur.* **2013**, *5*, 157–176. [CrossRef]
2. FAOSTAT. Available online: http://www.fao.org/faostat/en/#data/QC/visualize (accessed on 1 September 2020).
3. Daryanto, S.; Wang, L.; Jacinthe, P.A. Global synthesis of drought effects on maize and wheat production. *PLoS ONE* **2016**, *11*, e0156362. [CrossRef]
4. IPCC. *Climate Change 2014: Synthesis Report. Contribution of Working Groups I, II, and III to the Fifth Assessment Report of The Intergovernmental Panel on Climate Change*; Pachauri, R.K., Meyer, L.A., Eds.; IPCC: Geneva, Switzerland, 2014; ISBN 9789291691432.
5. IPCC. *Climate Change and Land: An IPCC Special Report on Climate Change, Desertification, Land Degradation, Sustainable Land Management, Food Security, and Greenhouse Gas Fluxes in Terrestrial Ecosystems*; Shukla, P.R., Skea, J., Calvo Buendia, E., Masson-Delmotte, V., Pörtner, H.-O., Roberts, D.C., Zhai, P., Slade, R., Connors, S., van Diemen, R., et al., Eds.; IPCC: Geneva, Switzerland, 2019.
6. Kahiluoto, H.; Kaseva, J.; Balek, J.; Olesen, J.E.; Ruiz-Ramos, M.; Gobin, A.; Kersebaum, K.C.; Takáč, J.; Ruget, F.; Ferrise, R.; et al. Decline in climate resilience of european wheat. *Proc. Natl. Acad. Sci. USA* **2019**, *116*, 123–128. [CrossRef] [PubMed]
7. Martínez-Alvarez, V.; Martin-Gorriz, B.; Soto-García, M. Seawater desalination for crop irrigation—A review of current experiences and revealed key issues. *Desalination* **2016**, *381*, 58–70. [CrossRef]
8. Dwivedi, S.L.; Ceccarelli, S.; Blair, M.W.; Upadhyaya, H.D.; Are, A.K.; Ortiz, R. Landrace Germplasm for Improving Yield and Abiotic Stress Adaptation. *Trends Plant Sci.* **2016**, *21*, 31–42. [CrossRef]
9. Bhat, J.A.; Deshmukh, R.; Zhao, T.; Patil, G.; Deokar, A.; Shinde, S.; Chaudhary, J. Harnessing High-throughput Phenotyping and Genotyping for Enhanced Drought Tolerance in Crop Plants. *J. Biotechnol.* **2020**, *324*, 248–260. [CrossRef] [PubMed]
10. Epstein, E. The anomaly of silicon in plant biology. *Proc. Natl. Acad. Sci. USA* **1994**, *91*, 11–17. [CrossRef]
11. Debona, D.; Rodrigues, F.A.; Datnoff, L.E. Silicon's Role in Abiotic and Biotic Plant Stresses. *Annu. Rev. Phytopathol.* **2017**, *55*, 85–107. [CrossRef]
12. Côté-Beaulieu, C.; Chain, F.; Menzies, J.G.; Kinrade, S.D.; Bélanger, R.R. Absorption of aqueous inorganic and organic silicon compounds by wheat and their effect on growth and powdery mildew control. *Environ. Exp. Bot.* **2009**, *65*, 155–161. [CrossRef]
13. Ma, J.F.; Yamaji, N. A cooperative system of silicon transport in plants. *Trends Plant Sci.* **2015**, *20*, 435–442. [CrossRef]
14. Bennett, D.M. Silicon deposition in the roots of *Hordeum sativum* Jess, *Avena sativa* L. and *Triticum aestivum* L. *Ann. Bot.* **1982**, *50*, 239–245. [CrossRef]
15. Lux, A.; Luxová, M.; Abe, J.; Tanimoto, E.; Hattori, T.; Inanaga, S. The dynamics of silicon deposition in the sorghum root endodermis. *New Phytol.* **2003**, *158*, 437–441. [CrossRef]
16. Yoshida, S.; Ohnishi, Y.; Kitagishi, K. Histochemistry of Silicon in Rice Plant. *Soil Sci. Plant Nutr.* **1962**, *8*, 1–5. [CrossRef]
17. Yamaji, N.; Sakurai, G.; Mitani-Ueno, N.; Ma, J.F. Orchestration of three transporters and distinct vascular structures in node for intervascular transfer of silicon in rice. *Proc. Natl. Acad. Sci. USA* **2015**, *112*, 11401–11406. [CrossRef]
18. Yoshida, S.; Ohnishi, Y.; Kitagishi, K. Chemical forms, mobility and deposition of silicon in rice plant. *Soil Sci. Plant Nutr.* **1962**, *8*, 15–21. [CrossRef]
19. Shakoor, S.A.; Bhat, M.A.; Mir, S.H. Phytoliths in Plants: A Review. *J. Bot. Sci.* **2014**, *3*, 10–24.
20. Hartley, S.E.; Fitt, R.N.; McLarnon, E.L.; Wade, R.N. Defending the leaf surface: Intra- and inter-specific differences in silicon deposition in grasses in response to damage and silicon supply. *Front. Plant Sci.* **2015**, *6*, 35. [CrossRef]
21. Sakai, W.; Thom, M. Localization of silicon in specific cell wall layers of the stomatal apparatus of sugar cane by use of energy dispersive X-ray analysis. *Ann. Bot.* **1979**, *44*, 245–248. [CrossRef]
22. Peleg, Z.; Saranga, Y.; Fahima, T.; Aharoni, A.; Elbaum, R. Genetic control over silica deposition in wheat awns. *Physiol. Plant.* **2010**, *140*, 10–20. [CrossRef] [PubMed]
23. Kumar, S.; Milstein, Y.; Brami, Y.; Elbaum, M.; Elbaum, R. Mechanism of silica deposition in sorghum silica cells. *New Phytol.* **2017**, *213*, 791–798. [CrossRef] [PubMed]
24. Thorne, S.J.; Hartley, S.E.; Maathuis, F.J.M. Is Silicon a Panacea for Alleviating Drought and Salt Stress in Crops? *Front. Plant Sci.* **2020**, *11*, 1221. [CrossRef]
25. Osakabe, Y.; Osakabe, K.; Shinozaki, K.; Tran, L.-S.P. Response of plants to water stress. *Front. Plant Sci.* **2014**, *5*, 86. [CrossRef]
26. Gong, H.; Zhu, X.; Chen, K.; Wang, S.; Zhang, C. Silicon alleviates oxidative damage of wheat plants in pots under drought. *Plant Sci.* **2005**, *169*, 313–321. [CrossRef]
27. Tale Ahmad, S.; Haddad, R. Study of silicon effects on antioxidant enzyme activities and osmotic adjustment of wheat under drought stress. *Czech J. Genet. Plant Breed.* **2011**, *47*, 17–27. [CrossRef]
28. Alzahrani, Y.; Kuşvuran, A.; Alharby, H.F.; Kuşvuran, S.; Rady, M.M. The defensive role of silicon in wheat against stress conditions induced by drought, salinity or cadmium. *Ecotoxicol. Environ. Saf.* **2018**, *154*, 187–196. [CrossRef]

29. Ibrahim, M.A.; Merwad, A.R.M.; Elnaka, E.A. Rice (*Oryza Sativa* L.) Tolerance to Drought Can Be Improved by Silicon Application. *Commun. Soil Sci. Plant Anal.* **2018**, *49*, 945–957. [CrossRef]
30. Merwad, A.R.M.A.; Desoky, E.S.M.; Rady, M.M. Response of water deficit-stressed *Vigna unguiculata* performances to silicon, proline or methionine foliar application. *Sci. Hortic.* **2018**, *228*, 132–144. [CrossRef]
31. Sonobe, K.; Hattori, T.; An, P.; Tsuji, W.; Eneji, E.; Tanaka, K.; Inanaga, S. Diurnal variations in photosynthesis, stomatal conductance and leaf water relation in sorghum grown with or without silicon under water stress. *J. Plant Nutr.* **2009**, *32*, 433–442. [CrossRef]
32. Yin, L.; Wang, S.; Liu, P.; Wang, W.; Cao, D.; Deng, X.; Zhang, S. Silicon-mediated changes in polyamine and 1-aminocyclopropane-1-carboxylic acid are involved in silicon-induced drought resistance in *Sorghum bicolor* L. *Plant Physiol. Biochem.* **2014**, *80*, 268–277. [CrossRef]
33. Wang, Y.; Zhang, B.; Jiang, D.; Chen, G. Silicon improves photosynthetic performance by optimizing thylakoid membrane protein components in rice under drought stress. *Environ. Exp. Bot.* **2019**, *158*, 117–124. [CrossRef]
34. Vandegeer, R.K.; Zhao, C.; Cibils-Stewart, X.; Wuhrer, R.; Hall, C.R.; Hartley, S.E.; Tissue, D.T.; Johnson, S.N. Silicon deposition on guard cells increases stomatal sensitivity as mediated by K^+ efflux and consequently reduces stomatal conductance. *Physiol. Plant.* **2021**, *171*, 358–370. [CrossRef]
35. Agarie, S.; Uchida, H.; Agata, W.; Kubota, F.; Kaufman, P.B. Effects of silicon on transpiration and leaf conductance in rice plants (*Oryza saliva* L.). *Plant Prod. Sci.* **1998**, *1*, 89–95. [CrossRef]
36. Ahmad, M.; El-Saeid, M.H.; Akram, M.A.; Ahmad, H.R.; Haroon, H.; Hussain, A. Silicon fertilization—A tool to boost up drought tolerance in wheat (*Triticum aestivum* L.) crop for better yield. *J. Plant Nutr.* **2016**, *39*, 1283–1291. [CrossRef]
37. Gong, H.; Chen, K.; Chen, G.; Wang, S.; Zhang, C. Effects of Silicon on Growth of Wheat Under Drought. *J. Plant Nutr.* **2003**, *26*, 1055–1063. [CrossRef]
38. Othmani, A.; Ayed, S.; Bezzin, O.; Farooq, M.; Ayed-Slama, O.; Slim-Amara, H.; Ben Younes, M. Effect of Silicon Supply Methods on Durum Wheat (*Triticum durum* Desf.) Response to Drought Stress. *Silicon* **2020**. [CrossRef]
39. Sattar, A.; Cheema, M.A.; Sher, A.; Ijaz, M.; Ul-Allah, S.; Nawaz, A.; Abbas, T.; Ali, Q. Physiological and biochemical attributes of bread wheat (*Triticum aestivum* L.) seedlings are influenced by foliar application of silicon and selenium under water deficit. *Acta Physiol. Plant.* **2019**, *41*, 146. [CrossRef]
40. Hosseini, S.A.; Maillard, A.; Hajirezaei, M.R.; Ali, N.; Schwarzenberg, A.; Jamois, F.; Yvin, J.-C. Induction of Barley Silicon Transporter HvLsi1 and HvLsi2, increased silicon concentration in the shoot and regulated Starch and ABA Homeostasis under Osmotic stress and Concomitant Potassium Deficiency. *Front. Plant Sci.* **2017**, *8*, 1359. [CrossRef]
41. Maillard, A.; Ali, N.; Schwarzenberg, A.; Jamois, F.; Yvin, J.C.; Hosseini, S.A. Silicon transcriptionally regulates sulfur and ABA metabolism and delays leaf senescence in barley under combined sulfur deficiency and osmotic stress. *Environ. Exp. Bot.* **2018**, *155*, 394–410. [CrossRef]
42. Massey, F.P.; Massey, K.; Roland Ennos, A.; Hartley, S.E. Impacts of silica-based defences in grasses on the feeding preferences of sheep. *Basic Appl. Ecol.* **2009**, *10*, 622–630. [CrossRef]
43. Soininen, E.M.; Bråthen, K.A.; Jusdado, J.G.H.; Reidinger, S.; Hartley, S.E. More than herbivory: Levels of silica-based defences in grasses vary with plant species, genotype and location. *Oikos* **2013**, *122*, 30–41. [CrossRef]
44. Ouzounidou, G.; Giannakoula, A.; Ilias, I.; Zamanidis, P. Alleviation of drought and salinity stresses on growth, physiology, biochemistry and quality of two *Cucumis sativus* L. cultivars by Si application. *Rev. Bras. Bot.* **2016**, *39*, 531–539. [CrossRef]
45. Parveen, A.; Liu, W.; Hussain, S.; Asghar, J.; Perveen, S.; Xiong, Y. Silicon priming regulates morpho-physiological growth and oxidative metabolism in maize under drought stress. *Plants* **2019**, *8*, 431. [CrossRef] [PubMed]
46. Maghsoudi, K.; Emam, Y.; Ashraf, M.; Pessarakli, M.; Arvin, M.J. Silicon application positively alters pollen grain area, osmoregulation and antioxidant enzyme activities in wheat plants under water deficit conditions. *J. Plant Nutr.* **2019**, *42*, 2121–2132. [CrossRef]
47. Lopes, M.S.; El-Basyoni, I.; Baenziger, P.S.; Singh, S.; Royo, C.; Ozbek, K.; Aktas, H.; Ozer, E.; Ozdemir, F.; Manickavelu, A.; et al. Exploiting genetic diversity from landraces in wheat breeding for adaptation to climate change. *J. Exp. Bot.* **2015**, *66*, 3477–3486. [CrossRef]
48. Merah, O.; Deleens, E.; Monneveux, P. Grain yield, carbon isotope discrimination, mineral and silicon content in durum wheat under different precipitation regimes. *Physiol. Plant.* **1999**, *107*, 387–394. [CrossRef]
49. Simpson, K.J.; Wade, R.N.; Rees, M.; Osborne, C.P. Still armed after domestication? Impacts of domestication and agronomic selection on silicon defences in cereals. *Funct. Ecol.* **2017**, *31*, 2108–2117. [CrossRef]
50. Michel, B.E. Evaluation of the Water Potentials of Solutions of Polyethylene Glycol 8000 Both in the Absence and Presence of Other Solutes. *Plant Physiol.* **1983**, *72*, 66–70. [CrossRef]
51. Reidinger, S.; Ramsey, M.H.; Hartley, S.E. Rapid and accurate analyses of silicon and phosphorus in plants using a portable X-ray fluorescence spectrometer. *New Phytol.* **2012**, *195*, 699–706. [CrossRef]
52. Johnson, J. Accurate Measurements of Low Z Elements in Sediments and Archaeological Ceramics Using Portable X-ray Fluorescence (PXRF). *J. Archaeol. Method Theory* **2014**, *21*, 563–588. [CrossRef]
53. R Core Team. *R: A Language and Environment for Statistical Computing*; R Foundation for Statistical Computing: Vienna, Austria, 2019. Available online: https://www.R-project.org/ (accessed on 27 April 2018).

54. Chen, C.T.; Kao, C.H. Osmotic stress and water stress have opposite effects on putrescine and proline production in excised rice leaves. *Plant Growth Regul.* **1993**, *13*, 197–202. [CrossRef]
55. Whalley, W.R.; Bengough, A.G.; Dexter, A.R. Water stress induced by PEG decreases the maximum growth pressure of the roots of pea seedlings. *J. Exp. Bot.* **1998**, *49*, 1689–1694. [CrossRef]
56. Ma, J.F.; Yamaji, N.; Tamai, K.; Mitani, N. Genotypic Difference in Silicon Uptake and Expression of Silicon Transporter Genes in Rice. *Plant Physiol.* **2007**, *145*, 919–924. [CrossRef] [PubMed]
57. Chiba, Y.; Mitani, N.; Yamaji, N.; Ma, J.F. *HvLsi1* is a silicon influx transporter in barley. *Plant J.* **2009**, *57*, 810–818. [CrossRef] [PubMed]
58. Pei, Z.F.; Ming, D.F.; Liu, D.; Wan, G.L.; Geng, X.X.; Gong, H.J.; Zhou, W.J. Silicon Improves the Tolerance to Water-Deficit Stress Induced by Polyethylene Glycol in Wheat (*Triticum aestivum* L.) Seedlings. *J. Plant Growth Regul.* **2010**, *29*, 106–115. [CrossRef]
59. Xu, L.; Islam, F.; Ali, B.; Pei, Z.; Li, J.; Ghani, M.A.; Zhou, W. Silicon and water-deficit stress differentially modulate physiology and ultrastructure in wheat (*Triticum aestivum* L.). *3 Biotech* **2017**, *7*, 173. [CrossRef]
60. Ruppenthal, V.; Zoz, T.; Steiner, F.; Do Carmo Lana, M.; Castagnara, D.D. Silicon does not alleviate the adverse effects of drought stress in soybean plants. *Semin. Agrar.* **2016**, *37*, 3941–3954. [CrossRef]
61. Hu, J.; Cai, X.; Jeong, B.R. Silicon Affects Root Development, Tissue Mineral Content, and Expression of Silicon Transporter Genes in Poinsettia (*Euphorbia pulcherrima* Willd.) Cultivars. *Plants* **2019**, *8*, 180. [CrossRef]
62. De Camargo, M.S.; Bezerra, B.K.L.; Holanda, L.A.; Oliveira, A.L.; Vitti, A.C.; Silva, M.A. Silicon Fertilization Improves Physiological Responses in Sugarcane Cultivars Grown Under Water Deficit. *J. Soil Sci. Plant Nutr.* **2019**, *19*, 81–91. [CrossRef]
63. Gunes, A.; Pilbeam, D.J.; Inal, A.; Coban, S. Influence of silicon on sunflower cultivars under drought stress, I: Growth, antioxidant mechanisms, and lipid peroxidation. *Commun. Soil Sci. Plant Anal.* **2008**, *39*, 1885–1903. [CrossRef]
64. Sapre, S.S.; Vakharia, D. Silicon induced physiological and biochemical changes under polyethylene glycol-6000 water deficit stress in wheat seedlings. *J. Environ. Biol.* **2017**, *38*, 313–319. [CrossRef]
65. Meunier, J.D.; Barboni, D.; Anwar-ul-Haq, M.; Levard, C.; Chaurand, P.; Vidal, V.; Grauby, O.; Huc, R.; Laffont-Schwob, I.; Rabier, J.; et al. Effect of phytoliths for mitigating water stress in durum wheat. *New Phytol.* **2017**, *215*, 229–239. [CrossRef] [PubMed]
66. Ahmad, F.; Aziz, T.; Maqsood, M.A. Effect of silicon application on wheat (*Triticum aestivum* L.) growth under water deficiency stress. *Emir. J. Food Agric.* **2007**, *19*, 1–7. [CrossRef]
67. Grašič, M.; Dobravc, M.; Golob, A.; Vogel-Mikuš, K.; Gaberščik, A. Water shortage reduces silicon uptake in barley leaves. *Agric. Water Manag.* **2019**, *217*, 47–56. [CrossRef]
68. Yang, R.; Howe, J.A.; Golden, B.R. Calcium silicate slag reduces drought stress in rice (*Oryza sativa* L.). *J. Agron. Crop Sci.* **2019**, *205*, 353–361. [CrossRef]
69. Chen, W.; Yao, X.; Cai, K.; Chen, J. Silicon alleviates drought stress of rice plants by improving plant water status, photosynthesis and mineral nutrient absorption. *Biol. Trace Elem. Res.* **2011**, *142*, 67–76. [CrossRef] [PubMed]

plants

MDPI

Article

Cloning and Characterization of Two Putative P-Type ATPases from the Marine Microalga *Dunaliella maritima* Similar to Plant H^+-ATPases and Their Gene Expression Analysis under Conditions of Hyperosmotic Salt Shock

Dmitrii A. Matalin [1,†], Dmitrii E. Khramov [1,†], Alexey V. Shuvalov [2], Vadim S. Volkov [1,*], Yurii V. Balnokin [1] and Larissa G. Popova [1,*]

[1] K.A.Timiryazev Institute of Plant Physiology RAS, 127276 Moscow, Russia; dmatalin@mail.ru (D.A.M.); khramov.de@yandex.ru (D.E.K.); balnokin@mail.ru (Y.V.B.)
[2] Engelhardt Institute of Molecular Biology RAS, 119991 Moscow, Russia; laursen1243@mail.ru
* Correspondence: vadim.s.volkov@gmail.com (V.S.V.); lora_gp@mail.ru (L.G.P.)
† D.A.M. and D.E.K. contributed equally to this work.

Abstract: The green microalga genus *Dunaliella* is mostly comprised of species that exhibit a wide range of salinity tolerance, including inhabitants of hyperhaline reservoirs. Na^+ content in *Dunaliella* cells inhabiting saline environments is maintained at a fairly low level, comparable to that in the cells of freshwater organisms. However, despite a long history of studying the physiological and molecular mechanisms that ensure the ability of halotolerant *Dunaliella* species to survive at high concentrations of NaCl, the question of how *Dunaliella* cells remove excess Na^+ ions entering from the environment is still debatable. For thermodynamic reasons it should be a primary active mechanism; for example, via a Na^+-transporting ATPase, but the molecular identification of Na^+-transporting mechanism in *Dunaliella* has not yet been carried out. Formerly, in the euryhaline alga *D. maritima*, we functionally identified Na^+-transporting P-type ATPase in experiments with plasma membrane (PM) vesicles which were isolated from this alga. Here we describe the cloning of two putative P-type ATPases from *D. maritima*, *Dm*HA1 and *Dm*HA2. Phylogenetic analysis showed that both ATPases belong to the clade of proton P-type ATPases, but the similarity between *Dm*HA1 and *Dm*HA2 is not high. The expression of *Dm*HA1 and *Dm*HA2 in *D. maritima* cells under hyperosmotic salt shock was studied by qRT-PCR. Expression of *DmHA1* gene decreases and remains at a relatively low level during the response of *D. maritima* cells to hyperosmotic salt shock. In contrast, expression of *DmHA2* increases under hyperosmotic salt shock. This indicates that *Dm*HA2 is important for overcoming hyperosmotic salt stress by the algal cells and as an ATPase it is likely directly involved in transport of Na^+ ions. We assume that it is the *Dm*HA2 ATPase that represents the Na^+-transporting ATPase.

Keywords: *Dunaliella*; cloning; expression; H^+-ATPase; microalgae; Na^+-ATPase; qRT-PCR; salt shock; salt tolerance

Citation: Matalin, D.A.; Khramov, D.E.; Shuvalov, A.V.; Volkov, V.S.; Balnokin, Y.V.; Popova, L.G. Cloning and Characterization of Two Putative P-Type ATPases from the Marine Microalga *Dunaliella maritima* Similar to Plant H^+-ATPases and Their Gene Expression Analysis under Conditions of Hyperosmotic Salt Shock. *Plants* **2021**, *10*, 2667. https://doi.org/10.3390/plants10122667

Academic Editor: Stefano Accoroni

Received: 29 October 2021
Accepted: 30 November 2021
Published: 3 December 2021

Publisher's Note: MDPI stays neutral with regard to jurisdictional claims in published maps and institutional affiliations.

1. Introduction

The genus of motile green unicellular algae *Dunaliella* belongs to the family Dunaliellaceae, which was described more than a hundred years ago [1]. Since then, representatives of this genus have become convenient model organisms in plant cell physiology for studying the cellular mechanisms of adaptation to unfavorable environmental factors, particularly, to increased salinity [2,3]. The genus *Dunaliella* includes freshwater species (*D. acodophila*, *D. lateralis*, *D. flagellate*), the marine/oligohaline/euryhaline species with optimum salinity for growth of about 2 to 4% NaCl (*D. tertiolecta*, *D. polymorpha*, *D. maritima*) and hypersaline/halophilic species with optimum salinity for growth >6% NaCl (*D. parva*, *D. salina*, *D. bioculata*) [4]. Primarily, representatives of the genus *Dunaliella* are known as inhabitants of hypersaline reservoirs [2,5]. For example, *D. salina* and *D. parva*, which

are found in saturated brines where the NaCl concentration reaches 100‰ (app. 1.7 M NaCl), provide the major part of biomass production of saline lakes [1]. Some *Dunaliella* species (*D. tertiolecta*, *D. maritima*) are marine/euhaline organisms; they show moderate resistance to NaCl compared to *D. salina* and *D. parva*. The optimal growth of these species is observed at 28–32% (app. 0.5 M NaCl), but these species are also able to grow at very high concentrations of NaCl reaching 1.5 M [6,7].

The ability of *Dunaliella* to grow in water reservoirs with variable salt concentration, is associated with the absence of a rigid cell wall and suggests that *Dunaliella* has effective systems of ionic and osmotic regulation necessary for life under changing environmental conditions. The question of maintaining osmotic balance in *Dunaliella* cells under conditions of high salinity has been well investigated in numerous studies. It was shown that the osmotic balance in *Dunaliella* is supported by the synthesis of a compatible osmolyte glycerol, which, depending on the concentration of NaCl in the medium, can accumulate to reach intracellular concentrations of 7.8 M [8–11].

At high concentrations Na^+ is toxic to cellular metabolism. High Na^+ concentrations over 100 mM have an inhibitory effect on protein synthesis, both in glycophytes and halophytes, including *Dunaliella* species [10,12–17]. Sodium is competing with potassium for allosteric sites of enzymes which leads to violations of cellular functions [18]. Sodium is also interacting with ion channels. For example, Na^+ ions change the gating of potassium outward rectifying currents (most likely carried by Shaker type K^+ channels) in root protoplasts of halophyte plant *Thellungiella* [19]. Moreover at the cellular level salt stress induces apoptosis [20] (briefly reviewed in [21,22]).

Like in all living organisms, Na^+ content in *Dunaliella* cells inhabiting saline environments is maintained at a fairly low level. Both in *Dunaliella* growing at 0.5 M NaCl and in species growing at 4 M NaCl in the medium, intracellular concentrations of Na^+ do not exceed 100 mM [23–28]. An interesting example is the halotolerant alga *D. salina*, which is a good unicellular eukaryotic model for studying salinity tolerance within the range of 0.05–5.5 M NaCl [25]. The cells of *D. salina* are small with a length about 10–11 μm, width of 6 μm and volume around 200 fL (or even smaller dimensions with a volume around 90–100 fL) [4]. Cytoplasmic Na^+ concentrations of about 90 mM (88 ± 28 mM) were reported in the alga using ^{23}Na-NMR spectroscopy [24] and were nearly the same (within the error of measurements) in the algal cells adapted to a wide range of external Na^+, from 0.1 to 4 M. Similar or even lower sodium concentrations below 100 mM were measured by other methods for the alga under 0.5–4 M sodium treatment [25,27].

However, despite a long history of studying the physiological and molecular mechanisms that ensure the ability of halotolerant *Dunaliella* species to survive at high concentrations of NaCl in the environment, the question of how *Dunaliella* cells get rid of excess Na^+ ions entering from the external environment is still debatable. In higher plants—organisms of the plant kingdom, which also include Dunaliellaceae—Na^+ homeostasis in cells is maintained by means of $\Delta\mu H^+$-dependent Na^+/H^+ antiporters at the plasma membrane and tonoplast, which export Na^+ from the cytoplasm to the external environment or to vacuoles (reviewed in [29–31]). The functioning of Na^+/H^+ antiporters is energized by active H^+-pumps that, at the expenses of ATP, produce H^+ gradients at the cell membranes. These H^+-pumps are P-type H^+-ATPase resident in plasma membranes and V-type H^+-ATPase and H^+-translocating pyrophosphatase of tonoplast [32]. Plasma membrane H^+-ATPases form a highly conservative subgroup of P-type ATPases. H^+-ATPases are ubiquitous and essential enzymes in yeast and higher plants where they ensure the driving force for uptake of nutrients, cytoplasmic pH-stat and regulation of cellular volume (reviewed in [33–35]). P-type H^+-ATPases have also been found in algae of various taxa [35–40].

It is important to mention one more structural peculiarity of Dunaliellaceae: along with the absence of a rigid cell wall, they also lack a large central vacuole. Since the alga has no central vacuole, the plasma membrane ATPase is considered to be the major means by which the intracellular Na^+ concentration is regulated. However, calculations demonstrated that under conditions which are typical for the habitats of halotolerant microalgae —i.e., in

environments where high concentrations of NaCl are combined with alkaline pH —there are thermodynamic restrictions for the export of Na^+ from cells of these organisms by means of $\Delta\mu H^+$-dependent Na^+/H^+ antiporter of the plasma membrane energized by H^+-ATPase [41]. If export of Na^+ from cytoplasm to the external medium by a secondary active $\Delta\mu H^+$-dependent Na^+/H^+ antiporter is not possible, then the Na^+ homeostasis of the cytoplasm has to be provided by a primary active mechanism, for example, by a Na^+-transporting ATPase, which will directly export Na^+ from the cytoplasm at the expenses of energy of ATP hydrolysis. The examples of such Na^+-pumps in eukaryotic kingdoms are the well-characterized Na^+, K^+-ATPase of animal cells [42] (reviewed in [43–45]) and the yeast-type Na^+-ATPase, ENA ATPase, which is found in different yeast species [46,47]. These enzymes, like the proton ATPases of the plant cell plasmalemma, belong to the family of P-type ATPases. P-type ATPases are relatively simply arranged integral membrane proteins that couple hydrolysis of ATP with transfer of small cations (Na^+, K^+, Ca^{2+}, H^+), heavy metal ions and phospholipids through biological membranes against their electrochemical gradients (reviewed in [48,49]). A characteristic feature of P-type ATPases is the formation of a transient phosphorylated intermediate during the catalytic cycle [50].

In algae of genus *Dunaliella*, a Na^+-transporting P-type ATPase was functionally identified in experiments with plasma membrane (PM) vesicles, which were isolated from the cells of green euryhaline microalga *D. maritima*. Under conditions when there was no proton gradient at the vesicle membrane ATP-dependent uptake of $^{22}Na^+$ by PM vesicles occurred thus indicating the functioning of a primary-energized Na^+-transporting mechanism in *D. maritima* PM, namely, a Na^+-transporting ATPase [51]. This enzyme as the other eukaryotic Na^+-ATPases is a P-type ATPase, since it has a characteristic feature of these ATPases, namely, sensitivity to micromolar concentrations of orthovanadate. As with the Na^+-ATPase of microalga *Tetraselmis viridis*, the Na^+-ATPase of *D. maritima* differs from both Na^+, K^+-ATPase of animal cells and yeast ENA ATPases based on a number of principal functional characteristics. The Na^+-ATPase of *D. maritima* does not transport K^+, it is an electrogenic uniporter [52]. This uniporter feature discriminates the Na^+-ATPase of *D. maritima* from the Na^+-ATPase of *T. viridis*, which uses Na^+ and H^+ as counterions. However, similar to the Na^+-ATPase of *T. viridis*, the Na^+-ATPase of *D. maritima* is highly selective for Na^+ [51,52]. Nevertheless, even though the Na^+-ATPase of *D. maritima* was discovered at the functional level over 20 years ago, the molecular identification of this enzyme has not yet been carried out.

Experiments to clone P-type ATPases from different *Dunaliella* species have been undertaken [53–55]. The cloned ATPases were either structurally similar to H^+-ATPases of plants (ATPases from *D. bioculata* [53], *D. acidophyla* and *D. salina* [54]) or similar to Ca^{2+}-ATPases (ATPase from *D. bioculata* [55]), but an enzyme which could be classified as a subgroup of Na^+-transporting ATPases by its general structural characteristics was not found.

Ambiguity over the molecular identification of the mechanism responsible for the export of Na^+ from *Dunaliella* cells is increased by the results of our bioinformatic study. In order to identify the gene of Na^+-ATPase for algae belonging to the genus *Dunaliella* we assembled *de novo* several transcriptomes of the microalga *D. tertiolecta* based on individual libraries of short RNA reads from *D. tertiolecta* available in free access in the Sequence Read Archive (SRA, NCBI) database. The assembled transcriptomes were examined *in silico* for possible signatures for P-type ATPases [56]. Coding sequences (CDS) for various P-type ATPases were found, but contrary to expectations, none of the assembled *D. tertiolecta* transcriptomes demonstrated a nucleotide sequence encoding a protein that could be unambiguously assigned to the Na^+-ATPase group. However, contigs containing CDS for two different hypothetical H^+-ATPases, HA1 (molecular weight 1131 aa) and HA2 (molecular weight 923 aa) have been identified. Contigs containing full-length CDS for these ATPases were found in all assembled transcriptomes indicating their relatively high abundance in the total transcript pool. The function of the proteins was supposed by their location on a P-type ATPase cladogram in the same clade with H^+-ATPases.

The similarity between ATPases HA1 (termed here as *Dt*HA1) and HA2 (termed as *Dt*HA2) was not high. ATPase *Dt*HA1 was identical (100% identical to amino acid residues) to H^+-ATPase of the plasma membrane of *D. bioculata* (GenBank CAA52107.1) and showed a high degree of similarity with H^+-ATPase from the acidophilic alga *D. acidophila* (P54210.1, UniProtKB/Swiss Prot Database). The other putative *D. tertiolecta* ATPase, *Dt*HA2, was similar (99% identical amino acid residues) to P-type ATPase of the halotolerant microalga *D. salina* (ABB88698.1, GenBank database). The phylogenetic analysis demonstrated that ATPase *Dt*HA1 is homologous to the proton pumps of higher plants, while ATPase *Dt*HA2 is homologous to H^+-ATPases of microalgae and parasitic protists [56].

Based on the assumption that the two different proton pumps in the plasmalemma of *D. tertiolecta* were unlikely to have a similar function, it was hypothesized that one of the predicted enzymes (transcripts of which were identified in *D. tertiolecta* transcriptome), *Dt*HA1, which is similar to the well-characterized H^+-ATPases of higher plants and the acidophilic microalga *D. acidophila* [54], is an H^+-ATPase and transfers protons while another ATPase, *Dt*HA2, may carry Na^+ ions.

This hypothesis is supported by some data obtained in the present work. Based on the sequences encoding *Dt*HA1 and *Dt*HA2 ATPases in the *de novo* assembled *D. tertiolecta* transcriptomes, primers were designed to amplify the coding sequences of homologous ATPases, *Dm*HA1 and *Dm*HA2 from the green euryhaline microalga *D. maritima*, which is closely related to alga *D. tertiolecta* [4,57] and was extensively characterized in our laboratory [7,14,51,52,58,59]. As mentioned above, the existence of Na^+-transporting ATPase in the plasma membrane of *D. maritima* was shown at the functional level [51]. The sequences *DmHA1* and *DmHA2* were cloned, their expression was studied in *D. maritima* cells under hyperosmotic salt shock, the similarities and differences in the structures of proteins *Dm*HA1 and *Dm*HA2 were analyzed *in silico*. The data obtained indicate that ATPase *Dm*HA2 may participate in export of Na^+ ions from *D. maritima* cells.

2. Materials and Methods

2.1. The Object of the Study and Conditions of Cultivation

The object of the study was the green euryhaline microalga *Dunaliella maritima* [60]. A suspension culture of the alga was grown in a liquid medium containing 0.5 M NaCl, pH 8: the complete composition of the medium is close to that of seawater and is given in [41]. *D. maritima* culture was cultured in glass vessels with a volume of 1 L, constantly bubbled with air containing 1.5% CO_2, and illuminated with white light from LB-20 fluorescent lamps for 14 h a day. Irradiance was 225 μmol photons m^{-2} s^{-1}.

A number of experiments also used a *D. maritima* culture growing in a medium with a low concentration of NaCl (0.1 M NaCl; "low-salt" culture). "Low-salt" culture was obtained by acclimating a "high-salt" culture of alga growing at 0.5 M NaCl to 0.1 M NaCl in the medium for at least 2 months. Passages of the algal culture to a fresh nutrient medium were carried out weekly.

2.2. Isolation of Total RNA from D. maritima Cells

For isolation of total RNA from *D. maritima* cells, 200 mL of alga cell suspension at the late logarithmic growth stage were taken, the culture density was about 1.5×10^7 cells/mL. The total RNA was isolated by the hot phenolic method according to de Vries et al. [61]. To remove the residual contaminant of genomic DNA, total RNA samples were treated with DNase I ("Fermentas", Thermo Fisher Scientific, Inc., Waltham, MA, USA) according to the manufacturer's protocol. RNA concentration and quality assessment by the ratio A_{260}/A_{280} were measured by NanoDrop ND1000 (Thermo Fisher Scientific, Inc., Waltham, MA, USA). The quality of isolated RNA was also confirmed by electrophoresis in 1% agarose gel.

2.3. cDNA Synthesis on the Total RNA Template

Samples of total RNA isolated from *D. maritima* cells were used to synthesize total cDNA in a reverse transcription reaction with MMLV-revertase ("Evrogen", Moscow, Russia) and a 12-dTVN oligo-dT primer. The reaction was carried out according to the manufacturer's protocol.

2.4. Amplification of the DmHA2 Partial Coding Sequence

The partial coding fragment of ATPase *Dm*HA2 was amplified on the template of the obtained total cDNA using degenerate primers (F: 5′-gAYAARACYggCACYCTCAC-3 'and R: 5′-TCRTTCACRCCATCACCYgT-3′) and the Encyclo Plus PCR kit ("Evrogen", Moscow, Russia).

2.5. Amplification of the Full-Length Sequences Encoding the DmHA1 and DmHA2

Amplification of the full-length *Dm*HA1 and *Dm*HA2 cDNA sequences was performed on the template of the total cDNA obtained using CloneAmp^{TM} HiFi PCR Premix kit optimized for high-fidelity PCR ("TaKaRa"/Takara Bio Inc., Shiga, Japan; cat # 638916). For amplification, gene-specific primers (Supplementary Table S1) were used, selected based on the assumed homology between the nucleotide sequences coding *D. maritima* ATPases and the corresponding sequences found in the assembled transcriptome of a closely related alga *D. tertiolecta* [56] (Supplementary S2). The primers were designed using the SnapGene Viewer software (from Insightful Science; available at https://www.snapgene.com/, accessed on 1 December 2021).

Additionally, the adaptors of 15–17 bp were added to the 5′-ends of the primers to make them complementary to the ends of linearized vector pMB1. The procedure was necessary for the vector constructions. The first 20 cycles of amplification were done using polymerase Encyclo ("Evrogen", Moscow, Russia) according to the protocol of the company, then 1 μL of the resulting PCR mix was used as a template for the further 32 cycles of amplification with the same primers and high fidelity polymerase from CloneAmp^{TM} HiFi PCR Premix kit ("TaKaRa"). Amplicons from the final PCR mix were used for assemblies of constructs based on vector pMB1, which was initially linearized by inverse PCR [62]. To linearize the vector, we also used CloneAmp^{TM} HiFi PCR Premix kit and the corresponding primers (Supplementary Table S1). Ligation of amplicons and the linearized pMB1 was performed using Gibson Assembly® Cloning Kit ("New England Biolabs", Ipswich, MA, USA) according to the protocol for the kit. The resulting constructs were routinely propagated in *E. coli* cells. The cloned *D. maritima* ATPase sequences were annotated in GenBank.

2.6. Analysis of DmHA1 and DmHA2 Expression under Hyperosmotic Salt Shock

Hyperosmotic salt shock for the cells of the alga *D. maritima* was created by adding 4.5 M NaCl solution to the "low-salt" cell suspension of the alga to a final concentration of 0.5 M NaCl. The cell suspension aliquots (200 mL) were taken at time intervals of 5, 15, 30, 60, 90, 120 and 180 min after the addition of NaCl and frozen in liquid nitrogen. Samples for cells growing at 0.1 M and at 0.5 M NaCl were also collected. Total RNA preparations were then obtained from the cell aliquots and used for cDNA synthesis in a reverse transcription reaction. The relative contents of *Dm*HA1 cDNA and *Dm*HA2 cDNA in the samples obtained were analyzed by quantitative real-time RT-PCR (qRT-PCR) with the LightCycler® 96 Instrument (Roche Diagnostics Corporation, Indianopolis, IN, USA). Reaction mix (20 μL) included 5 μL (100 ng) of cDNA template, 4 μL of ready-made reaction mixture with intercalating fluorescent dye SYBR Green (5 × SYBR Green I qPCRmix-HS SYBR, "Evrogen", Moscow, Russia), 1 μL of each primer for qRT-PCR (Table S1) (the final concentration of each primer was 0.5 μM), 9 μL mQH_2O. The amplification program was the following: 5 min at 95 °C, 45 cycles of 20 s at 95 °C, 20 s at 58 °C, 20 s at 72 °C. The specificity of PCR products was confirmed by the melting curve at the end of the amplification cycle. The sizes of the target fragments were 186 bp for *Dm*HA1 and 196 bp

for *Dm*HA2. Gene of *Dunaliella* β-tubulin was selected as a reference gene, it was cloned by us and annotated in GenBank (ID: MW679534). The size of the synthesized fragment of β-tubulin was 127 bp.

The data obtained were processed using the software for the LightCycler® 96 Instrument (Roche Diagnostics Corporation, Indianopolis, IN, USA), where the $2^{-\Delta\Delta Ct}$ method is used for relative transcription level calculations. The fold changes are represented as (final values–initial values)/initial values. The results are for 3 biological replicates.

2.7. Determination of Na^+ Content in D. maritima Cells under Hyperosmotic Salt Shock

Aliquots (10 mL) of alga cell suspension were taken before and at 5, 10, 15, 20, 30, 40, 60, 90, 120, 150 and 180 min after a sharp increase in the salt concentration in the medium. The alga cells were separated from the external medium by centrifugation through a layer of isotonic washing solution containing 1 M mannitol and 20 mM $Ca(NO_3)_2$ [7]. Distilled water (3 mL) was added to the cell precipitate, which caused cell lysis. Then the cell fragments were precipitated by centrifugation and the content of Na^+ ions in the supernatant was determined using a flame photometer Leki FP 640 ("Leki", Finland). To calculate intracellular ion concentrations, the quantity of ions obtained was attributed to the total volume of cells in the sample. The cell volume was determined by the Okamoto and Suzuki method [63] by the difference in the electrical conductivity of the medium and the cell suspension using the OK-102/1 conductometer (Radelkis, Budapest, Hungary).

2.8. Bioinformatic Methods

The frequency of the codons usage in the green microalgae for design of the degenerate primers was determined according to the Codon Usage Database website (http://www.kazusa.or.jp, accessed on 1 December 2021). Virtual translation of nucleotide sequences into amino acid sequences was carried out using the on-line service on the ExPASy portal (http://web.expasy.org/translate/, accessed on 1 December 2021). Molecular weight, theoretical isoelectric point and the grand average of hydropathicity (GRAVY) of the ATPase proteins were analyzed by the ExPASy compute MW/pI tool (http://web.expasy.org/protparam/, accessed on 1 December 2021). The subcellular localizations of the ATPases were predicted using the on-line tools WoLF PSORT II prediction on the GenScript server (https://www.genscript.com/tools/wolf-psort/, accessed on 1 December 2021). The homology of amino acid sequences of *Dm*HA1 and *Dm*HA2 was determined using Protein BLAST (Basic Local Alignment Search Tool) at NCBI portal (National Center Biotechnology Information, http://www.ncbi.nlm.nih.gov, accessed on 1 December 2021). To determine the phylogenetic relations of *Dm*HA1 and *Dm*HA2 with the known P-type H^+- and Na^+- ATPases, the amino acid sequences of the ATPases were extracted from NCBI portal. Multiple alignment of the ATPase sequences was performed using ClustalW analysis in "MEGA X" software [64]. The phylogenetic tree of the ATPases was constructed using the maximum likelihood method also by means of "MEGA X" software. The topology of *Dm*HA1 and *Dm*HA2 ATPases and the location of the transmembrane domains (TMD) were predicted using the CCTOP (Constrained Consensus TOPology) online service (http://cctop.enzim.ttk.mta.hu, accessed on 1 December 2021), which predicts a consistent model using 10 TMD prediction software tools (HMMTOP, Memsat, Octopus, Philius, Phobius, Pro, Prodiv, Scampi, ScampiMsa, TMHMM).

3. Results and Discussion

In the first stages of the study, cloning of a partial coding sequence (CDS) of the P-type ATPase of the microalgae *D. maritima* was carried out. This was done to check the similarity of the sequences encoding the *D. maritima* ATPases with the orthologous sequences from the phylogenetically related microalga *D. tertiolecta* [57]. The *D. tertiolecta* sequences were previously identified by us in the *de novo* assembled transcriptome of this microalga [56]. To amplify the fragment of CDS for P-type ATPase from *D. maritima* we used degenerate primers which were designed according to the structural features of P-type ATPases.

P-type ATPases have a relatively simple structure. Typically, these enzymes consist of a single catalytic subunit with a molecular weight of 90–140 kDa and have a similar three-dimensional organization though they may vary in size. These are integral membrane proteins containing, depending on the affiliation of the ATPase to a particular subfamily of P-type ATPases [65], 6–10 transmembrane segments (α-helices) which form a transmembrane domain, small and large cytoplasmic loops forming a large cytoplasmic domain and N- and C-ends lying in the cytoplasm [50]. However, despite the general similarity of tertiary structures, the primary structures of P-type ATPases generally are not very similar [65]. Nevertheless, in each enzyme belonging to this class, 8 regions in the amino acid sequence are present that have a high degree of homology among all P-type ATPases. In turn, there are highly conserved regions within these areas. As a rule, rather short amino acid motifs (PGD, PAD, TGES, DKTGTLT, KGAP, DPPR, MVTGD, TGDGVND) located in the catalytic cytoplasmic domain of the enzyme and involved in ATP binding and hydrolysis are strictly invariable [66,67].

The most conserved sequence present almost unchanged in all P-type ATPases, is the DKTGTLT sequence. It is located within a large cytoplasmic loop of the ATPase protein, its aspartate is phosphorylated during the catalytic cycle of the enzyme due to gamma phosphate transfer from ATP, and it is this autophosphorylation that is a characteristic feature of P-type ATPases. Another rather long conservative sequence typical for P-type ATPases, TGDGVND, is located in the "hinge" joint area. This sequence connects the large cytoplasmic domain with the C-terminal hydrophobic domain and is involved in conformational changes during the catalytic cycle of ATPase. The DKTGTLT and TGDGVND sequences are located at a distance of 300–400 amino acids from each other [67]. Degenerate primers for amplification of the fragment of P-type ATPase from *D. maritima* were designed based on these two highly conserved regions of amino acid sequences, taking into account the frequency of codon usage in green microalgae. With the degenerate primers, a 771 nucleotide cDNA fragment was amplified by RT-PCR on the total RNA template obtained from the cells of the microalga *D. maritima* growing at 0.5 M NaCl in the medium. The resulting fragment was sequenced (Supplementary S3). It turned out that it is completely identical to the part of the nucleotide sequence identified *in silico* in the *de novo* assembled transcriptome of *D. tertiolecta* and encoding an ATPase termed HA2 (*Dt*HA2) [56]. Consequently, we termed the corresponding sequence in *D. maritima* *DmHA2*.

The identity of nucleotide sequences encoding fragments of ATPases, *Dm*HA2 in *D. maritima* and *Dt*HA2 in *D. tertiolecta*, gave us reasons to use gene-specific primers (Supplementary Table S1) for amplification of full-size sequences encoding *Dm*HA1 and *Dm*HA2 of *D. maritima*. The design of the primers was carried out on the basis of full-size nucleotide sequences-orthologs, found in silico in *de novo* assembled transcriptome of the microalga *D. tertiolecta* (Supplementary S2). Using these primers, amplicons of 3631 and 2894 nucleotides in size were obtained on the template of the total RNA from *D. maritima* cells and annotated in GenBank (ID: MK510928.1 and KX832225.1, respectively). Significantly, these amplicons turned out to be almost identical to the contigs from the *de novo* assembled transcriptome of *D. tertiolecta* containing the coding sequences for *Dt*HA1 and *Dt*HA2 ATPases (Supplementary S2). The amplicons obtained contained full-length open reading frames for two proteins. Based on the deduced amino acid sequences these proteins were characterized as P-type ATPases and termed as *Dm*HA1 (1131 aa, GenBank with ID: QEH60479.1) and *Dm*HA2 (923 aa, GenBank ID: AQM50087.1). Remarkably, the amino acid sequences of *Dm*HA1 and *Dm*HA2 as well as their nucleotide sequences have a slight similarity: for paired alignment about 27% of identical and 42% of similar amino acid residues can be detected (Supplementary S4). Sequence analysis of *Dm*HA1 and *Dm*HA2 revealed that they possess the conserved motifs typical for P-type ATPases. Computed parameters of *Dm*HA1 and *Dm*HA2 are presented in Table 1.

Table 1. Molecular properties of *Dm*HA1 and *Dm*HA2 based on their deduced amino acid sequences (computed parameters).

Properties	*Dm*HA1	*Dm*HA2
Protein accession number (GenBank ID)	QEH60479.1	AQM50087.1
Number of amino acids	1131	923
Subunit size (kDa)	123.4	100
pI	5.35	5.62
GRAVY index *	0.030	0.166
Subcellular localization	plasma membrane	plasma membrane
The proteins with highest homology scores **	P54211.1 (100% identity) *** P54210.1 (75% identity) ***	ABB88698.1 (99% identity) ***

* GRAVY (Grand average of hydropathicity) indicates the solubility of the proteins: positive GRAVY is for hydrophobic proteins; negative GRAVY is for hydrophilic ones. ** Identity for aa sequences is shown. *** P54211.1, H^+-ATPase *D. bioculata*; P54210.1, H^+-ATPase *D. acidophila*; ABB88698.1, P-type ATPase *D. salina.*

Cloned from *D. maritima* ATPases, *Dm*HA1 and *Dm*HA2, turned out to be very similar to cloned ATPases from other *Dunaliella* species (Figure 1, Table 1). For example, *Dm*HA1 is almost identical to H^+-ATPase from *D. bioculata* (GenBank ID: P54211.1; 100% identical amino acids) and is very similar to H^+-ATPase from *D. acidophila* (GenBank ID: P54210.1, about 75% of identical amino acids). The *Dm*HA2 ATPase is similar to the enzyme from the extremely halotolerant *D. salina* (GenBank ID: ABB88698.1, about 99% of identical amino acids).

Phylogenetic analysis showed that ATPases *Dm*HA1 and *Dm*HA2 belong to the clade of proton P-type ATPases (Figure 2). However, within the clade of putative proton ATPases, the two cloned *D. maritima* ATPases are located in different subclades: *Dm*HA1 protein is similar to the well-characterized proton pumps of higher plants and *S. cerevisiae*, while *Dm*HA2 ATPase is similar to the less studied putative proton ATPases of microalgae and parasitic protists. The transport of monovalent cations (as well as H^+ transport) has not been demonstrated for the ATPases from this subclade. It should be noted that for most cases the coding sequences of proteins included in the second clade have not been determined experimentally but based on genomic sequencing while the functions of these proteins are predicted and have not been experimentally determined so far.

Using programs for prediction of transmembrane domains in proteins we obtained consistent topological models for *Dm*HA1 and *Dm*HA2 (Figure 3). The modeling demonstrated that both are integral membrane proteins with 10 transmembrane segments. This number of transmembrane segments is typical for P-type ATPases which belong to subfamilies P2 (includes Na^+-ATPases) and P3 (includes H^+-ATPases) of P-type ATPases [67]. The analysis of structure for the two ATPases demonstrates that the highest similarity lies within the region of 100–700 amino acids (Supplementary S4). This region includes the small cytoplasmic domain, the 3rd and the 4th transmembrane helices and the large cytoplasmic domain, and it is the region which contains all the important conservative parts of P-type ATPases [66]. This region is linked to the details of the catalytic cycle that are common for all P-type ATPases independently of their ion selectivity: binding of ATP and Mg^{2+} ions as reaction cofactor, formation of phosphorylated intermediate, conformational changes of the enzyme [45]. The similarity of *Dm*HA1 and *Dm*HA2 within the hydrophobic C-terminal part of the proteins, where modeling predicted transmembrane segments M4, M5, M6 and M8 involved in the formation of the transmembrane pathway for the transferred cation and playing a critical role in its high-affinity binding [33], is not high. It may suggest that *Dm*HA1 and *Dm*HA2 transport different cations. It is also worth mentioning that sometimes the substitution of a single amino acid can change the ion selectivity of enzyme, in particular swopping H^+ transport for that of Na^+ ions [68].

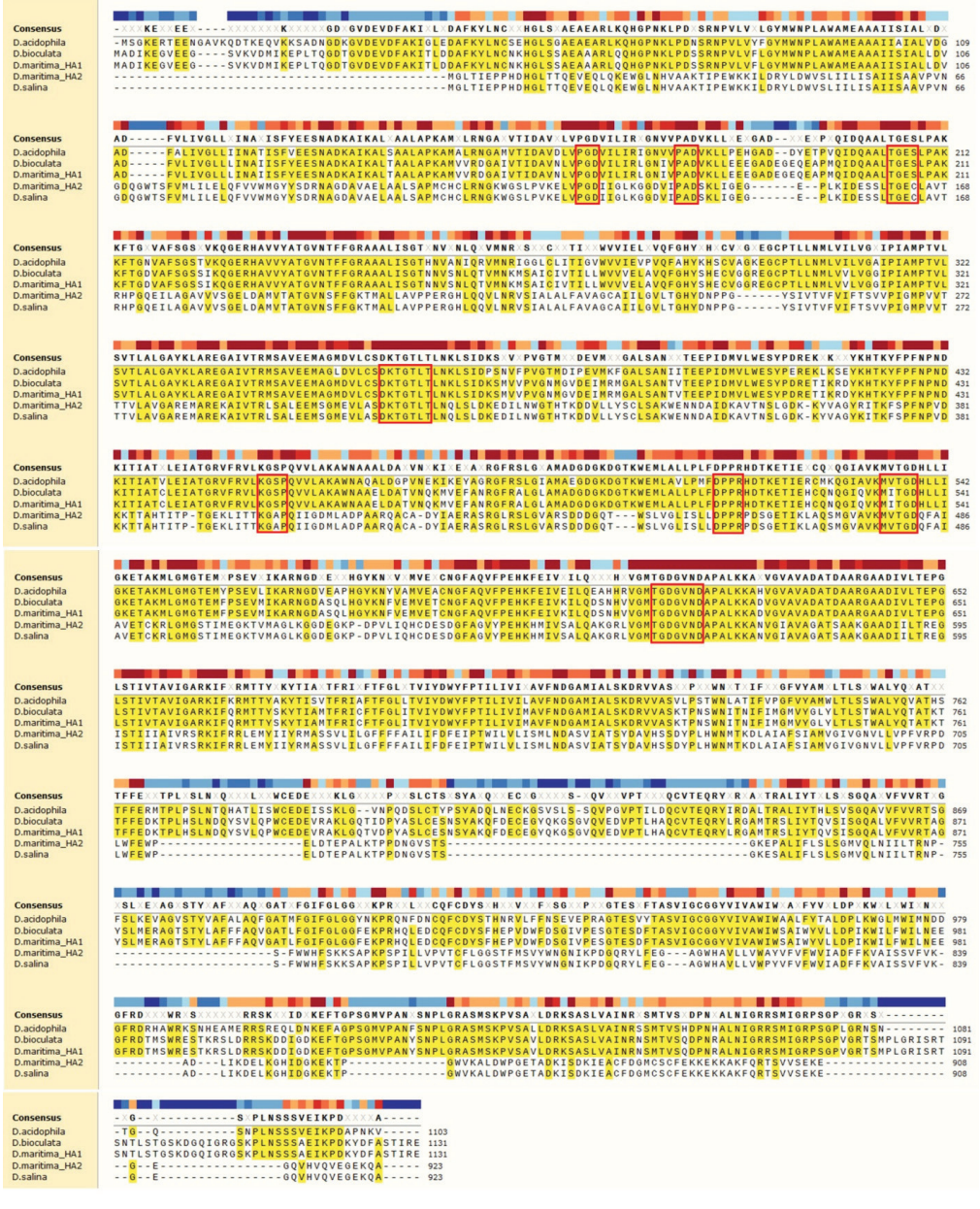

Figure 1. Multiple alignment of aa sequences of ATPases from *Dunaliella* species. The identical amino acids are shown in yellow background, and the conserved amino acids in P-type ATPases are highlighted by frames. The proteins for alignment: *D. acidophila*, P54210.1; *D. bioculata*, P54211.1; *D. maritima*_HA1, QEH60479.1; *D. maritima*_HA2, AQM50087.1; *D. salina*, ABB88698.1.

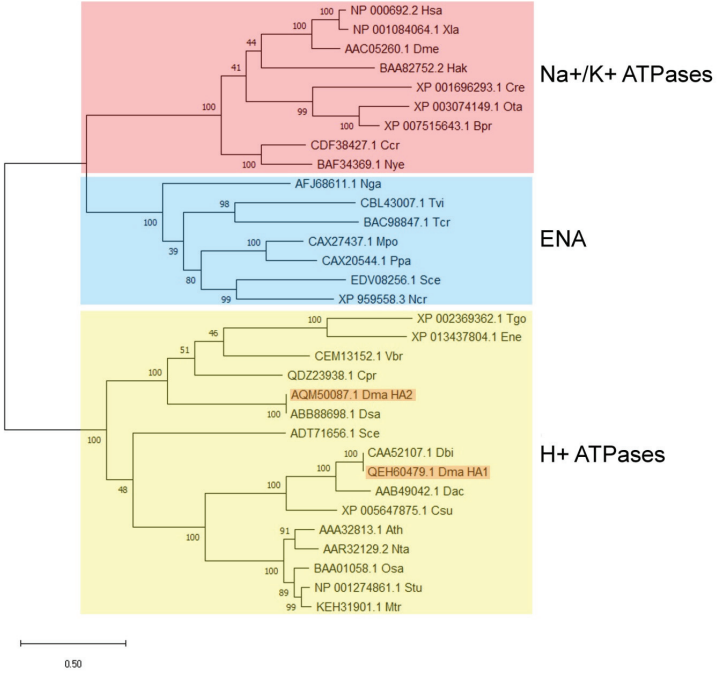

Figure 2. Cladogram of P-type H^+-ATPases and Na^+-ATPases from different organisms. Amino acid sequences from the following organisms are included in the analysis: Ath, *Arabidopsis thaliana*; Bpr, *Bathycoccus prasinos*; Ccr, *Chondrus crispus*; Cpr, *Chloropicon primus*; Cre, *Chlamidomonas reinhadtii*; Csu, *Coccomyxa subellipsoidea*; Dac, *Dunaliella acidophila*; Dbi, *Dunaliella bioculata;* Dma, *Dunaliella maritima*; Dme, *Drosophila melanogaster*; Dsa, *Dunaliella salina*; Ene, *Eimeria necatrix*; Hak, *Heterosigma akashiwo*; Has, *Homo sapiens*; Mpo, *Marchantia polymorpha*; Mtr, *Medicago truncatula*; Ncr, *Neurospora crassa*; Nga, *Nannochloropsis gaditana*; Nta, *Nicotiana tabacum*; Nye, *Neopyropia yezoensis;* Osa, *Oryza sativa*; Ota, *Ostreococcus tauri*; Ppa, *Physcomitrella patens*; Sce, *Saccharomyces cerevisiae*; Stu, *Solanum tuberosum*; Tcr, *Trypanosoma cruzi*; Tgo, *Toxoplasma gondii*; Tvi, *Tetraselmis viridis*; *Vbr, Vitrella brassicaformis*; Xla, *Xenopus laevis*.

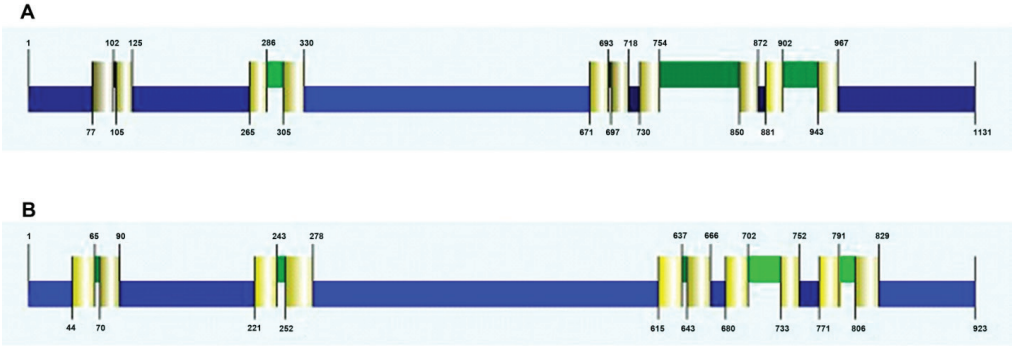

Figure 3. Predicted topology of *Dm*HA1 ((**A**), 1131 aa) and *Dm*HA2 ATPases ((**B**), 923 aa) and the location of the transmembrane domains (TMD) (colored pale yellow). Cytoplasmic areas (N-terminus, small and large cytoplasmic loops, C-terminus) are colored blue, extracellular protein areas are colored green. The figure illustrating the consistent model derived by the CCTOP (Constrained Consensus TOPology) online service (http://cctop.enzim.ttk.mta.hu, accessed on 1 December 2021) is taken from the Philius prediction (http://cctop.enzim.ttk.mta.hu, accessed on 1 December 2021).

Since the similarity of amino acid sequences for *Dm*HA1 and *Dm*HA2 was not high, the proteins are likely not isoforms of one protein and may have different functions. In this case, the *Dm*HA1 ATPase, which is similar to the well-characterized proton pumps of higher plants, is most likely a proton pump, while *Dm*HA2 could be a Na^+-transporting ATPase.

Na^+-transporting P-type ATPases have been identified functionally, as well as at the molecular level, in representatives of other eukaryotes: marine brown algae (kingdom *Chromista*) [69,70], protozoa (kingdom *Protista*) [71], green and red microalgae (kingdom *Plantae*) [41,72] and in primitive terrestrial plants, bryophytes [73]. Unlike the highly conservative H^+-ATPase of P-type, the features of Na^+-ATPases from various organisms may differ significantly. For example, the brown marine alga *Heterosigma akashiwo* and red alga *Porphyra yezoensis* have Na^+-ATPases similar to Na^+, K^+-ATPases of animal cells [72,74]. Na^+-ATPases in yeast form a special group of yeast-type ATPases (so-called ENA ATPases), which have low selectivity with respect to Na^+ and K^+ ions [47]. Na^+-ATPases of protozoa are very similar to yeast ENA ATPases [71]. The Na^+-transporting ATPase that was discovered in the green marine microalga *Tetraselmis viridis* [41], differs functionally from both animal Na^+, K^+-ATPase and yeast-type ENA ATPase. Unlike animal Na^+, K^+-ATPase that transport 3 Na^+ per 2 K^+, the ATPase from *T. viridis* does not transport K^+ but uses the H^+ ion as the counterion for Na^+, i.e., during the catalytic cycle it exchanges Na^+ for H^+ with odd (not even) stoichiometry (the exact stoichiometry of the transport cycle is not yet known) [75]. In contrast with the yeast-type ENA ATPases with low selectivity between Na^+ and K^+ [47], the Na^+-ATPase of *T. viridis* has high selectivity for Na^+ [76].

To identify a potential candidate for the role of Na^+-transporting ATPase in *D. maritma*, the expression of the *DmHA1* and *DmHA2* genes under hyperosmotic salt shock was studied. Algal culture acclimated to relatively low salt concentrations (0.1 M NaCl) in the medium was used in these experiments. Hyperosmotic salt shock was created by adding NaCl to the cell suspension to a final concentration of 0.5 M. During the response of the cells to hyperosmotic salt shock, a significant induction of the *DmHA2* gene occurred, while the expression of the *DmHA1* gene decreased and mostly remained at a relatively low level (Figure 4): the level of *Dm*HA2 transcripts was significantly higher than that for *Dm*HA1 during the response of *Dunaliella* cells to hyperosmotic salt shock. The maximum expression of *DmHA2* gene was observed at 90 min after adding NaCl to the cell suspension. After 90 min, the level of *DmHA2* transcripts gradually decreased and returned approximately to initial values after 3 h. The expression of *DmHA1* slightly increased at 90 min (compared to 60 min) after the sharp rise of external Na^+ concentration (Figure 4A). This increase of *DmHA1* expression could be explained by general biochemical reactions in response to hyperosmotic shock: they lead to synthesis of intracellular compatible osmolyte glycerol [9,77] and can acidify cytoplasm [78]. Plasma membrane H^+-ATPase is a main player in the cytoplasmic pH-stat (e.g., [49]), hence its activation (including at the transcriptional level) is required to alleviate or prevent the cytoplasmic acidification.

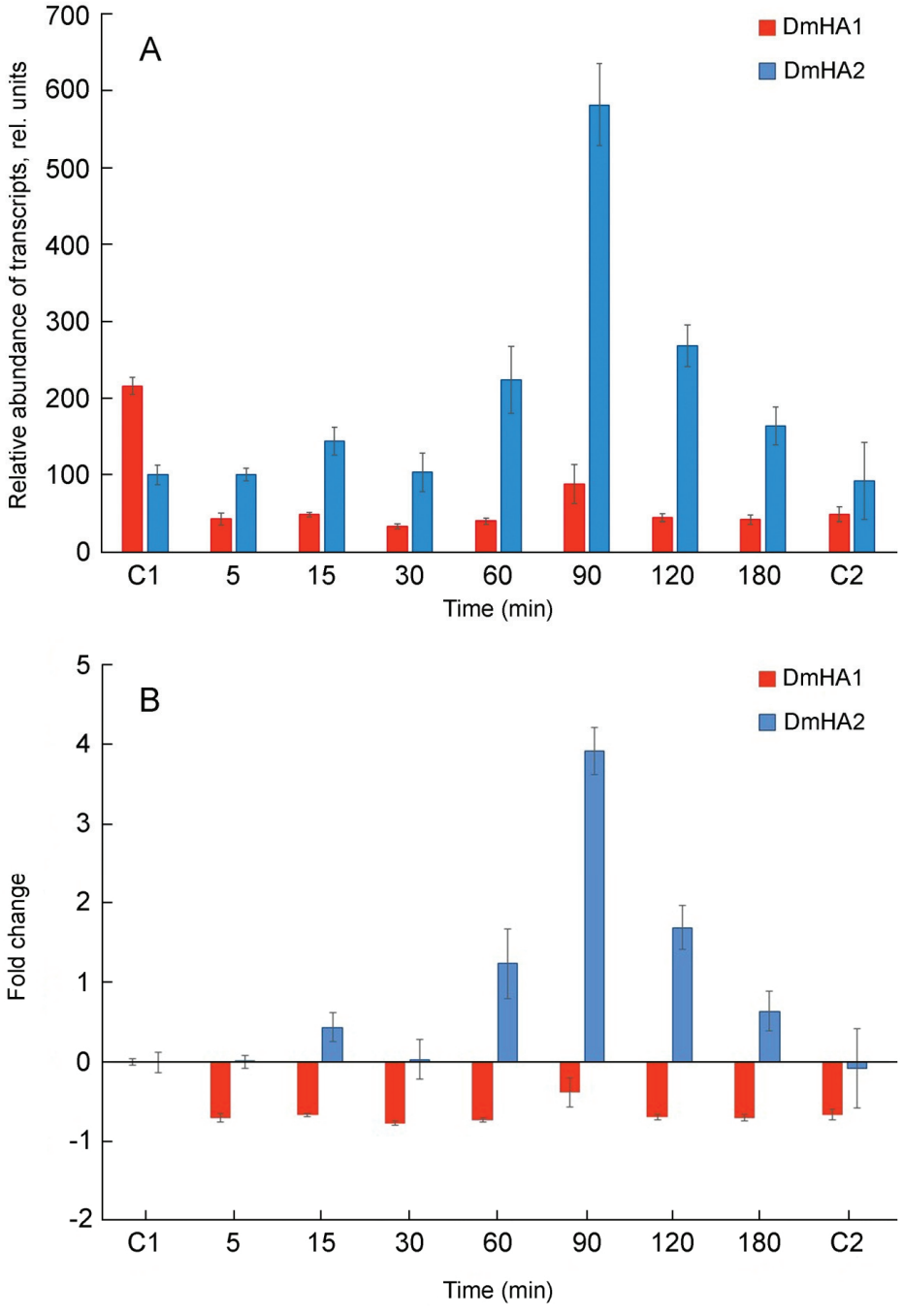

Figure 4. qRT-PCR analysis of *DmHA1* and *DmHA2* expression during the response of *D. maritima* cells to hyperosmotic salt shock. Sodium concentration in the medium was dramatically increased at "zero" time point. Points "C1" and "C2" represent the values of the expression of the ATPase genes in the algal cells growing at 0.1 M NaCl and 0.5 M NaCl in the medium, respectively. (**A**) relative abundance of transcripts; (**B**) recalculated fold changes of gene expression.

The dynamics of changes in the *DmHA2* gene expression corresponded to the dynamics of changes in intracellular Na^+ concentrations in *D. maritima* under conditions of hyperosmotic salt shock (Figure 5). Immediately following the increase in the external salt concentration, an increase in intracellular Na^+ concentrations (the so-called "entry phase") was observed. After some time, the growth of intracellular concentrations of Na^+ was replaced by a drop ("pumping phase"). Na^+ concentration in *D. maritima* cells, increased as a result of the hyperosmotic salt shock, but returned to the new steady-state level by 90–120 min after the increase in salt concentration in the medium. This decrease of intracellular Na^+ concentrations is accompanied by increased synthesis of glycerol [77] which finally becomes responsible for the osmotic balance in the algal cells [8–10]. The delayed maximum expression of *DmHA2* (at 90 min) compared to intracellular Na^+ concentrations (peaked at 40 min) probably indicates a required threshold or specific signature of Na^+ signal for induction of *DmHA2* gene while the excess Na^+ ions are removed earlier by activation of pumping achieved mostly at translational or post-translational levels. The new steady-state level of intracellular Na^+ concentration stabilizes though the expression of *DmHA2* decreases after 90 min of salt shock. It is likely that high expression of *DmHA2* is not necessary for cells under the new stationary conditions: Na^+ entry might be limited now by low Na^+ permeability of plasma membrane which is known for *Dunaliella* [7]. Therefore, it seems that intracellular concentration of Na^+ under stationary conditions is rather regulated by membrane permeability than by high expression of ATPase. The observed kinetics of intracellular Na^+ changes indicates that the mechanisms responsible for pumping Na^+ ions out of alga cells work efficiently and are able to restore ionic homeostasis. A significant induction of *DmHA2* with an increase in the NaCl concentration in the medium indicates that the ATPase encoded by this gene is necessary for the alga cells to overcome hyperosmotic salt stress and, as a P-type transport ATPase, is probably directly involved in the export of Na^+ ions from the alga cells, i.e., *Dm*HA2 might be a Na^+-transporting enzyme. It is interesting to note (Figure 4A) that expression of *DmHA1* is higher than expression of *DmHA2* at 0.1 M NaCl in the external medium while the opposite pattern (higher expression of *DmHA2*) was seen for 0.5 M NaCl and that *D. maritima* grows less well at 0.1 M NaCl than at higher external 0.5 M NaCl (personal unpublished results). It is likely that under the low salt conditions (0.1 M external NaCl) the energization of the algal plasma membrane is insufficient for energy-dependent uptake of nutrients, which also often involves symport with Na^+ ions [79–81], as the energization is realized by an electrogenic Na^+-pump (e.g., [82]) (presumably *Dm*HA2). The low membrane energization could be a consequence of a low Na^+ concentration gradient at the membrane. This low energization may require activation of the electrogenic proton pump (presumably *Dm*HA1), which also participates in generation of electric membrane potential; it then stimulates voltage-dependent nutrient transport processes. Higher external NaCl concentration (0.5 M NaCl), on the other hand, provides better opportunities for algal plasma membrane energization at the expenses of Na^+-ATPase, so that the cells do not need the high expression of the H^+-ATPase seen at the high concentration of NaCl in the medium.

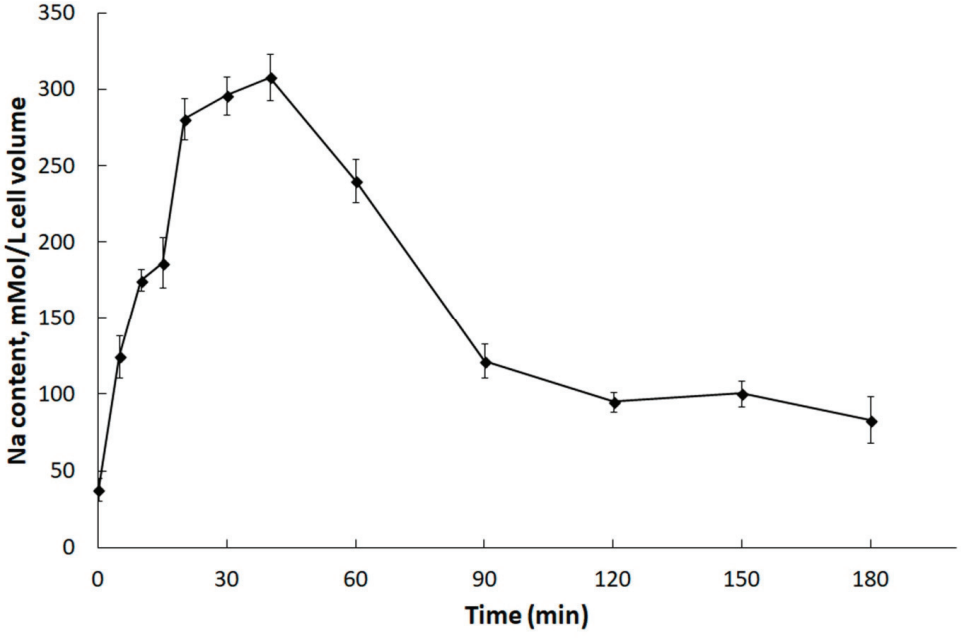

Figure 5. Changes in concentrations of Na^+ ions in *D. maritima* cells under hyperosmotic salt shock. The alga was grown in a medium containing 0.1 M NaCl. At "zero" time, the salt concentration in the cell suspension was increased to 0.5 M. Each point on the graph is the average of 4 analytical replications. The abscissa axis indicates the incubation time of algal cells in hypertonic salt medium.

4. Conclusions

The coexistence of proton pumps and Na^+-transporting ATPases has been demonstrated for plasma membranes of many unicellular eukaryotes, for yeast, microalgal cells and protists [76,83–85]. The situation is likely typical for cells that live in media with rapidly changing ion (especially Na^+) concentrations and pH; it demands the ability to activate different ion transport mechanisms to restore ion homeostasis of the cells.

Euryhaline green microalgae *D. maritima* inhabits shallow coastal basins and lagoons that are characterized by variable salinity [1,3]. Therefore, *D. maritima* is able to withstand sharp salinity changes and grow in a wide range of salinity [7,86]. Earlier, in experiments with plasma membrane vesicles isolated from *D. maritima* cells it was demonstrated using optical probes that both H^+-ATPase and Na^+-ATPase are functional in the *D. maritima* plasma membrane [51,59]. Both enzymes are P-type ATPases, which is typical for plasma membrane ATPases of eukaryotes. The data from the functional studies can be correlated with the results of the present research where coding sequences of two putative ATPases of *D. maritima*, *Dm*HA1 and *Dm*HA2, were cloned and analyzed. One of the enzymes, *Dm*HA1, is a conceivable proton pump since it shows high similarity to H^+-ATPase of higher plants and to the H^+-ATPase of *D. acidophila*. The latter is a freshwater species, its ATPase is overexpressed as the pH of the medium shifts to the region of acidic values, and the proton transfer function of the latter enzyme is beyond doubt [54]. Expression of *Dm*HA1 decreases and remains at a low level during the response of *D. maritima* cells to the hyperosmotic salt shock (Figure 4).

In contrast, expression of *DmHA2* increases under hyperosmotic salt shock. This indicates that the protein encoded by the gene is important for overcoming hyperosmotic salt stress experienced by the algal cells. The protein *Dm*HA2 is presumably a P-type ion transporting ATPase that takes a direct part in transport of Na^+ ions; i.e., it represents

a Na^+-transporting ATPase. Results of our experiments investigating the expression of *DmHA1* and *DmHA2* agree well with the results of research where the changes in the plasma membrane proteome of *D. salina* were analyzed under hyperosmotic salt shock [87]. This proteomic analysis revealed upregulation of a protein similar to ATPase with GenBank ID ABB88698.1. A noteworthy observation is that *Dm*HA2 demonstrates high similarity with exactly this ATPase (Table 1).

Phylogenetic analysis showed that *Dm*HA2 is similar to the poorly-studied ATPases of other microalgae and parasitic protists, whose subclade on the phylogenetic tree is in the same clade with H^+-ATPases of higher plants (Figure 2). However, the functions of the enzymes which are in the clade with *Dm*HA2, have not yet been experimentally characterized and their sequences are taken from the results on genome sequencing of the corresponding species. Hence, the characterization of the enzymes as H^+-ATPases is still rather preliminary. The ion selectivity in three-dimensional protein structure is often determined by amino acids located on different transmembrane segments of the enzyme. They selectively coordinate the ion carried by the ATPase along the path of its movement through the membrane [88,89]. The ion-binding sites are unexpectedly similar for Ca^{2+}-ATPases, Na^+, K^+-ATPase and H^+, K^+-ATPase; small changes in the ion binding sites of the enzymes are likely not the only reason determining the ion selectivity of these enzymes [90]. The binding of the "correct" ion neutralizes the negative charge in protein transmembrane segment and induces the conformation changes that lead to occlusion of the transferred ion [90]. Therefore, *in silico* prediction of ion selectivity for an ATPase requires experimental confirmation. For example, Na^+-ATPase from yeast, ENA1, was initially identified as a putative calcium P-type ATPase on the basis of its sequence characteristics [91]. Two years later its capacity to extrude Na^+, Li^+ and K^+ was reported [92]. Obviously, further research is needed to characterize functionally the cloned ATPases of *D. maritima*.

Supplementary Materials: The following are available online at https://www.mdpi.com/2223-7747/10/12/2667/s1, Table S1: Primers used in the study, S2: Contigs from the *de novo* assembled transcriptome of *D. tertiolecta* containing the coding sequences for *Dt*HA1 and *Dt*HA2 ATPases, S3: Partial coding sequence for *Dm*HA2, S4: Alignment of aa sequences of DmHA1 (QEH60479.1) and DmHA2 (AQM50087.1) ATPases from *D. maritima*. The identical amino acids are shown in black, and the conserved amino acids in P-type ATPases are highlighted by frames.

Author Contributions: Conceived and designed the experiments: L.G.P. and Y.V.B. Performed the experiments: D.A.M., D.E.K., A.V.S. and V.S.V. Analyzed the data: D.A.M., D.E.K., A.V.S. and L.G.P. Wrote and revised the paper: L.G.P. and V.S.V. Supervision, L.G.P.; project administration, L.G.P.; funding acquisition, L.G.P., Y.V.B. and V.S.V. All authors have read and agreed to the published version of the manuscript.

Funding: The reported study was funded by Russian Foundation for Basic Research, project No. 20-04-00903.

Institutional Review Board Statement: Not applicable.

Informed Consent Statement: Not applicable.

Data Availability Statement: Available data are presented in the manuscript and supplementary material; the sequences are deposited in GenBank.

Acknowledgments: The Authors thank Timothy J. Flowers for advising on the Manuscript before the submission and three anonymous Reviewers for their valuable comments and suggestions on our Manuscript.

Conflicts of Interest: The authors declare no conflict of interest.

References

1. Oren, A. A hundred years of *Dunaliella* research: 1905–2005. *Saline Syst.* **2005**, *1*, 2. [CrossRef] [PubMed]
2. Avron, M.; Ben-Amotz, A. (Eds.) *Dunaliella: Physiology, Biochemistry, and Biotechnology*; CRC Press: Boca Raton, FL, USA, 1992.
3. Borowitzka, M.A.; Siva, C.J. The taxonomy of the genus *Dunaliella* (Chlorophyta, *Dunaliella* Les) with emphasis on the marine and halophilic species. *J. Appl. Phycol.* **2007**, *19*, 567–590. [CrossRef]

4. Massjuk, N.P. *Morphology, Taxonomy, Ecology and Geographic Distribution of the Genus Dunaliella Teod. and Prospects for Its Potential Utilization*; Naykova Dumka: Kiev, Ukraine, 1973; p. 242. (In Russian)
5. Ginzburg, M. *Dunaliella*: A green alga adapted to salt. *Adv. Bot. Res.* **1987**, *14*, 93–183.
6. Ben-Amotz, A. Adaptation of the unicellular alga *Dunaliella parva* to a saline environment. *J. Phycol.* **1975**, *11*, 50–54. [CrossRef]
7. Balnokin, Y.V.; Mazel, Y.Y. Permeability of the plasma membrane to sodium ions in halophilic algae of the genus *Dunaliella*. *Soviet Plant Physiol.* **1985**, *32*, 23–30.
8. Wegmann, K. Osmotic regulation of photosynthetic glycerol production in *Dunaliella*. *Biochim. Biophys. Acta* **1971**, *234*, 317–323. [CrossRef]
9. Ben-Amotz, A.; Avron, M. The role of glycerol in the osmotic regulation of the halophilic alga *Dunaliella parva*. *Plant Physiol.* **1973**, *51*, 875–878. [CrossRef]
10. Borowitzka, L.J.; Brown, A.D. The salt relations of marine and halophilic species of the unicellular green alga, *Dunaliella*. The role of glycerol as a compatible solute. *Arch. Microbiol.* **1974**, *96*, 37–52. [CrossRef] [PubMed]
11. Gimmler, H.; Hartung, W. Low permeability of the plasma membrane of *Dunaliella parva* for solutes. *J. Plant Physiol.* **1988**, *133*, 165–172. [CrossRef]
12. Johnson, M.K.; Johnson, E.J.; MacElroy, R.D.; Speer, H.L.; Bruff, B.S. Effects of salts on the halophilic alga *Dunaliella viridis*. *J. Bacteriol.* **1968**, *95*, 1461–1468. [CrossRef]
13. Pollard, A.; Jones, W.G.W. Enzyme activities in concentrated solutions of glycinbetain and other solutes. *Planta* **1979**, *144*, 291–298. [CrossRef]
14. Balnokin, Y.V.; Medvedev, A.V. Effects of ions on electron transport in chloroplasts of the halophilic alga *Dunaliella*. *Soviet Plant Physiol.* **1980**, *27*, 1229–1236.
15. Flowers, T.J.; Dalmond, D. Protein synthesis in halophytes–the influence of potassium sodium, and magnesium in vitro. *Plant Soil* **1992**, *146*, 153–161. [CrossRef]
16. Maathuis, F.J.M.; Amtmann, A. K^+ nutrition and Na^+ toxicity: The basis of cellular K^+/Na^+ ratios. *Ann. Bot.* **1999**, *84*, 123–133. [CrossRef]
17. Hasegawa, P.M.; Bressan, R.A.; Zhu, J.K.; Bohner, H.J. Plant cellular and molecular responses to high salinity. *Annu. Rev. Plant Physiol. Plant Mol. Biol.* **2000**, *51*, 463–499. [CrossRef] [PubMed]
18. Bhandal, I.S.; Malik, C.P. Potassium estimation uptake, and its role in the physiology and metabolism of flowering plants. *Int. Rev. Cytol.* **1988**, *110*, 205–254. [CrossRef]
19. Volkov, V.; Amtmann, A. *Thellungiella halophila*, a salt-tolerant relative of *Arabidopsis thaliana*, has specific root ion-channel features supporting K^+/Na^+ homeostasis under salinity stress. *Plant J.* **2006**, *48*, 342–353. [CrossRef]
20. Huh, G.H.; Damsz, B.; Matsumoto, T.K.; Reddy, M.P.; Rus, A.M.; Ibeas, J.I.; Narasimhan, M.L.; Bressan, R.A.; Hasegawa, P.M. Salt causes ion disequilibrium-induced programmed cell death in yeast and plants. *Plant J.* **2002**, *29*, 649–659. [CrossRef]
21. Shabala, S. Salinity and programmed cell death: Unraveling mechanisms for ion specific signaling. *J. Exp. Bot.* **2009**, *60*, 709–711. [CrossRef]
22. Demidchik, V.; Cuin, T.A.; Svistunenko, D.; Smith, S.J.; Miller, A.J.; Shabala, S.; Sokolik, A.; Yurin, V. *Arabidopsis* root K^+-efflux conductance activated by hydroxyl radicals: Single-channel properties, genetic basis and involvement in stress-induced cell death. *J. Cell Sci.* **2010**, *123*, 1468–1479. [CrossRef]
23. Ehrenfeld, J.; Cousin, J.L. Ionic regulation of the unicellular green alga *Dunaliella tertiolecta*. *J. Membr. Biol.* **1982**, *70*, 47–57. [CrossRef]
24. Bental, M.; Degani, H.; Avron, M. ^{23}Na NMR studies of the intracellular sodium ion concentration in the halotolerant alga *Dunaliella salina*. *Plant Physiol.* **1988**, *87*, 813–817. [CrossRef] [PubMed]
25. Katz, A.; Avron, M. Determination of intracellular osmotic volume and sodium concentration in *Dunaliella*. *Plant Physiol.* **1985**, *78*, 817–820. [CrossRef] [PubMed]
26. Katz, A.; Pick, U.; Avron, M. Characterization and reconstitution of the Na^+/H^+ antiporter from the plasma membrane of the halophilic alga *Dunaliella*. *Biochim. Biophys. Acta* **2001**, *1504*, 423–431. [CrossRef]
27. Pick, U.; Karni, L.; Avron, M. Determination of ion content and ion fluxes in the halotolerant alga *Dunaliella salina*. *Plant Physiol.* **1986**, *81*, 92–96. [CrossRef]
28. Shumkova, G.A.; Popova, L.G.; Balnokin, Y.V. Export of Na^+ from cells of the halotolerant microalga *Dunaliella maritima*: Na^+/H^+ antiporter or primary Na^+-pump? *Biochemistry* **2000**, *65*, 1080–1087.
29. Pardo, J.M.; Cubero, B.; Leidi, E.O.; Quintero, F.J. Alkali cation exchanger: Roles in cellular homeostasis and stress tolerance. *J. Exp. Bot.* **2006**, *57*, 1181–1199. [CrossRef]
30. Rodriguez-Rosales, M.P.; Galvez, F.J.; Huertas, R.; Aranda, M.N.; Baghour, M.; Cagnac, O.; Venema, K. Plant NHX cation/proton antiporters. *Plant Signal. Bahavior* **2009**, *4*, 265–276. [CrossRef] [PubMed]
31. Yamaguchi, T.; Hamamoto, S.; Uozumi, N. Sodium transport system in plant cells. *Front. Plant Sci.* **2013**, *4*, 410. [CrossRef]
32. Gaxiola, R.A.; Palmgren, M.G.; Schumacher, K. Plant proton pumps. *FEBS Lett.* **2007**, *581*, 2204–2214. [CrossRef]
33. Morsomme, P.; Boutry, M. The plant plasma membrane H^+-ATPase: Structure, function and regulation. *Biochim. Biophys. Acta* **2000**, *1465*, 1–16. [CrossRef]
34. Duby, G.; Boutry, M. The plant plasma membrane proton pump ATPase: A highly regulated P-type ATPase with multiple physiological roles. *Pfluggers Arch.–Eur. J. Physiol.* **2009**, *457*, 645–655. [CrossRef] [PubMed]

35. Zhang, S.; Habets, M.; Breuninger, H.; Dolan, L.; Offringa, R.; van Duijn, B. Evolutionary and functional analysis of a *Chara* plasma membrane H^+-ATPase. *Front. Plan Sci.* **2020**, *10*, 1707. [CrossRef]
36. Ohta, H.; Shirakawa, H.; Uchida, K.; Yoshida, M.; Matuo, Y.; Enami, I. Cloning and sequencing of the gene encoding the plasma membrane H^+-ATPase from an acidophilic red alga, *Cyanidium caldarium*. *Biochim. Biophys. Acta* **1997**, *1319*, 9–13. [CrossRef]
37. Harada, A.; Fukuhara, T.; Takagi, S. Photosynthetic control of the plasma membrane H+-ATPase in Vallisneria leaves. II. Presence of putative isogenes and a protein equipped with a C-terminal autoinhibitory domain. *Planta* **2002**, *214*, 870–876. [CrossRef]
38. Masashi, T. Cell physiological aspects of the plasma membrane electrogenic H^+ pump. *J. Plant Res.* **2003**, *116*, 419–442. [CrossRef]
39. Matsuzaki, M.; Misumi, O.; Shin-I, T.; Maruyama, S.; Takahara, M.; Miyagishima, S.Y.; Mori, T.; Nishida, K.; Yagisawa, F.; Nishida, K.; et al. Genome sequence of the ultrasmall unicellular red alga *Cyanidioschyzon merolae* 10D. *Nature* **2004**, *428*, 653–657. [CrossRef]
40. Prochnik, S.E.; Umen, J.; Nedelcu, A.M.; Hallmann, A.; Miller, S.M.; Nishii, I.; Ferris, P.; Kuo, A.; Mitros, T.; Fritz-Laylin, L.K.; et al. Genomic analysis of organismal complexity in the multicellular green alga *Volvox carteri*. *Science* **2010**, *329*, 223–226. [CrossRef]
41. Balnokin, Y.; Popova, L.; Gimmler, H. Further evidence for an ATP-driven sodium pump in the marine alga *Tetraselmis (Platymonas) viridis*. *J. Plant Physiol.* **1997**, *150*, 264–270. [CrossRef]
42. Skou, J.C. Nobel Lecture. The identification of the sodium pump. *Biosci. Rep.* **1998**, *18*, 155–169. [CrossRef] [PubMed]
43. Scheiner-Bobis, G. The sodium pump. *Eur. J. Biochem.* **2002**, *269*, 2424–2433. [CrossRef] [PubMed]
44. Glinn, I.M. A hundred years of sodium pumping. *Annu. Rev. Physiol.* **2002**, *64*, 1–18. [CrossRef]
45. Jorgensen, P.L.; Hakansson, K.O.; Karlish, J.D. Structure and mechanism of Na, K-ATPase: Functional site and their interactions. *Annu. Rev. Physiol.* **2003**, *65*, 817–849. [CrossRef] [PubMed]
46. Benito, B.; Garciadeblas, B.; Rodriguez-Navarro, A. Potassium- or sodium-efflux ATPase, a key enzyme in the evolution of fungi. *Microbiology* **2002**, *148*, 933–941. [CrossRef] [PubMed]
47. Rodriguez-Navarro, A.; Benito, B. Sodium or potassium efflux ATPase. A fungal, bryophyte, and protozoal ATPase. *Biochim. Biophys. Acta* **2010**, *1798*, 1841–1853. [CrossRef] [PubMed]
48. Scarborough, G.A. Structure and function of the P-type ATPases. *Curr. Opin. Cell Biol.* **1999**, *11*, 517–522. [CrossRef]
49. Palmgren, M.G.; Nissen, P. P-type ATPases. *Annu. Rev. Biophys.* **2011**, *40*, 243–266. [CrossRef] [PubMed]
50. Palmgren, M.G.; Harper, J.F. Pumping with plant P-type ATPases. *J. Exp. Bot.* **1999**, *50*, 883–893. [CrossRef]
51. Popova, L.G.; Shumkova, G.A.; Andreev, I.M.; Balnokin, Y.V. Functional identification of electrogenic Na^+-translocating ATPase in the plasma membrane of the halotolerant microalga *Dunaliella maritima*. *FEBS Lett.* **2005**, *579*, 5002–5006. [CrossRef]
52. Popova, L.G.; Kornilova, A.G.; Shumkova, G.A.; Andreev, I.M.; Balnokin, Y.V. Na^+-transporting ATPase in the plasma membrane of halotolerant microalga *Dunaliella maritima* operates as a Na^+-uniporter. *Russ. J. Plant Physiol.* **2006**, *53*, 474–480. [CrossRef]
53. Wolf, A.H.; Slayman, C.W.; Gradmann, D. Primary structure of the plasma membrane H^+-ATPase from the halotolerant alga *Dunaliella bioculata*. *Plant Mol. Biol.* **1995**, *28*, 657–666. [CrossRef]
54. Weiss, M.; Pick, U. Primary structure and effect of pH on the expression of the plasma membrane H^+-ATPase from *Dunaliella acidophila* and *Dunaliella salina*. *Plant Physiol.* **1996**, *112*, 1693–1702. [CrossRef] [PubMed]
55. Raschke, B.C.; Wolf, A.H. Molecular cloning of a P-type Ca(2+)-ATPase from the halotolerant alga *Dunaliella bioculata*. *Planta* **1996**, *200*, 78–84. [CrossRef]
56. Popova, L.G.; Belyaev, D.V.; Shuvalov, A.V.; Yurchenko, A.A.; Matalin, D.A.; Khramov, D.E.; Orlova, Y.V.; Balnokin, Y.V. In silico analysis of transcriptomes of the marine green microalga *Dunaliella tertiolecta*: Identification of sequences encoding P-type ATPases. *Mol. Biol.* **2018**, *52*, 520–531. [CrossRef]
57. Guiry, M.D.; Guiry, G.M. Algae Base. World-Wide Electronic Publication, National University of Ireland, Galway. 2021. Available online: http://www.algaebase.org (accessed on 1 December 2021).
58. Balnokin, Y.V.; Medvedev, A.V. Na^+, K^+, and H^+ transport across the plasmalemma of K^+-deficient cells of the halophilic alga *Dunaliella maritima*. *Soviet Plant Physiol.* **1984**, *31*, 805–809.
59. Popova, L.G.; Shumkova, G.A.; Andreev, I.M.; Balnokin, Y.V. Na^+-dependent electrogenic ATPase from the plasma membrane of the halotolerant microalga *Dunaliella maritima*. *Dokl. Biochem. Biophys.* **2000**, *375*, 235–238. [CrossRef]
60. Massjuk, N.P. New taxa of the genus *Dunaliella* Teod. Part I. *Ukr. Bot. J.* **1973**, *30*, 175–178.
61. de Vries, S.; Hoge, H.; Bisseling, T. Isolation of total and polysomal RNA from plant tissues. In *Plant Molecular Biology Manual*; Gelvin, S.B., Schilperoort, R.A., Verma, D.P.S., Eds.; Kluwer Academic Publishers: Dordrecht, The Netherlands, 1988; pp. 1–13.
62. Ochman, H.; Gerber, A.S.; Hartl, D.L. Genetic applications of an inverse polymerase chain reaction. *Genetics* **1988**, *120*, 621–623. [CrossRef]
63. Okamoto, H.; Suzuki, Z. Intracellular concentration of ions in a halophilic strain of Chlamydomonas. I. Concentration of Na^+, K^+ and Cl^- in the cell. *Z. Allg. Microbiol.* **1964**, *4*, 350–357. [CrossRef]
64. Kumar, S.; Stecher, G.; Li, M.; Knyaz, C.; Tamura, K. MEGA X: Molecular evolutionary genetic analysis across computing platforms. *Mol. Biol. Evol.* **2018**, *35*, 1547–1549. [CrossRef]
65. Axelsen, K.; Palmgren, M.G. Evolution and substrate specificities in the P-type ATPase superfamily. *J. Mol. Evol.* **1998**, *46*, 84–101. [CrossRef]
66. Møller, J.V.; Juul, B.; le Maire, M. Structural organization, ion transport and energy transduction of P-type ATPases. *Biochim. Biophys. Acta* **1996**, *1286*, 1–51. [CrossRef]

67. Thever, M.D.; Saier, M.H., Jr. Bioinformatic characterization of P-type ATPase encoded within the fully sequenced genomes of 26 eukaryotes. *J. Membr. Biol.* **2009**, *229*, 115–130. [CrossRef]
68. Kaim, G.; Dimroth, P. Construction, expression and characterization of a plasmid-encoded Na^+-specific ATPase hybrid consisting of *Propionigenium modestum* F0-ATPase and *Escherichia coli* F1-ATPase. *Eur. J. Biochem.* **1994**, *222*, 615–623. [CrossRef]
69. Wada, M.; Satoh, S.; Kasamo, K.; Fujii, T. Presence of a Na^+-activated ATPase in the plasma membrane of the marine raphidophycean *Heterosigma akashiwo*. *Plant Cell Physiol.* **1989**, *30*, 923–928. [CrossRef]
70. Shono, M.; Wada, M.; Fujii, T. Partial purification of a Na^+-ATPase from the plasma membrane of the marine alga *Heterosigma akashiwo*. *Plant Physiol.* **1995**, *108*, 1615–1621. [CrossRef] [PubMed]
71. Iizumi, K.; Mikami, Y.; Hashimoto, M.; Nara, T.; Hara, Y.; Aoki, T. Molecular cloning and characterization of ouabain-insensitive Na^+-ATPase in the parasitic protist *Trypanosoma cruzi*. *Biochim. Biophys. Acta* **2006**, *1758*, 738–746. [CrossRef] [PubMed]
72. Uji, T.; Hirata, R.; Mikami, K.; Mizuta, H.; Saga, N. Molecular characterization and expression analysis of sodium pump genes in the marine red alga *Porphyra yezoensis*. *Mol. Biol. Rep.* **2012**, *39*, 7973–7980. [CrossRef] [PubMed]
73. Fraile-Escanciano, A.; Garciadeblas, B.; Rodriguez-Navarro, A.; Benito, B. Role of ENA ATPase in Na^+ efflux at high pH in bryophytes. *Plant Mol. Biol.* **2009**, *71*, 599–608. [CrossRef] [PubMed]
74. Shono, M.; Wada, M.; Hara, Y.; Fujii, T. Molecular cloning of Na^+-ATPase cDNA from a marine alga, *Heterosigma akashiwo*. *Biochim. Biophys. Acta* **2001**, *1511*, 193–199. [CrossRef]
75. Balnokin, Y.V.; Popova, L.G.; Pagis, L.Y.; Andreev, I.M. The Na^+-translocating ATPase in the plasma membrane of the marine microalga *Tetraselmis viridis* catalyzes a Na^+/H^+ exchange. *Planta* **2004**, *219*, 332–337. [CrossRef]
76. Pagis, L.Y.; Popova, L.G.; Andreev, I.M.; Balnokin, Y.V. Ion specificity of Na^+-transporting systems in the plasma membrane of the halotolerant alga *Tetraselmis* (*Platymonas*) *viridis*. *Russ. J. Plant Physiol.* **2001**, *48*, 281–286. [CrossRef]
77. Zakhozhii, I.G.; Matalin, D.A.; Popova, L.G.; Balnokin, Y.V. Responses of photosynthetic apparatus of the halotolerant microalga *Dunaliella maritima* to hyperosmotic salt shock. *Russ. J. Plant Physiol.* **2012**, *59*, 42–49. [CrossRef]
78. Chen, H.; Lu, Y.; Jiang, J.-G. Comparative analysis on the key enzymes of the glycerol cycle metabolic pathway in *Dunaliella salina* under osmotic stressess. *PLoS ONE* **2012**, *7*, e37578. [CrossRef]
79. Walker, N.A.; Sanders, D. Sodium-coupled solute transport in charophyte algae: A general mechanism for transport energization in plant cells? *Planta* **1991**, *185*, 443–445. [CrossRef]
80. Chan, C.X.; Reyes-Prieto, A.; Bhattacharya, D. Red and green algal origin of diatom membrane transporters: Insights into environmental adaptation and cell evolution. *PLoS ONE* **2011**, *6*, e29138. [CrossRef] [PubMed]
81. Chan, C.X.; Zäuner, A.; Wheeler, G.; Grossman, A.R.; Prochnik, S.E.; Blouin, N.A.; Zhuang, Y.; Benning, C.; Berg, G.M.; Yarish, C.; et al. Analysis of Porphyra membrane transporters demonstrates gene transfer among photosynthetic eukaryotes and numerous sodium-coupled transport systems. *Plant Physiol.* **2012**, *158*, 2001–2012. [CrossRef] [PubMed]
82. Raven, J.A.; Beardall, J. Energizing the plasmalemma of marine photosynthetic organisms: The role of primary active transport. *J. Mar. Biol. Assoc. UK* **2020**, *100*, 333–346. [CrossRef]
83. Ambesi, A.; Miranda, M.; Petrov, V.V.; Slayman, C.W. Biogenesis and function of the yeast plasma membrane H^+-ATPase. *J. Exp. Biol.* **2000**, *203*, 155–160. [CrossRef]
84. Van Der Heyden, N.; Docampo, R. Proton and sodium pumps regulate the plasma membrane potential of different stages of *Trypanosoma cruzi*. *Mol. Biochem. Parasitol.* **2002**, *120*, 127–139. [CrossRef]
85. Ruiz, A.; Ariño, J. Function and regulation of the *Saccharomyces cerevisiae* ENA sodium ATPase system. *Eukaryot. Cell* **2007**, *6*, 2175–2181. [CrossRef] [PubMed]
86. Balnokin, Y.V. Ion homeostasis and osmoregulation in halotolerant microalgae. *Russ. J. Plant Physiol.* **1993**, *40*, 498–506.
87. Katz, A.; Waridel, P.; Shevchenko, A.; Pick, U. Salt-induced changes in the plasma membrane proteome of the halotolerant alga Dunaliella salina as revealed by Blue-Native gel electrophoresis and nanoLC-MC/MS analysis. *Mol. Cell. Proteom.* **2007**, *6*, 1459–1472. [CrossRef] [PubMed]
88. Ogawa, H.; Toyoshima, C. Homology modeling of the cation binding sites of Na^+, K^+-ATPase. *Proc. Natl. Acad. Sci. USA* **2002**, *99*, 15977–15982. [CrossRef] [PubMed]
89. Palmgren, M.G.; Buch-Pedersen, M.J.; Møller, A.L. Mechanism of proton pumping by plant plasma membrane H^+-ATPase. *Ann. N. Y. Acad. Sci.* **2003**, *986*, 188–197. [CrossRef]
90. Bublitz, M.; Poulsen, H.; Morth, J.P.; Nissen, P. In and out of the cation pumps: P-type ATPase structure revisited. *Curr. Opin. Struct. Biol.* **2010**, *20*, 431–439. [CrossRef] [PubMed]
91. Rudolf, H.K.; Anteli, A.; Fink, G.B.; Buckley, C.M.; Dorman, T.E.; LeVitre, J.; Davidow, L.S.; Mao, J.I.; Moir, D.T. The yeast secretory pathway is perturbed by mutations in PMR1, a member of a Ca^{2+}-ATPase family. *Cell* **1989**, *58*, 133–145. [CrossRef]
92. Haro, R.; Garciadeblas, B.; Rodriguez-Navarro, A. A novel P-type ATPase from yeast involved in sodium transport. *FEBS Lett.* **1991**, *291*, 189–191. [CrossRef]

plants

MDPI

Article

Molecular Cloning and Characterization of SaCLCd, SaCLCf, and SaCLCg, Novel Proteins of the Chloride Channel Family (CLC) from the Halophyte *Suaeda altissima* (L.) Pall

Olga I. Nedelyaeva *, Larissa G. Popova, Vadim S. Volkov * and Yurii V. Balnokin

K.A. Timiryazev Institute of Plant Physiology RAS, 127276 Moscow, Russia; lora_gp@mail.ru (L.G.P.); balnokin@mail.ru (Y.V.B.)

* Correspondence: olga.nedelyaeva@yandex.ru (O.I.N.); vadim.s.volkov@gmail.com (V.S.V.)

Abstract: Coding sequences of the CLC family genes *SaCLCd*, *SaCLCf*, and *SaCLCg*, the putative orthologs of *Arabidopsis thaliana AtCLCd*, *AtCLCf*, and *AtCLCg* genes, were cloned from the euhalophyte *Suaeda altissima* (L.) Pall. The key conserved motifs and glutamates inherent in proteins of the CLC family were identified in SaCLCd, SaCLCf, and SaCLCg amino acid sequences. SaCLCd and SaCLCg were characterized by higher homology to eukaryotic (human) CLCs, while SaCLCf was closer to prokaryotic CLCs. Ion specificities of the SaCLC proteins were studied in complementation assays by heterologous expression of the *SaCLC* genes in the *Saccharomyces cerevisiae GEF1* disrupted strain Δ*gef1*. *GEF1* encoded the only CLC family protein, the Cl^- transporter Gef1p, in undisrupted strains of this organism. Expression of *SaCLCd* in Δ*gef1* cells restored their ability to grow on selective media. The complementation test and the presence of both the "gating" and "proton" conservative glutamates in SaCLCd amino acid sequence and serine specific for Cl^- in its selectivity filter suggest that this protein operates as a Cl^-/H^+ antiporter. By contrast, expression of *SaCLCf* and *SaCLCg* did not complement the growth defect phenotype of Δ*gef1* cells. The selectivity filters of SaCLCf and SaCLCg also contained serine. However, SaCLCf included only the "gating" glutamate, while SaCLCg contained the "proton" glutamate, suggesting that SaCLCf and SaCLCg proteins act as Cl^- channels. The *SaCLCd*, *SaCLCf*, and *SaCLCg* genes were shown to be expressed in the roots and leaves of *S. altissima*. In response to addition of NaCl to the growth medium, the relative transcript abundances of all three genes of *S. altissima* increased in the leaves but did not change significantly in the roots. The increase in expression of *SaCLCd*, *SaCLCf*, and *SaCLCg* in the leaves in response to increasing salinity was in line with Cl^- accumulation in the leaf cells, indicating the possible participation of SaCLCd, SaCLCf, and SaCLCg proteins in Cl^- sequestration in cell organelles. Generally, these results suggest the involvement of SaCLC proteins in the response of *S. altissima* plants to increasing salinity and possible participation in mechanisms underlying salt tolerance.

Keywords: *Suaeda altissima*; anion transporters; chloride channel family; CLC family; halophytes; molecular cloning; salt tolerance; *SaCLCd*; *SaCLCf*; *SaCLCg*

Citation: Nedelyaeva, O.I.; Popova, L.G.; Volkov, V.S.; Balnokin, Y.V. Molecular Cloning and Characterization of SaCLCd, SaCLCf, and SaCLCg, Novel Proteins of the Chloride Channel Family (CLC) from the Halophyte *Suaeda altissima* (L.) Pall. *Plants* **2022**, *11*, 409. https://doi.org/10.3390/plants11030409

Academic Editor: Wei Ma

Received: 30 December 2021
Accepted: 29 January 2022
Published: 2 February 2022

Publisher's Note: MDPI stays neutral with regard to jurisdictional claims in published maps and institutional affiliations.

1. Introduction

Soil salinization is a significant problem in agriculture. Salt-affected soils occupy more than 6% of the earth's land surface (800 million hectares) and, according to various estimates, 20–50% of irrigated land [1–3]. The annual losses from salinization in the world currently exceed US $27 billion [4]. The decrease in yield caused by salinity is due to the fact that the vast majority of agricultural crops are salt-sensitive plants, also known as glycophytes [5–8]. NaCl in soil results in disturbances in plant–water relations and causes Na^+ and Cl^- accumulation up to toxic levels in the cytoplasm [7,9–11].

Halophytes are plants of saline habitats that have evolved mechanisms to adequately regulate Na^+ and Cl^- concentrations in cytoplasm and acquire nutrients, in particular nitrate, under soil salinization [12–14]. The transport of the cations Na^+ and K^+ under

salt stress is relatively well studied [6,15–21]. However, much less is known about the transport of anions. Despite the fact that anion flow into cells is hindered by the plasma membrane electric potential, negative from the cytoplasmic side, Cl^- ions at high external concentrations may passively enter the cells and accumulate in the cytoplasm [9,22,23]. Sensitivity of many plants to Cl^- is known to be even higher than to Na^+ [24,25]. To grow under soil salinization, plants, including halophytes, need to maintain relatively low Cl^- concentrations in their cytoplasm. For example, the Cl^- concentration in the leaf cytoplasm of *Suaeda maritima* growing in 340 mM NaCl was estimated to be approximately 90 mM [26]. One of the main reasons for low NO_3^- availability in plants on salt-affected soils is direct competition of NO_3^- with Cl^- for high-affinity anionic transporters [27–30]. However, nitrate deficiency in halophytes under chloride salinity is less pronounced than in glycophytes [28–30]. The ion-transporting proteins of halophytes have been assumed to differ in primary structure, and accordingly in physicochemical properties, from their orthologs in glycophytes [7,29–31]. However, researchers have paid little attention to anion transporters despite the supposedly higher efficiency of nitrate transporters of halophytes compared to their orthologs from glycophytes. There are abundant published data on the physiology of salt tolerance in glycophytes but practically no information on the genes encoding anion-transporting proteins of halophytes, which provide absorption, delivery to cells and intracellular regulation of anions, even under strong salinization.

In glycophytes, anion channels and transporters from the CLC (chloride channel) family play key roles in anionic homeostasis, salinity tolerance, and nitrogen nutrition [32–34]. CLC proteins are found in representatives of all kingdoms [35–38]. In addition to chloride channels, this family includes anion/proton exchangers (Cl^-/H^+ and NO_3^-/H^+ antiporters) [38]. Contrary to the situation in glycophytes, CLC channels have hardly been studied in halophytes.

In plants, CLC proteins are localized mainly in endomembranes, where they perform many different functions, such as carrying out electrogenic transport of NO_3^- from cytosol into vacuoles [39,40], regulating cytoplasmic concentrations of NO_3^- [41], and participating in acidification of organelles and assumedly in the regulation of their transmembrane electric potential [38]. By analogy with mammalian CLCs, it can be suggested that due to neutralization of positive charges accumulating in organelles as a result of the operation of V-type H^+-ATPase, the anion/H^+ exchange executed by plant CLCs promotes compartmentalization of anions in organelles and converts electrical potential into ΔpH. The latter can be subsequently used by secondary transporters as an energy source for transport of diverse substances across the organellar membranes [42]. Cl^- transporters are also involved in vesicular trafficking [43–45].

Seven genes of the CLC family have been cloned from *A. thaliana*, namely AtCLCa–e. While the functions and physiological roles of their products have been extensively investigated [32–34,46], the halophyte orthologs of CLC family proteins remain barely studied. The molecular cloning and functional characterization of proteins from halophytes are important for elucidating the mechanisms underlying plant salt tolerance and improving crop resistance to soil salinity by genetic manipulations [47–50].

Recently, we cloned *SaCLCa1* and *SaCLCc1*, the putative orthologs of *AtCLCa* and *AtCLCc* encoding NO_3^-/H^+ and Cl^-/H^+ antiporters of *A. thaliana*, respectively, from the euhalophyte *Suaeda altissima* [51,52]. In the present work, we describe the cloning of other genes of the CLC family from *S. altissima*, namely *SaCLCd*, *SaCLCf*, and *SaCLCg*, the putative orthologs of *AtCLCd*, *AtCLCf*, and *AtCLCg*, and investigate anion selectivity of the encoded proteins. The anion selectivity of SaCLCd, SaCLCf, and SaCLCg was examined in complementation assays by heterologous expression of their genes in the *Saccharomyces cerevisiae GEF1* disruption mutant Δ*gef1*. *GEF1* is the only gene from the CLC family in *S. cerevisiae*, and the protein Gef1p is characterized by Cl^- specificity [53]. Relative *SaCLCd*, *SaCLCf*, and *SaCLCg* transcript levels as well as Cl^- content in organs and their biomass were also measured for *S. altissima* plants grown at various NaCl concentrations.

2. Materials and Methods

2.1. Plant Material

Seeds of *S. altissima* (L.) Pall. were collected from plants growing in the wild on the shores of Lake Elton, a salt lake located in Russia (Volgograd region). The seeds were germinated in wet sand at 21–23 °C. After three weeks, the seedlings were transplanted into a 3 L glass container (4 plants per container) on an aerated Robinson and Downton [54] nutrient solution, supplemented with 250, 500, and 750 mM NaCl or without salt. Plants were then grown in a growth chamber under controlled environmental conditions in water culture at 24 °C and air relative humidity of 60–70%. The plants were illuminated with high-pressure sodium lamps DNaZ_400 "Reflux" ("Minimax", Saint Petersburg, Russia) with a photoperiod of 16 h/8 h (day/night) and a light intensity of 300 μmol photons/(m^2·s). Plants that were 45 days old were used in the experiments. For total RNA extraction, leaves and roots of *S. altissima* were sampled (approximately 1 g fresh weight of each sample) and frozen in liquid nitrogen for further use.

2.2. Total RNA Extraction and First-Strand cDNA Synthesis

Total RNA samples from *S. altissima* organs were obtained by the hot phenol procedure of Yourieva et al. [55] and used as templates for first-strand cDNA synthesis. For the amplification of 3′- and 5′-ends of *CLC* transcript sequences using Step-Out RACE technology, synthesis of first-strand cDNA was carried out with Mint reverse transcriptase ("Evrogen", Moscow, Russia) according to the protocol from the manufacturer. For cloning cDNA of CLC family genes and quantitative analysis of *SaCLCd*, *SaCLCf*, and *SaCLCg* transcripts in *S. altissima* organs, synthesis of first-strand cDNA was carried out using total RNA, $(dT)_{15}$ primer, and MMLV reverse transcriptase ("Evrogen", Moscow, Russia).

2.3. Amplification of SaCLCd, SaCLCf, and SaCLCg cDNA Partial Sequences

First, we performed an *in silico* search for the sequences homologous to the *AtCLCd*, *AtCLCf*, and *AtCLCg* genes in the *de novo* assembled by us transcriptomes of *Suaeda fruticosa* (L.) Forssk, which is a closely related species of *S. altissima* [51,56]. To do this, the contigs of the assembled transcriptomes were translated into amino acid sequences and search for the sequences related to the CLC family proteins was accomplished in the obtained arrays. AtCLCd, AtCLCf, and AtCLCg proteins were used as queries. The primers for amplification of partial cDNA fragments of *S. altissima* homologous genes (Table S1) were then designed using the contigs identified in the assembled *S. fruticosa* transcriptomes and encoding partial sequences of putative chloride channels/transporters. With these primers, the partial cDNAs of *S. altissima* CLC genes were amplified from cDNA template using Encyclo DNA polymerase ("Evrogen", Moscow, Russia) and sequenced.

2.4. Cloning of the Full-Length SaCLCd, SaCLCf, and SaCLCg cDNA Sequences

Based on the partial *SaCLCd*, *SaCLCf*, and *SaCLCg* sequences obtained, the forward and reverse primer sets were designed for amplification of the 3′- and 5′-end fragments (Table S1). With these primers, we amplified the 3′- and 5′-end fragments of *SaCLCd*, *SaCLCf*, and *SaCLCg* (~1000–1500 bp) by 3′- and 5′-rapid amplification of cDNA ends (3′- and 5′-RACE) using the Step-Out RACE technology and cloned them into vector pAL2-T ("Evrogen", Moscow, Russia). Cloned 3′- and 5′-ends fragments of *SaCLCd*, *SaCLCf*, and *SaCLCg* cDNA were then sequenced. Partial sequences (central fragments, the 3′- and 5′-end fragments of *SaCLCd*, *SaCLCf*, and *SaCLCg*) were then combined *in silico*, and the resulting complete coding sequences for *SaCLCd*, *SaCLCf*, and *SaCLCg* contained open reading frames (ORFs) for proteins of 793, 587, and 776 amino acids (aa), respectively. Experimentally, the full-size *SaCLCd*, *SaCLCf*, and *SaCLCg* cDNA sequences were amplified with a CloneAmpPCR PreMix kit ("TaKaRa"/Takara Bio Inc., Shiga, Japan; cat # 638916) using pairs of the forward and reverse primers (Table S1) and total first-strand cDNA as a template. The amplified *SaCLCd*, *SaCLCf*, and *SaCLCg* cDNAs were cloned into shuttle vector pMB1, which are designed for expression of proteins in yeast cells [57], under the control of the strong

constitutive promoter *GPD1*. A linear form of pMB1 was amplified using the pair of primers (Table S1). The recombinant plasmids pMB1–*SaCLCd*, pMB1–*SaCLCf*, and pMB1–*SaCLCg* were obtained by fusion of *SaCLCd*, *SaCLCf*, and *SaCLCg* cDNAs and the linear form of pMB1 using a Gibson Assembly Cloning kit ("New England Biolabs", Ipswich, MA, USA). The cloned *SaCLCd, SaCLCf,* and *SaCLCg* were sequenced, and the obtained sequences were deposited in GenBank.

2.5. Heterologous Expression of the SaCLCd, SaCLCf, and SaCLCg Genes in Δgef1 Yeast Mutant

S. cerevisiae mutant strain Δ*gef1* that was created by us earlier [51,52] was transformed with constructs pMB1–*SaCLCd*, pMB1–*SaCLCf*, and pMB1–*SaCLCg* using the lithium protocol [58]. To explore the growth characteristics of the mutant strain Δ*gef1* and the transformants, yeast cells were plated on a number of agarized (2%) selective media described in [59], namely (1) rich YPD medium consisting of 1% yeast extract, 2% peptone, and 2% dextrose (as a fermentable carbon source); (2) rich YPEG medium consisting of 1% yeast extract, 2% peptone, 2% ethanol, and 2% glycerol (as a nonfermentable carbon source); (3) minimal synthetic medium SD [60] supplemented with 2% dextrose and buffered with 50 mM Mes-Tris, pH 7.0; and (4) minimal synthetic medium SR supplemented with 2% raffinose as a nonfermentable carbon source and buffered with 50 mM Mes-Tris, pH 7.0. Yeast cells were left to grow on the selective media for two days (YPD), three days (YPD, YPEG, and SD) or four days (SR) at 28 °C. To study the effect of Mn^{2+} on yeast cell growth, $MnCl_2$ or $MnSO_4$ were added to the media at final concentrations of 2 or 3 mM. To set up iron deficiency, ferrosin, which is an iron chelator, was added to the media at a final concentration of 1 mM.

2.6. Quantitative Analysis of SaCLCd, SaCLCf, and SaCLCg Transcripts in S. altissima Organs

The cDNA templates for *SaCLCd*, *SaCLCf*, and *SaCLCg* fragment amplification were synthesized on the templates of total RNAs isolated from roots and leaves of *S. altissima* plants grown on nutrient media with various NaCl concentrations. Quantitative analysis of *SaCLCd*, *SaCLCf*, and *SaCLCg* transcripts was performed by the qRT-PCR method using a LightCycler® 96 system (Roche Diagnostics Corporation, Indianopolis, IN, USA). A reaction mixture with intercalating dye SYBR Green I ("Evrogen", Moscow, Russia) was used. To amplify the *SaCLCd*, *SaCLCf*, and *SaCLCg* fragments, the pairs of primers were used (Table S1). Target gene mRNA expression levels were normalized for the *S. altissima* actin gene *SaAct7* (GenBank, acc. no. MK615596.1) and the elongation factor 1 alpha gene *SaeEF1alpha* (GenBank, acc. no. MN076325.1). To amplify the *SaAct7* and *SaeEF1alpha* fragments, the primer pairs were used (Table S1). Results were based on three to five biological replicates. The results obtained were processed by LightCycler 96SW 1.1 software. The expression of the selected reference genes was quite stable with fold changes not exceeding 0.4 under the chosen experimental conditions.

2.7. Primer Design

Primers for qPCR-RT experiments were designed by Light Cycler96 Probe Design software (https://lifescience.roche.com/, accessed on 15 December 2021). Other primers were designed using Oligo 7 software (https://www.oligo.net/, accessed on 15 December 2021) or Primer Blast software (https://www.ncbi.nlm.nih.gov/tools/primer-blast/, accessed on 15 December 2021). The primers are listed in Table S1.

2.8. Bioinformatic Analysis of Amino Acid Sequences

Multiple alignment of amino acid sequences of CLC proteins was performed by MAFFT software using on-line service (https://www.ebi.ac.uk/Tools/msa/mafft/, accessed on 15 December 2021). The phylogenetic tree of plant CLC family proteins was created by Molecular Evolutionary Genetic Analysis (MEGA) 11 software (https://www.megasoftware.net/, accessed on 15 December 2021) using the maximum likelihood method based on the Jones–Taylor–Thornton model [61] (1000 bootstrap replication performed).

Protein topology was predicted by MEMSAT-SVM software (http://bioinf.cs.ucl.ac.uk/software_downloads/memsat/, accessed on 15 December 2021). Intracellular localization of the proteins was predicted with the DeepLoc 1.0 software's eukaryotic protein subcellular localization predictor (http://www.cbs.dtu.dk/services/DeepLoc-1.0/index.php, accessed on 15 December 2021).

2.9. Determination of Chloride Content in S. altissima Organs

Water extracts from *S. altissima* roots and leaves were prepared by incubating samples that were dried for 1 day at 90 °C and then ground in boiling deionized water for 10 min. Concentrations of Cl^- in the extracts were determined by titration with Hg^{2+} using a Top Buret H digital burette (Eppendorf, Wesseling-Berzdorf, Germany).

2.10. Statistical Analysis

Statistical analysis of the data was made by one-way analysis of variance (ANOVA). A p-value < 0.05 was considered to be statistically significant. * $p \leq 0.05$; ** $p \leq 0.01$; *** $p \leq 0.001$. Standard deviations are given. Correlation coefficients were calculated in the Excel program.

3. Results

Coding nucleotide sequences of *SaCLCd*, *SaCLCf*, and *SaCLCg*, genes from the halophyte *S. altissima*, were determined based on the putative similarity of these genes to homologous genes from the halophyte *S. fruticosa*. As a result of *in silico* searches of sequences related to the *CLC* family in the *de novo* assembled transcriptome of *S. fruticosa* [51,56], the contigs containing the partial coding regions of three sequences homologous to the *A. thaliana CLC* genes were designated by us as *SfCLCd*, *SfCLCf*, and *SfCLCg*. The contigs from *S. fruticosa* served as a base for identification of the full-size coding sequences of the target *S. altissima* genes by a rapid amplification of 3´- and 5´-cDNA ends. The cDNAs of the *SaCLCd*, *SaCLCf*, and *SaCLCg* genes thus obtained were then cloned and sequenced. The cloned cDNAs of *SaCLCd* (GenBank, acc. no. OK626332), *SaCLCf* (GenBank, acc. no. OK626333), and *SaCLCg* (GenBank, acc. no. OK626334) genes contained open reading frames (ORFs) encoding polypeptides consisting of 793, 587, and 776 amino acids, with calculated molecular masses of 87.6, 62.3, and 85.8 kDa, respectively. SaCLCd and SaCLCg were of molecular masses close to those of most plant and animal CLC proteins [37,62–65]. SaCLCf was noticeably smaller than the other two proteins. It should be noted that similar but smaller CLC proteins have been found in other plants. The *AtCLCf* gene encodes two forms of the AtCLCf protein, one with molecular mass of 83.5 kDa (781 a.a., At1g55620.2) and a shorter one with molecular mass of 62.5 kDa (586 a.a., At1g55620.1) [37] (Figure S1). Moreover, shortened *CLCf* transcripts with corresponding shortened proteins were revealed in transcriptomes of grape (*Vitis vinifera*) (GenBank: NP_001268117.1), pistachio (*Pistacia vera*) (GenBank: XP_031257549.1), and alfalfa (*Medicago truncatula*) (GenBank: KEH32883.1).

Each of the three proteins identified in *S. altissima* contained three conserved motifs (Figure 1) that are a distinctive feature of all CLC proteins. In the amino acid sequences of the SaCLC proteins, the motifs occupied the positions given in Table S2. The motifs of two proteins, SaCLCd and SaCLCg, were found to match the next sequences, namely (1) GxGxPE, (2) GKxGPxxH, and (3) PxxGxLF revealed earlier in *A. thaliana* [32]. The three homologous motifs identified in SaCLCf, namely (1) SSKSSQ, (2) GPEGPSVD, and (3) AVAGCFF, differed from those of SaCLCd and SaCLCg and were almost identical to the motifs of AtCLCf (Figure S1).

According to [66], the conserved motifs in CLC proteins are involved in the formation of the anion-conducting pathway through membrane, in determination of channel ionic selectivity, and in gating of anion-conducting pathway. The motif GSGIPE and its putative homolog SSKSSQ (Figure 1) are functional as selectivity filters [66,67]. The amino acid occupying the second position in the motifs has been shown to be responsible for anionic

specificity of the CLC protein, namely proline (P) for NO_3^- and serine (S) for Cl^- [68,69]. The GSGIPE (SSKSSQ in SaCLCf) motif of the *S. altissima* CLC proteins identified in the current study included serine in the second position, thus suggesting involvement of these proteins in chloride transport.

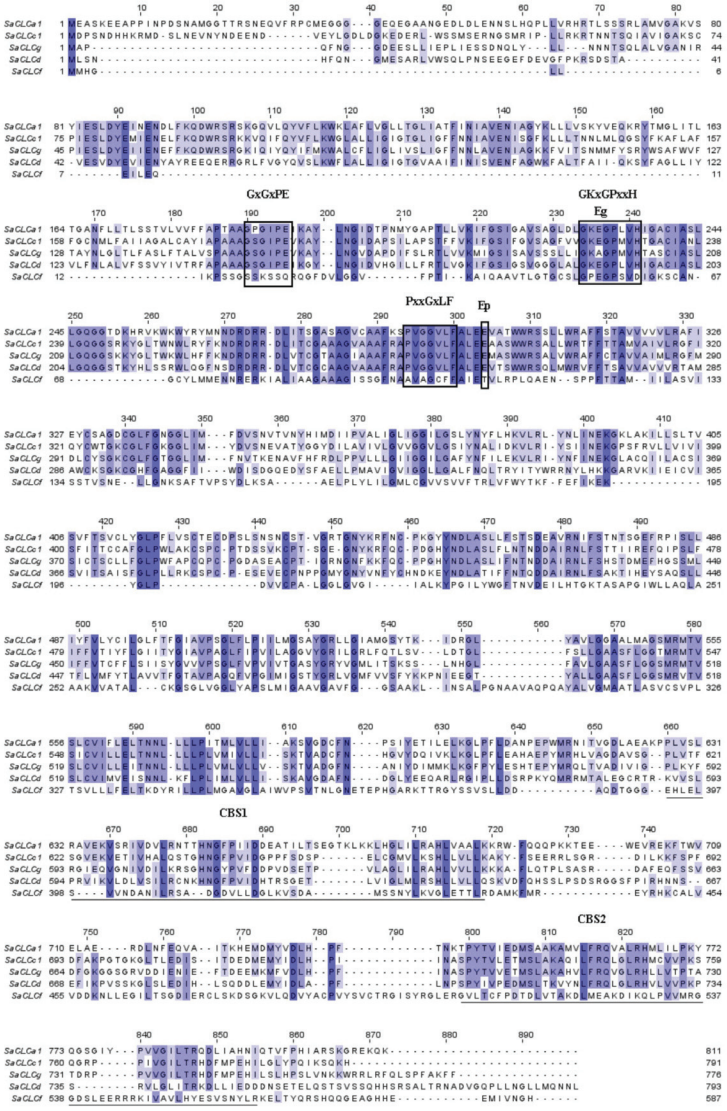

Figure 1. Alignment of the amino acid sequences of CLC proteins from *S. altissima*: SaCLCa1 (GenBank, acc. no. ANG09048.1), SaCLCc1 (GenBank, acc. no. AVQ93350.1), SaCLCd (GenBank, acc. no. OK626332), SaCLCf (GenBank, acc. no. OK626333), and SaCLCg (GenBank, acc. no. OK626334). The alignment was performed in the MAFFT program and visualized in Jalview 2.11.1.4 program [70]. The conserved amino acid motifs (GxGxPE, GKxGPxxH and PxxGxLF) are framed. GxGxPE motif is a selective filter. Eg and Ep are the key glutamates of the CLC family proteins. The intensity of staining for amino acid residues depicts the degree of their identity (percentage identity). CBS1 and CBS2 domains are underlined.

Two conserved glutamates, Eg ("gating" glutamate) and Ep ("proton" glutamate), play key roles in the functioning of anion/H^+ antiporters of the CLC family [36,71]. Eg participates in the gating of the transmembrane anion path, whereas Ep is necessary for H^+ translocation [72]. We found both conserved glutamates inherent in CLC anion/H^+ antiporters in only the SaCLCd amino acid sequence. Only "gating" glutamate (Eg) was found in SaCLCf, and only "proton" glutamate (Ep) was found in SaCLCg (Table S2). This suggests that the ion transport mechanisms differ from anion/proton antiport for SaCLCf and SaCLCg.

Like other CLCs, SaCLCd, SaCLCf, and SaCLCg contain the regulatory cystathionine beta synthase (CBS) domains CBS1 and CBS2 in the hydrophilic region at the C-terminus (Figure 1; Table S2).

According to the topology models predicted by the MEMSAT-SVM software, SaCLCd, SaCLCf, and SaCLCg are integral membrane proteins. They form 11, 7, and 9 transmembrane domains, respectively, with the N- and C-ends of the protein located on opposite sides of the membrane.

Phylogenetic analysis (Figure 2) revealed a similarity between SaCLCd, SaCLCf, and SaCLCg and CLC family representatives from other plants. Therefore, we named the cloned genes of *S. altissima* CLC proteins based on their similarity to *A. thaliana* CLC proteins characterized earlier.

The known CLCs can be divided into two subfamilies. One of them is characterized by a higher homology to eukaryotic (mostly human) CLCs; the representatives of the other are closer to prokaryotic CLCs [37,45]. Accordingly, in our cladogram of plant CLCs, the proteins were also divided into two clusters (Figure 2). We found SaCLCd and SaCLCg in the first "eukaryotic" cluster and SaCLCf in the second "prokaryotic" one. Interestingly, according to predictions obtained with the DeepLoc 1.0 software, "eukaryotic" SaCLCd and SaCLCg as well as "prokaryotic" SaCLCf were more likely to be localized to the vacuolar membrane (P_{SaCLCd} = 0.59; P_{SaCLCf} = 0.34; P_{SaCLCg} = 0.64) than to the plasma membrane (P_{SaCLCd} = 0.39; P_{SaCLCf} = 0.18; P_{SaCLCg} = 0.32). However, the "prokaryotic" SaCLCf gave indications of localization in mitochondria (P_{SaCLCf} = 0.19), endoplasmic reticulum (P_{SaCLCf} = 0.11), plastids (P_{SaCLCf} = 0.11), or Golgi network (P_{SaCLCf} = 0.05), which could be linked to the symbiogenetic (or partially symbiogenetic) origin of the organelles.

To elucidate the transport functions of SaCLCd, SaCLCf, and SaCLCg proteins, we used the previously generated [51,52] knockout mutant strain Δ*gef1* of *S. cerevisiae*. Such mutants have successfully been used earlier for clarifying anion selectivity of CLC proteins from diverse organisms [24,59,73–76]. The Gef1p protein, encoded by *GEF1*, transports chloride and is the single member of the chloride channel family in *S. cerevisiae*. Knockout mutation of the *GEF1* gene caused disturbances in a range of cellular processes and led to corresponding phenotypic manifestations [53,59]. The growth of Δ*gef1* was suppressed on rich media containing nonfermentable carbon sources (glycerol, ethanol, acetate, lactate, and raffinose) and iron in reduced concentrations and on media with fermentable carbon sources (glucose, fructose, and mannose) at pH 7.0. As the solubility of iron salts decreases upon moderate alkalization, the availability of iron for yeast cells was also lowered to pH $\geq$ 7.0. Suppressed growth of Δ*gef1* was also found on media containing cations (Li^+, Mn^{2+}, Ca^{2+}, Mg^{2+}, and tetramethylammonium$^+$) in toxic concentrations.

We transformed the yeast mutant strain Δ*gef1* by the constructs pMB1–*SaCLCd*, pMB1–*SaCLCf*, and pMB1–*SaCLCg* created on the basis of the shuttle vector pMB1 and containing sequences *SaCLCd*, *SaCLCf*, and *SaCLCg* under control of the strong constitutive *GPD1* promoter. To determine the phenotype of the transformants, the strains obtained were plated on the agarized selective diagnostic media described above (Figure 3). According to Gaxiola et al. [59], Δ*gef1* cells fail to grow on Fe-deficient medium YPEG with nonfermentable carbon sources and on both SD and SR synthetic media at pH 7.0. In our experiments, growth of Δ*gef1* cells failed under an Fe-deficient setup when Fe chelator ferrozine was added to YPEG medium with ethanol and glycerol as carbon sources. The same was the case when the pH was adjusted to 7.0 for SD and SR media. The growth of the

mutant strain Δ*gef1* on rich YPD medium was also inhibited by Mn^{2+} ions at concentrations of 2 or 3 mM (Figure 3).

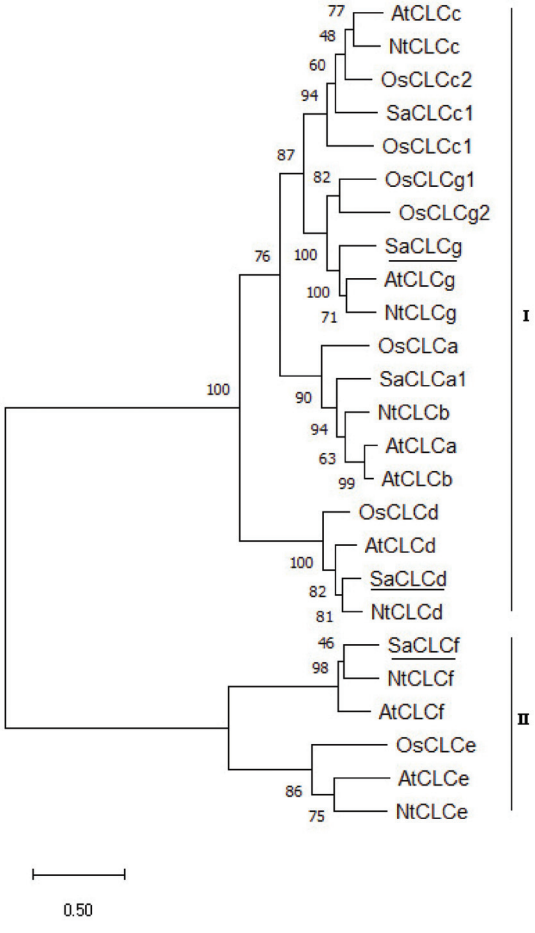

Figure 2. Phylogenetic tree of CLC family proteins of *A. thaliana*, *O. sativa*, *N. tabacum*, and *S. altissima*. AtCLCa (NP_198905.1), AtCLCb (NP_189353.1), AtCLCc (NP_199800.1), AtCLCd (NP_197996.1), AtCLCe (NP_567985.1), AtCLCf (NP_564698.1), AtCLCg (NP_198313.2), OsCLC1 (XP_015633162.1), OsCLC2 (XP_015622009.1), OsCLC3 (XP_015626588.1), OsCLC4 (AAO19370.1), OsCLC5 (XP_015636607.1), OsCLC6 (XP_015650515.1), OsCLC7 (XP_015620662.1), NtCLCc (NP_001312418.1), NtCLCb (NP_001312163.1), NtCLCd (XP_016512457.1), NtCLCe (XP_016461326.1), NtCLCf (XP_009787963.1), NtCLCg (XP_016468444.1), SaCLCa1 (ANG09048.1), SaCLCc1 (AVQ93350.1), SaCLCd (OK626332), SaCLCf (OK626333), and SaCLCg (OK626334). All protein sequences were taken from the protein database (NCBI). Subgroup I is the "eukaryotic" branch, and subgroup II is the "prokaryotic" branch. The phylogenetic tree was built in the MEGA 11 using the maximum likelihood method based on the Jones–Taylor–Thornton model. The number of bootstrap replicates was 1000; the values of bootstrap support are indicated near the nodes. Scale: 0.5 substitutions per site.

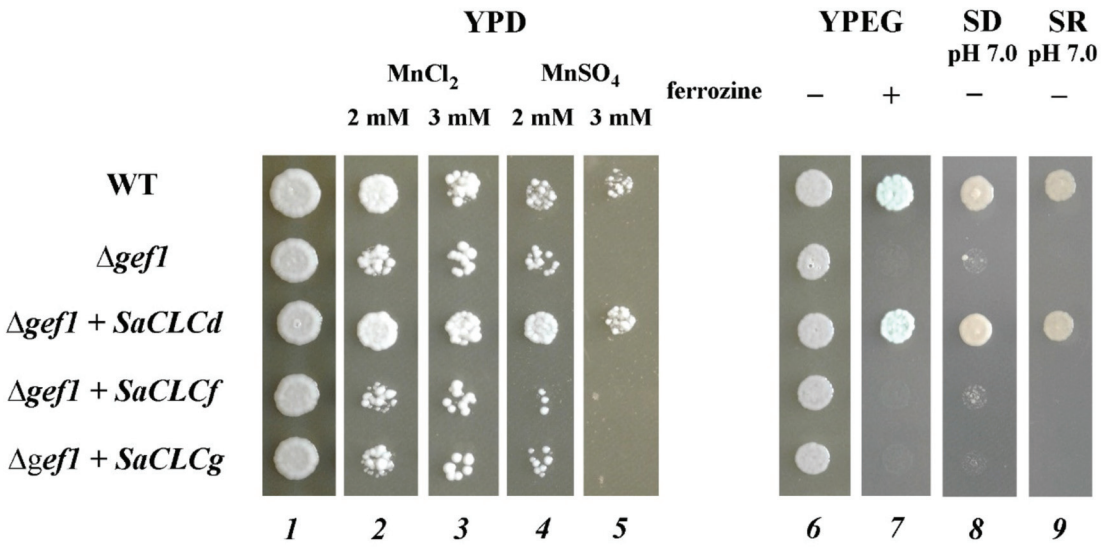

Figure 3. The growth of the yeast mutant Δ*gef1* transformed with *SaCLCd*, *SaCLCf*, and *SaCLCg* genes. Controls: wild-type W3031A and the mutant Δ*gef1* transformed with vector pMB1. Selective media: lanes 1—YPD (YPD medium: 1% yeast extract, 2% peptone, and 2% dextrose; 2 days of cells growth); 2—YPD + 2 mM $MnCl_2$ (2 days); 3—YPD + 3 mM $MnCl_2$ (2 days); 4—YPD + 2 mM $MnSO_4$ (3 days); 5—YPD + 3 mM $MnSO_4$ (3 days); 6—YPEG (rich YPEG medium: 1% yeast extract, 2% peptone, 2% ethanol, and 2% glycerol; 3 days); 7—YPEG + 1 mM ferrozine (Fe^{2+} chelator) (3 days); 8—SD, pH 7.0 (minimal synthetic medium [60] supplemented with 2% dextrose; 3 days); 9—SR, pH 7.0 (minimal synthetic medium supplemented with 2% raffinose; 4 days). Approximately 10^5 of the yeast cells were plated on selective media.

Expression of *SaCLCf* or *SaCLCg* did not restore the growth of Δ*gef1* colonies on the selective media. However, growth restoration of Δ*gef1* occurred when the mutant strain was transformed with the construct pMB1–*SaCLCd* (Figure 3), indicating the recovery of Cl^-/H^+ exchanger function in the mutant cells.

To gain further insight into the putative physiological functions of SaCLCd, SaCLCf, and SaCLCg, we investigated expression of genes encoding these proteins in the roots and leaves of *S. altissima* plants grown under increasing NaCl concentrations in the nutrient solution. We also determined the growth characteristics of *S. altissima* plants and the contents of chloride in *S. altissima* organs under these conditions. The growth of *S. altissima* was stimulated for both roots and shoots at 250 mM NaCl and stimulated for roots even at 500 mM NaCl, while inhibition (compared to 0 mM NaCl) only started at 750 mM NaCl (Figure 4a). Chloride was accumulated in *S. altissima* organs under salinity. The contents of chloride in the root and leaf tissues of *S. altissima* linearly increased with increasing NaCl concentration in the nutrient solution, and the increase was more pronounced in the leaves than in the roots (Figure 4b). With NaCl addition, concentration of chloride in the leaves were only slightly lower than that in the nutrient solution and much higher than that in the roots. At 750 mM NaCl in the nutrient solution, the concentration of chloride in the roots was less than half that in the leaves and in the nutrient solution.

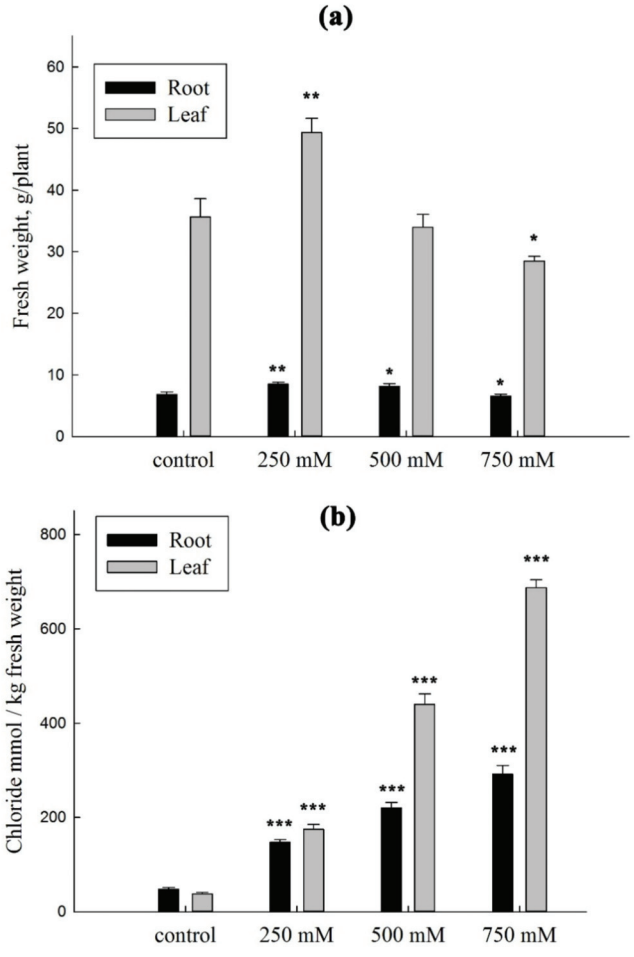

Figure 4. Fresh weights (**a**) and chloride contents (**b**) of leaves and roots of *S. altissima* grown at various NaCl concentrations in the nutrient medium. A p-value < 0.05 was considered to be statistically significant. * $p \leq 0.05$; ** $p \leq 0.01$; *** $p \leq 0.001$. Standard deviations are given.

The expression of *SaCLCd*, *SaCLCf*, and *SaCLCg* genes showed different patterns for roots and leaves of the euhalophyte under increasing salinity (Figure 5), although changes in the transcript levels were similar for all three genes. In the leaves, the relative quantity of *SaCLCd*, *SaCLCf*, and *SaCLCg* transcripts grew linearly as the salt concentration in the medium increased. Correlation coefficients (R^2) between chloride content and the level of expression of *SaCLCd*, *SaCLCf*, and *SaCLCg* genes were 0.946, 0.975 and 0.951, respectively. In the roots, the relative quantity of the *CLC* transcripts did not change significantly with increasing salinity. The minor changes observed in the expression of *CLCs* genes in the roots were in good agreement with smooth and relatively moderate changes in the Cl^- content in this organ (Figure 4b). In the leaves, a significant accumulation of Cl^- ions, observed from the elevation of NaCl concentration in the medium, corresponded to a noticeable increase in the expression of *SaCLCd*, *SaCLCf*, and *SaCLCg*, indicating the possible participation of CLC proteins that were presumably residing in the tonoplast and mediating vacuolar ion accumulation.

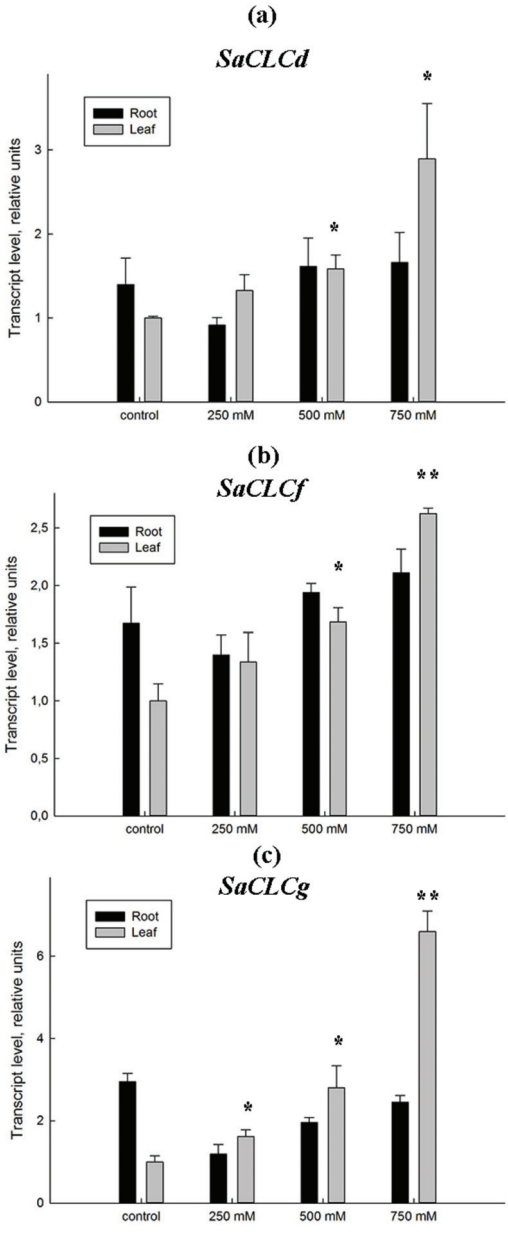

Figure 5. Relative abundance of the *SaCLCd* (**a**), *SaCLCf* (**b**), and *SaCLCg* (**c**) transcripts in the roots (dark bars) and leaves (light bars) of *S. altissima* plants grown at various NaCl concentrations in the plant growth medium. The actin gene *SaAct7* was used as internal reference gene. Similar results were obtained with *SaAct7* and *SaeEF1alpha* as reference genes, so the data are presented for the actin gene only. Data shown are means ± SD from three independent experiments. The results were deduced from three biological replicates, and each of them were performed in three analytical replicates. A p-value < 0.05 was considered to be statistically significant. * $p \leq 0.05$; ** $p \leq 0.01$.

4. Discussion

In this work, we cloned *SaCLCd*, *SaCLCf*, and *SaCLCg* genes of CLC family, the putative orthologs of *AtCLCd*, *AtCLCf*, and *AtCLCg* genes, from the euhalophyte *S. altissima*. The primary structure, membrane topology, and phylogenetic analysis of the cloned genes confirmed that they belong to the chloride channel family and have common properties both with representatives of this family from other plant species and with each other. At the same time, the three cloned *S. altissima* CLC proteins displayed some differences.

SaCLCd, like the homologous *A. thaliana* gene *AtCLCd*, belongs to the "eukaryotic" subfamily of *CLC* family genes (Figure 2) [37,45,52]. Amino acid sequences of both SaCLCd and AtCLCd contained the two conserved glutamates Eg and Ep (Figure 1), a hallmark of the "eukaryotic" subfamily of CLC proteins [71,77]. Serine in the second position of GSGxPE motif (Figure 1) indicates a preference for Cl^- over NO_3^- in anionic specificity of both these proteins [45,59]. Bioinformatic predictions located the corresponding protein for *SaCLCd* to tonoplast or plasma membrane with combined probability of 0.98.

In complementation analyses, AtCLCd is often used as a positive control for heterologous expression of CLC genes from diverse organisms in the *Saccharomyces cerevisiae GEF1* disrupted strain Δ*gef1*. Expression of *AtCLCd* in the Δ*gef1* strain invariably rescues the growth defect phenotype of the latter [37,52,59,78]. Like *AtCLCd*, the expression of *SaCLCd* gene also complemented the growth defect phenotype of the Δ*gef1* yeast mutant. The cells of Δ*gef1* transformed with the construct pMB1–*SaCLCd*, in contrast to Δ*gef1* cells transformed with empty vector pMB1, demonstrated indistinguishable growth from that of WT *S. cerevisiae* cells on selective media (Figure 3). Altogether, these results indicate that SaCLCd operates as an anion/H^+ exchanger rather than an anion channel.

SaCLCf belongs to the "prokaryotic" subfamily of *CLC* family genes (Figure 2). AtCLCf, the homolog of SaCLCf protein, is currently the least studied protein of the AtCLC family, and its subcellular localization, transport functions, and physiological role are not yet fully clarified. The available data concerning its localization and functions are contradictory. For yeast grown on selective media [59], complementation of the growth defect phenotype of Δ*gef1* was observed in the mutant cells expressing AtCLCf [37]. However, Lv and coworkers [78] did not obtain complementation of the Δ*gef1* mutant phenotype in response to the expression of this gene. According to [37], AtCLCf mainly resides in *cis*-Golgi compartments and, to a lesser extent, in the *trans*-Golgi network. However, a recent work [45] demonstrated that the relation of AtCLCf is predominantly to the *trans*-Golgi network/early endosomes (TGN/EE), where it colocalizes with V-ATPase (VHA-a1) as well as AtCLCd. The authors suggested that AtCLCd and AtCLCf transfer Cl^- into the endosomal lumen and, together with V-ATPase, are likely involved in regulation of pH and chloride concentration in the lumen of the *trans*-Golgi network and in late endosomes. Our bioinformatic predictions located the homolog of AtCLCf protein, SaCLCf, to tonoplast or plasma membrane with a combined probability of 0.52. Arguably, SaCLCf is equally likely to be located in the Golgi network or endosome membranes, similar to the AtCLCf protein.

We failed to complement the growth defect phenotype of the yeast mutant strain Δ*gef1* by expressing SaCLCf in its cells (Figure 3). Given the presence of serine in the second position of the SaCLCf conserved motif SSKSSQ (Figure 1), which indicates chloride specificity of this protein [66,67], the complementation failure could be because SaCLCf functions as a chloride channel and not as a Cl^-/H^+ antiporter. In line with the result, amino acid sequence of SaCLCf did not contain Ep, the conserved glutamate (Figure 1), playing a key role in the H^+ transport through membrane [71,77]. In relation to these data, it should be noted that "neutralization" of "proton" glutamate E203 in prokaryotic CLC-ec1 by mutation E270Q abolished H^+ coupling to Cl^- transport [72]. However, the suggestion that CLCfs act as chloride channels did not find support in a recently proposed hypothesis [45]. It was hypothesized that in members of the "prokaryotic" subfamily AtClCe and AtClCf, the function of "proton" glutamate might be performed by a glutamate other than the Ep of the "eukaryotic" CLC subfamily and that these "prokaryotic" representatives of the CLC

family are likely antiporters [45]. Generally, the operation mechanism of SaCLCf, like that of AtCLCf, remains to be elucidated.

The third gene *SaCLCg*, the homolog of *AtCLCg*, was a member of the "eukaryotic" subfamily of *S. altissima CLCs*. The presence of serine in the *SaCLCg* protein in the second position of the conserved motif GSGIPE, canonic for the "eukaryotic" CLC subfamily, indicated chloride selectivity of SaCLCg. Expression of *SaCLCg* in cells of the yeast mutant strain Δ*gef1* did not complement its growth defect phenotype (Figure 3) like the expression of the *AtCLCg* homolog [78]. This fact, together with the missing "gating" glutamate in its amino acid sequence (Figure 1), indicates that SaCLCg, like its homolog from *Arabidopsis*, is a chloride channel rather than a Cl^-/H^+ antiporter. The importance of Eg for functioning "eukaryotic" anion/H^+ antiporters is highlighted by the fact that mutating the "gating" glutamate E203 to alanine in AtCLCa expressed in *Xenopus* oocytes resulted in uncoupled anion conductance [71]. AtCLCg, most likely a Cl^- channel [33,38,71], is expressed in mesophyll, phloem, and hydathode cells of mature leaves as well in root cells; the protein was shown to localize in tonoplast [46,78]. AtCLCg was suggested to be involved in sequestering Cl^- ions in vacuoles, phloem recirculation, guttation, and xylem loading, thereby providing tolerance to salt stress [46]. Minimizing xylem loading and subsequent transport of Cl^- to the shoot might contribute to salt tolerance by keeping photosynthetic tissues away from Cl^- overaccumulation [9]. The euhalophytes have evolved another strategy for growth under salinity. These plants translocate absorbed Na^+ and Cl^- to the shoots and accumulate them preferentially in leaf vacuoles [14,79,80]. This maintains cytoplasmic Na^+ and Cl^- concentrations at nontoxic levels and contributes to water potential gradient setup in the system, namely soil–root–shoot, which promotes continuous water flow in the ascending direction [81]. Greater Na^+ and Cl^- accumulation in *S. altissima* leaves than in the roots and the growth stimulation in response to increase in NaCl concentration in the medium (Figure 4) are in line with patterns of SaCLCd, SaCLCf, and SaCLCg expression in these organs under saline conditions (Figure 5). Results of the study of *SaCLC* gene expression in the roots and leaves of plants grown at different NaCl concentrations in the medium showed that abundance of *SaCLCd*, *SaCLCf*, and *SaCLCg* transcripts did not change significantly in the roots with increasing salinity in the nutrient solution (Figure 5). However, in the leaves, a substantial increase in *SaCLCd*, *SaCLCf*, and *SaCLCg* transcript levels was observed under these conditions, which implies the participation of the proteins encoded by these genes in Cl^- accumulation in leaf organelles.

5. Conclusions

In this study, we cloned coding sequences of three novel chloride channel family genes *SaCLCd*, *SaCLCf*, and *SaCLCg*, the putative orthologs of *A. thaliana AtCLCd*, *AtCLCf*, and *AtCLCg* genes, from the euhalophyte *S. altissima*. The growth of this euhalophyte was stimulated by 250 mM NaCl, while inhibition only started from 750 mM. This is an extremely unusual feature for most plants, including agricultural ones that are glycophytes. However, global climate change and soil salinization have made us consider the importance of halophytes. In plants, members of the chloride channel family transport Cl^- and NO_3^- across membranes of intracellular organelles and account for a number of physiological functions. The results of a complementation assay using yeast expression system as well as bioinformatic analyses of the proteins encoded by these genes indicate that SaCLCd protein is a Cl^-/H^+ antiporter, while the SaCLCf and SaCLCg proteins are likely Cl^- channels. The results of qRT-PCR analyses showed that expression of all three genes was activated in the leaves with increase in NaCl concentration in the growth medium, suggesting the involvement of the SaCLCd, SaCLCf, and SaCLCg proteins in the response of *S. altissima* to NaCl. All three encoded proteins share common properties with the proteins of CLC family representatives from glycophytes, particularly the presence of conserved motifs, conserved glutamates, and regulatory CBS domains in amino acid sequences. However, differences between the proteins of *S. altissima* and their putative orthologs from glycophytes remain to be elucidated. Future investigations of the proteins, such as studies aimed at revealing their

intracellular localization and distribution in whole plant, functional studies employing heterological expression systems, and examination of the physiochemical and structural protein features, could clarify differences between halophyte and glycophyte proteins and give clues to understanding the processes underlying salinity tolerance and ways to improve them by methods of molecular genetics.

Supplementary Materials: The following supporting information can be downloaded at: https://www.mdpi.com/article/10.3390/plants11030409/s1, Figure S1: Alignment of the amino acid sequences SaCLCf (GenBank, acc. no. OK626333), AtCLCf_long (GenBank, acc. no. NP_564698.1), and AtCLCf_short (GenBank, acc. no. NP_849813.1) performed in the MAFFT program and visualized in Jalview 2.11.1.4 program [70]. The intensity of the staining of amino acid residues corresponds to the degree of their identity (Percentage Identity), Table S1: List of the primers used in the study, Table S2: Conserved amino acids motifs and residues in SaCLCd, SaCLCf and SaCLCg sequences and their coordinates.

Author Contributions: Y.V.B.: conceptualization, validation, funding acquisition, writing—original draft preparation, and supervision; O.I.N.: methodology, investigation, curation of data, funding acquisition, and formal analysis; V.S.V. and L.G.P.: formal analysis, funding acquisition, and writing—review and editing. All authors have read and agreed to the published version of the manuscript.

Funding: The research was carried out within the state assignment of Ministry of Science and Higher Education of the Russian Federation (theme No. 121040800153-1).

Institutional Review Board Statement: Not applicable.

Informed Consent Statement: Not applicable.

Data Availability Statement: All data included in this study are available upon request by contact with the corresponding author. The cloned *SaCLCd*, *SaCLCf*, and *SaCLCg* cDNA were deposited in GenBank (acc. no. OK626332, OK626333, and OK626334, respectively).

Acknowledgments: The Authors thank Timothy J. Flowers for advising on the Manuscript before submission. We remember with gratitude the former head of the Group of Genetic Engineering of Fungi (Bioengineering Centre, Russian Academy of Sciences) Mikhail El'darov who left the world prematurely, who kindly provided the pMB1 vector. The Authors are grateful to E.E. Fedorova, head of the Group of Plant–Microbial Interactions of K.A. Timiryazev Plant Physiology Institute of Russian Academy of Sciences, for critical reading of the manuscript.

Conflicts of Interest: The authors declare no conflict of interest.

References

1. Flowers, T.J. Salinisation and horticultural production. *Sci. Hortic.* **1999**, *78*, 1–4.
2. UNESCO. World Water Quality Portal Unesco. Available online: https://en.unesco.org/waterqualitymonitor (accessed on 20 December 2021).
3. Ismail, A.M.; Horie, T. Genomics, Physiology, and Molecular Breeding Approaches for Improving Salt Tolerance. *Annu. Rev. Plant Biol.* **2017**, *68*, 405–434. [CrossRef] [PubMed]
4. Qadir, M.; Quillérou, E.; Nangia, V.; Murtaza, G.; Singh, M.; Thomas, R.J.; Drechsel, P.; Noble, A.D. Economics of salt-induced land degradation and restoration. *Nat. Resour. Forum* **2014**, *38*, 282–295. [CrossRef]
5. Wang, B.; Davenport, R.J.; Volkov, V.; Amtmann, A. Low unidirectional sodium influx into root cells restricts net sodium accumulation in Thellungiella halophila, a salt-tolerant relative of Arabidopsis thaliana. *J. Exp. Bot.* **2006**, *57*, 1161–1170. [CrossRef] [PubMed]
6. Apse, M.P.; Blumwald, E. Na^+ transport in plants. *FEBS Lett.* **2007**, *581*, 2247–2254. [CrossRef] [PubMed]
7. Munns, R.; Tester, M. Mechanisms of salinity tolerance. *Annu. Rev. Plant Biol.* **2008**, *59*, 651–681. [CrossRef] [PubMed]
8. Yamaguchi, T.; Hamamoto, S.; Uozumi, N. Sodium transport system in plant cells. *Front. Plant Sci.* **2013**, *4*, 410. [CrossRef] [PubMed]
9. Teakle, N.L.; Tyerman, S.D. Mechanisms of Cl^- transport contributing to salt tolerance. *Plant Cell Environ.* **2010**, *33*, 566–589. [CrossRef]
10. Agarwal, P.K.; Shukla, P.S.; Gupta, K.; Jha, B. Bioengineering for salinity tolerance in plants: State of the art. *Mol. Biotechnol.* **2013**, *54*, 102–123. [CrossRef]

11. Mbarki, S.; Sytar, O.; Cerda, A.; Zivcak, M.; Rastogi, A.; He, X.; Zoghlami, A.; Abdelly, C.; Brestic, M. Strategies to mitigate the salt stress effects on photosynthetic apparatus and productivity of crop plants. In *Salinity Responses and Tolerance in Plants*; Kumar, V., Wani, S.H., Penna, S., Tran, L.S.P., Eds.; Springer: Cham, Switzerland, 2018; Volume 1, pp. 85–136. ISBN 9783319756714.
12. Flowers, T.J.; Galal, H.K.; Bromham, L. Evolution of halophytes: Multiple origins of salt tolerance in land plants. *Funct. Plant Biol.* **2010**, *37*, 604–612. [CrossRef]
13. Shabala, S. Learning from halophytes: Physiological basis and strategies to improve abiotic stress tolerance in crops. *Ann. Bot.* **2013**, *112*, 1209–1221. [CrossRef]
14. Flowers, T.J.; Munns, R.; Colmer, T.D. Sodium chloride toxicity and the cellular basis of salt tolerance in halophytes. *Ann. Bot.* **2015**, *115*, 419–431. [CrossRef] [PubMed]
15. Shi, H.; Ishitani, M.; Kim, C.; Zhu, J.K. The Arabidopsis thaliana salt tolerance gene SOS1 encodes a putative Na^+/H^+ antiporter. *Proc. Natl. Acad. Sci. USA.* **2000**, *97*, 6896–6901. [CrossRef] [PubMed]
16. Shi, H.; Quintero, F.J.; Pardo, J.M.; Zhu, J.K. The putative plasma membrane Na^+/H^+ antiporter SOS1 controls long-distance NA+ transport in plants. *Plant Cell* **2002**, *14*, 465–477. [CrossRef] [PubMed]
17. Tester, M.; Davenport, R. Na^+ tolerance and Na^+ transport in higher plants. *Ann. Bot.* **2003**, *91*, 503–527. [CrossRef] [PubMed]
18. Davenport, R.J.; Muñoz-Mayor, A.; Jha, D.; Essah, P.A.; Rus, A.; Tester, M. The Na^+ transporter AtHKT1;1 controls retrieval of Na^+ from the xylem in *Arabidopsis*. *Plant Cell Environ.* **2007**, *30*, 497–507. [CrossRef] [PubMed]
19. James, R.A.; Blake, C.; Zwart, A.B.; Hare, R.A.; Rathjen, A.J.; Munns, R. Impact of ancestral wheat sodium exclusion genes Nax1 and Nax2 on grain yield of durum wheat on saline soils. *Funct. Plant Biol.* **2012**, *39*, 609–618. [CrossRef]
20. Reguera, M.; Bassil, E.; Blumwald, E. Intracellular NHX-Type cation/H^+ antiporters in plants. *Mol. Plant* **2014**, *7*, 261–263. [CrossRef]
21. Wang, Z.; Hong, Y.; Zhu, G.; Li, Y.; Niu, Q.; Yao, J.; Hua, K.; Bai, J.; Zhu, Y.; Shi, H.; et al. Loss of salt tolerance during tomato domestication conferred by variation in a Na^+/K^+ transporter. *EMBO J.* **2020**, *39*, e103256. [CrossRef] [PubMed]
22. Pantoja, O.; Dainty, J.; Blumwald, E. Cytoplasmic Chloride Regulates Cation Channels in the Vacuolar Membrane of Plant Cells. *J. Membr. Biol.* **1992**, *125*, 219–229. [CrossRef]
23. White, P.J.; Broadley, M.R. Chloride in soils and its uptake and movement within the plant: A review. *Ann. Bot.* **2001**, *88*, 967–988. [CrossRef]
24. Wei, P.; Wang, L.; Liu, A.; Yu, B.; Lam, H.M. GmCLC1 confers enhanced salt tolerance through regulating chloride accumulation in soybean. *Front. Plant Sci.* **2016**, *7*, 1082. [CrossRef] [PubMed]
25. Li, B.; Tester, M.; Gilliham, M. Chloride on the move. *Trends Plant Sci.* **2017**, *22*, 236–248. [CrossRef] [PubMed]
26. Flowers, T.J.; Yeo, A.R. Ion relation of salt tolerance. In *Solute Transport in Plant Cells and Tissues*; Baker, D., Hall, J., Eds.; Longman Scientific and Technical: Harlow, UK, 1988; pp. 392–413.
27. Rubinigg, M.; Posthumus, F.; Ferschke, M.; Elzenga, J.T.M.; Stulen, I. Effects of NaCl salinity on 15N-nitrate fluxes and specific root length in the halophyte Plantago maritima L. *Plant Soil* **2003**, *250*, 201–213. [CrossRef]
28. Song, J.; Ding, X.; Feng, G.; Zhang, F. Nutritional and osmotic roles of nitrate in a euhalophyte and a xerophyte in saline conditions. *New Phytol.* **2006**, *171*, 357–366. [CrossRef]
29. Kudo, N.; Fujiyama, H. Responses of halophyte Salicornia bigelovii to different forms of nitrogen source. *Pedosphere* **2010**, *20*, 311–317. [CrossRef]
30. Yuan, J.F.; Feng, G.; Ma, H.Y.; Tian, C.Y. Effect of nitrate on root development and nitrogen uptake of Suaeda physophora under NaCl salinity. *Pedosphere* **2010**, *20*, 536–544. [CrossRef]
31. Niu, X.; Bressan, R.A.; Hasegawa, P.M.; Pardo, J.M. Ion homeostasis in NaCI stress environments. *Plant Physiol.* **1995**, *109*, 735–742. [CrossRef]
32. Barbier-Brygoo, H.; Vinauger, M.; Colcombet, J.; Ephritikhine, G.; Frachisse, J.M.; Maurel, C. Anion channels in higher plants: Functional characterization, molecular structure and physiological role. *Biochim. Biophys. Acta Biomembr.* **2000**, *1465*, 199–218. [CrossRef]
33. Zifarelli, G.; Pusch, M. CLC transport proteins in plants. *FEBS Lett.* **2010**, *584*, 2122–2127. [CrossRef]
34. Nedelyaeva, O.I.; Shuvalov, A.V.; Balnokin, Y.V. Chloride Channels and Transporters of the CLC Family in Plants. *Russ. J. Plant Physiol.* **2020**, *67*, 767–784. [CrossRef]
35. Jentsch, T.J.; Friedrich, T.; Schriever, A.; Yamada, H. The CLC chloride channel family. *Pflugers Arch. Eur. J. Physiol.* **1999**, *437*, 783–795. [CrossRef] [PubMed]
36. Miller, C. ClC chloride channels viewed through a transporter lens. *Nature* **2006**, *440*, 484–489. [CrossRef] [PubMed]
37. Marmagne, A.; Vinauger-Douard, M.; Monachello, D.; De Longevialle, A.F.; Charon, C.; Allot, M.; Rappaport, F.; Wollman, F.A.; Barbier-Brygoo, H.; Ephritikhine, G. Two members of the Arabidopsis CLC (chloride channel) family, AtCLCe and AtCLCf, are associated with thylakoid and golgi membranes, respectively. *J. Exp. Bot.* **2007**, *58*, 3385–3393. [CrossRef]
38. Barbier-Brygoo, H.; De Angeli, A.; Filleur, S.; Frachisse, J.-M.; Gambale, F.; Thomine, S.; Wege, S. Anion channels/transporters in plants: From molecular bases to regulatory networks. *Annu. Rev. Plant Biol.* **2011**, *62*, 25–51. [CrossRef]
39. De Angeli, A.; Monachello, D.; Ephritikhine, G.; Frachisse, J.M.; Thomine, S.; Gambale, F.; Barbier-Brygoo, H. The nitrate/proton antiporter AtCLCa mediates nitrate accumulation in plant vacuoles. *Nature* **2006**, *442*, 939–942. [CrossRef]
40. Isayenkov, S.; Isner, J.C.; Maathuis, F.J.M. Vacuolar ion channels: Roles in plant nutrition and signalling. *FEBS Lett.* **2010**, *584*, 1982–1988. [CrossRef]

41. Wege, S.; De Angeli, A.; Droillard, M.J.; Kroniewicz, L.; Merlot, S.; Cornu, D.; Gambale, F.; Martinoia, E.; Barbier-Brygoo, H.; Thomine, S.; et al. Phosphorylation of the vacuolar anion exchanger AtCLCa is required for the stomatal response to abscisic acid. *Sci. Signal.* **2014**, *7*, ra65. [CrossRef]
42. Jentsch, T.J.; Pusch, M. CLC chloride channels and transporters: Structure, function, physiology, and disease. *Physiol. Rev.* **2018**, *98*, 1493–1590. [CrossRef]
43. von der Fecht-Bartenbach, J.; Bogner, M.; Krebs, M.; Stierhof, Y.D.; Schumacher, K.; Ludewig, U. Function of the anion transporter AtCLC-d in the *trans*-Golgi network. *Plant J.* **2007**, *50*, 466–474. [CrossRef]
44. Guo, W.; Zuo, Z.; Cheng, X.; Sun, J.; Li, H.; Li, L.; Qiu, J.L. The chloride channel family gene CLCd negatively regulates pathogen-associated molecular pattern (PAMP)-triggered immunity in Arabidopsis. *J. Exp. Bot.* **2014**, *65*, 1205–1215. [CrossRef]
45. Scholl, S.; Hillmer, S.; Krebs, M.; Schumacher, K. ClCd and ClCf act redundantly at the trans—Golgi network/early endosome and prevent acidification of the Golgi stack. *J. Cell Sci.* **2021**, *134*, jcs258807. [CrossRef] [PubMed]
46. Nguyen, C.T.; Agorio, A.; Jossier, M.; Depré, S.; Thomine, S.; Filleur, S. Characterization of the chloride channel-like, AtCLCg, involved in chloride tolerance in Arabidopsis thaliana. *Plant. Cell Physiol.* **2015**, *57*, 764–775. [CrossRef]
47. Ashraf, M.; Akram, N.A. Improving salinity tolerance of plants through conventional breeding and genetic engineering: An analytical comparison. *Biotechnol. Adv.* **2009**, *27*, 744–752. [CrossRef] [PubMed]
48. Volkov, V. Salinity tolerance in plants. Quantitative approach to ion transport starting from halophytes and stepping to genetic and protein engineering for manipulating ion fluxes. *Front. Plant Sci.* **2015**, *6*, 873. [CrossRef] [PubMed]
49. Mishra, A.; Tanna, B. Halophytes: Potential resources for salt stress tolerance genes and promoters. *Front. Plant Sci.* **2017**, *8*, 829. [CrossRef] [PubMed]
50. Jha, R.; Patel, J.; Mishra, A.; Jha, B. Introgression of halophytic salt stress-responsive genes for developing stress tolerance in crop plants. In *Halophytes and Climate Change: Adaptive Mechanisms and Potential Uses*; Hasanuzzaman, M., Shabala, S., Fujita, M., Eds.; CABI: Boston, MA, USA, 2019; pp. 275–286.
51. Nedelyaeva, O.I.; Shuvalov, A.V.; Mayorova, O.V.; Yurchenko, A.A.; Popova, L.G.; Balnokin, Y.V.; Karpichev, I.V. Cloning and functional analysis of SaCLCc1, a gene belonging to the chloride channel family (CLC), from the halophyte *Suaeda altissima* (L.) Pall. *Dokl. Biochem. Biophys.* **2018**, *481*, 186–189. [CrossRef] [PubMed]
52. Nedelyaeva, O.I.; Shuvalov, A.V.; Karpichev, I.V.; Beliaev, D.V.; Myasoedov, N.A.; Khalilova, L.A.; Khramov, D.E.; Popova, L.G.; Balnokin, Y.V. Molecular cloning and characterisation of SaCLCa1, a novel protein of the chloride channel (CLC) family from the halophyte *Suaeda altissima* (L.) Pall. *J. Plant Physiol.* **2019**, *240*, 152995. [CrossRef] [PubMed]
53. López-Rodríguez, A.; Cárabez Trejo, A.; Coyne, L.; Halliwell, R.F.; Miledi, R.; Martínez-Torres, A. The product of the gene GEF1 of Saccharomyces cerevisiae transports Cl—across the plasma membrane. *FEMS Yeast Res.* **2007**, *7*, 1218–1229. [CrossRef] [PubMed]
54. Robinson, S.P.; Downton, W.J.S. Potassium, sodium and chloride ion concentrations in leaves and isolated chloroplasts of the halophyte Suaeda australis R. Br. *Aust. J. Plant Physiol.* **1985**, *12*, 471–479. [CrossRef]
55. Yuorieva, N.O.; Voronkov, A.S.; Tereshonok, D.V.; Osipova, E.S.; Platonova, E.V.; Belyaev, D.V. An assay for express screening of potato transformants by GFP fluorescence. *Mosc. Univ. Biol. Sci. Bull.* **2018**, *73*, 69–75. [CrossRef]
56. Shuvalov, A.V.; Yurchenko, A.A.; Nedelyaeva, O.I.; Myasoedov, N.A.; Karpichev, I.V.; Khalilova, L.A.; Popova, L.G.; Balnokin, Y.V. Identification of Some Anion Transporter Genes in the Halophyte *Suaeda altissima* (L.) Pall. and Their Expression under Nitrate Deficiency and Salinity. *Russ. J. Plant Physiol.* **2021**, *68*, 873–882. [CrossRef]
57. Eldarov, M.A.; Baranov, M.V.; Dumina, M.V.; Shgun, A.A.; Andreeva, N.A.; Trilisenko, L.V.; Kulakovskaya, T.V.; Ryasanova, L.P.; Kulaev, I.S. Polyphosphates and exopolyphosphatase activities in the yeast Saccharomyces cerevisiae under overexpression of homologous and heterologous PPN1 genes. *Biochemistry* **2013**, *78*, 946–953. [CrossRef] [PubMed]
58. Sambrook, J.; Fritsch, E.F.; Maniatis, T. *Molecular Cloning: A Laboratory Manual*; Cold Spring Harbor Laboratory Press: New York, NY, USA, 1989; p. 1546.
59. Gaxiola, R.A.; Yuan, D.S.; Klausner, R.D.; Fink, G.R. The yeast CLC chloride channel functions in cation homeostasis. *Proc. Natl. Acad. Sci. USA* **1998**, *95*, 4046–4050. [CrossRef] [PubMed]
60. Sherman, F. Getting started with yeast. In *Guide to Yeast Genetics and Molecular Biology*; Christine, G., Gerald, R.F., Eds.; Academic Press: San Diego, CA, USA, 1991; pp. 3–21.
61. Jones, D.T.; Taylor, W.R.; Thornton, J.M. The rapid generation of mutation data matrices from sequences. *Bioinformatics* **1992**, *8*, 275–282. [CrossRef]
62. Hechenberger, M.; Schwappach, B.; Fischer, W.N.; Frommer, W.B.; Jentsch, T.J.; Steinmeyer, K. A family of putative chloride channels from Arabidopsis and functional complementation of a yeast strain with a CLC gene disruption. *J. Biol. Chem.* **1996**, *271*, 33632–33638. [CrossRef]
63. Lurin, C.; Geelen, D.; Barbier-Brygoo, H.; Guern, J.; Maurel, C. Cloning and functional expression of a plant voltage-dependent chloride channel. *Plant Cell* **1996**, *8*, 701–711. [CrossRef]
64. Jentsch, T.J.; Steinmeyer, K.; Schwarz, G. Primary structure of Torpedo marmorata chloride channel isolated by expression cloning in Xenopus oocytes. *Nature* **1990**, *348*, 510–514. [CrossRef]
65. Jentsch, T.J. CLC chloride channels and transporters: From genes to protein structure, pathology and physiology. *Crit. Rev. Biochem. Mol. Biol.* **2008**, *43*, 3–36. [CrossRef]
66. Jentsch, T.J. Discovery of CLC transport proteins: Cloning, structure, function and pathophysiology. *J. Physiol.* **2015**, *593*, 4091–4109. [CrossRef]

67. Dutzler, R. The structural basis of ClC chloride channel function. *Trends Neurosci.* **2004**, *27*, 315–320. [CrossRef] [PubMed]
68. Zifarelli, G.; Pusch, M. Conversion of the 2 Cl^-/1 H^+ antiporter ClC-5 in a NO_3^-/H^+ antiporter by a single point mutation. *EMBO J.* **2009**, *28*, 175–182. [CrossRef] [PubMed]
69. Wege, S.; Jossier, M.; Filleur, S.; Thomine, S.; Barbier-Brygoo, H.; Gambale, F.; De Angeli, A. The proline 160 in the selectivity filter of the Arabidopsis NO_3^-/H^+ exchanger AtCLCa is essential for nitrate accumulation in planta. *Plant J.* **2010**, *63*, 861–869. [CrossRef] [PubMed]
70. Waterhouse, A.M.; Procter, J.B.; Martin, D.M.A.; Clamp, M.; Barton, G.J. Jalview Version 2—A multiple sequence alignment editor and analysis workbench. *Bioinformatics* **2009**, *25*, 1189–1191. [CrossRef]
71. Bergsdorf, E.Y.; Zdebik, A.A.; Jentsch, T.J. Residues important for nitrate/proton coupling in plant and mammalian CLC transporters. *J. Biol. Chem.* **2009**, *284*, 11184–11193. [CrossRef]
72. Accardi, A.; Walden, M.; Nguitragool, W.; Jayaram, H.; Williams, C.; Miller, C. Separate ion pathways in a Cl^-/H^+ exchanger. *J. Gen. Physiol.* **2005**, *126*, 563–570. [CrossRef]
73. Miyazaki, H.; Uchida, S.; Takei, Y.; Hirano, T.; Marumo, F.; Sasaki, S. Molecular cloning of CLC chloride channels in Oreochromis mossambicus and their functional complementation of yeast CLC gene mutant. *Biochem. Biophys. Res. Commun.* **1999**, *255*, 175–181. [CrossRef]
74. Kida, Y.; Uchida, S.; Miyazaki, H.; Sasaki, S.; Marumo, F. Localization of mouse CLC-6 and CLC-7 mRNA and their functional complementation of yeast CLC gene mutant. *Histochem. Cell Biol.* **2001**, *115*, 189–194. [CrossRef]
75. Nakamura, A.; Fukuda, A.; Sakai, S.; Tanaka, Y. Molecular cloning, functional expression and subcellular localization of two putative vacuolar voltage-gated chloride channels in rice (*Oryza sativa* L.). *Plant Cell Physiol.* **2006**, *47*, 32–42. [CrossRef]
76. Wei, P.; Che, B.; Shen, L.; Cui, Y.; Wu, S.; Cheng, C.; Liu, F.; Li, M.W.; Yu, B.; Lam, H.M. Identification and functional characterization of the chloride channel gene, GsCLC-c2 from wild soybean. *BMC Plant Biol.* **2019**, *19*, 1–15. [CrossRef]
77. Accardi, A. Structure and gating of CLC channels and exchangers. *J. Physiol.* **2015**, *593*, 4129–4138. [CrossRef] [PubMed]
78. Lv, Q.D.; Tang, R.; Liu, H.; Gao, X.S.; Li, Y.Z.; Zheng, H.Q.; Zhang, H.X. Cloning and molecular analyses of the Arabidopsis thaliana chloride channel gene family. *Plant Sci.* **2009**, *176*, 650–661. [CrossRef]
79. Flowers, T.J.; Troke, P.F.; Yeo, A.R. The Mechanism of Salt Tolerance in Halophytes. *Annu. Rev. Plant Physiol.* **1977**, *28*, 89–121. [CrossRef]
80. Flowers, T.J.; Colmer, T.D. Plant salt tolerance: Adaptations in halophytes. *Ann. Bot.* **2015**, *115*, 327–331. [CrossRef] [PubMed]
81. Balnokin, Y.V.; Kotov, A.A.; Myasoedov, N.A.; Khailova, G.F.; Kurkova, E.B.; Lun'kov, R.V.; Kotova, L.M. Involvement of long-distance Na^+ transport in maintaining water potential gradient in the medium-root-leaf system of a halophyte *Suaeda altissima*. *Russ. J. Plant Physiol.* **2005**, *52*, 489–496. [CrossRef]

MDPI
St. Alban-Anlage 66
4052 Basel
Switzerland
Tel. +41 61 683 77 34
Fax +41 61 302 89 18
www.mdpi.com

Plants Editorial Office
E-mail: plants@mdpi.com
www.mdpi.com/journal/plants

MDPI
St. Alban-Anlage 66
4052 Basel
Switzerland

Tel: +41 61 683 77 34

www.mdpi.com

ISBN 978-3-0365-4518-9